Facoltà di Scienze Matematiche Fisiche e Naturali

Dottorato in Fisica - XVIII Ciclo

ELECTRICAL AND ALL-OPTICAL POLING OF NONLINEAR OPTICAL MATERIALS: RELAXATION DYNAMICS

Ph.D. Student:

Alessia Quatela

Supervisors:

Prof. Mauro Casalboni

Università di Roma "Tor Vergata"

Dr. Fabio De Matteis

Università di Roma "Tor Vergata"

Referee:

Prof. Francesco Michelotti

Università di Roma "La Sapienza"

2005-2006

to the memory of Felice

INDEX

Introduction

Efforts to accelerate Internet data traffic always seem to hit speed bumps. Let us consider an electrooptic modulator, which encodes signals onto the light beams that carry data along optical fibers. Today's high-speed systems, operating at 40 Gb/s, depend on $LiNbO_3$ modulators with a bandwidth of 43-44 GHz. But at faster modulation, the signals start to degrade. An alternative approach to overcome such difficulties is the use of organic molecules endowed with strong nonlinearities incorporated into matrices using different molecular design approaches. Such matrices are polymers and organic-inorganic hybrids, synthesized by sol-gel technique. In particular, the last systems seem to be excellent photonic media because of their high optical quality and extremely low optical losses. Therefore, combining inorganic glass and organic functional molecules is probably one of the best way of getting optical nonlinearity as in organic systems and mechanical stability as an inorganic one. Nowadays, alternative route to crystalline-based devices are being investigated by many research laboratories worldwide.

A team of researchers at Lucent Technologies' Bell Labs, in a work published on Science in the 13 November **2002** issue, estimates that a bandwidth of 150-170 GHz could be achieved in a polymer modulator and a detectable modulation signal at 1.6 THz could be produced (in $LiNbO_3$ the largest bandwidth quoted in the literature was 105 GHz). The team mixed a commercially available chromophore into the polymer polymethylmethacrylate or Lucite. It was possible to make a composite with higher electrooptic coefficient than $LiNbO_3$, 60-70 pm/V as opposed to 30 pm/V. The coefficient defines the rate at which the refraction index changes in response to an applied field, and the faster that rate is, the lower the system drive voltage can be in the experiment. Since high input voltage is one cause of signal degradation, a lower voltage allows the polymer to perform better.

Such advantages are obtained at the cost of some additional post-deposition procedures. After deposition, this composed material is centrosymmetric and, as such, is not endowed of second order properties. Poling, i.e. the orientation of the molecular dipoles, is necessary in order to break this centrosymmetry. By poling, the dipoles can be oriented parallel or perpendicular to the film plane. Linear (Polarized Absorption Spectroscopy-*PAS*) and nonlinear (Second Harmonic Generation-*SHG*) characterizations can be performed on the studied systems in order to reveal the orientation.

For practical uses, nonlinear optical (NLO) materials must possess both large nonlinearity and temporal stability. Industrial requirements demand poled second order nonlinear optical materials must retain at least 80% of its initial nonlinear activity at an operating temperature of

70°C for a period of 5 years. They must also withstand brief excursions to device processing temperatures of 250°C and higher. A careful analysis of the orientation mechanism is therefore of fundamental importance. Orientation relaxation in poled systems arises from thermal re-orientational effects whose rate is governed by the mobility of the molecules in the matrix. The mobility is in turn determined by a number of parameters including glass transition temperature (T_g) and free volume content. Thus, measure of SHG is a diagnostic tool for studying relaxation processes. For these reasons, temperature is often chosen as degrading agent and polar order decay monitored by SHG in accelerated aging tests.

The present thesis is motivated by the attempt to find practical polymeric or hybrid organic-inorganic materials for electrooptic devices, paying particular attention to the macroscopic second order nonlinearity, the raise and decay of the poled order responsible for the nonlinearity and on the chemical nature of the systems identified as promising materials. The work is pursued mainly under the *ODEON*• European project and performed in the *NeMO*•• laboratory at the University of Roma "Tor Vergata". The aim of the project is the development of innovative multifunctional nanomaterials for optoelectronics specially suitable for electrooptic modulators. *ODEON* is engaged in such challenge, gathering skills from eleven first class European scientific and industry institutions operating on functional polymers, sol-gel based materials, chromophore synthesis and device fabrication.

Two different poling methods are investigated and discussed: *corona* and *all-optical poling*. The first technique, developed in the *NeMO* laboratory, involves a dc electric field, used to orient the dipoles of the material at a temperature where the molecule dipoles can rotate. The second one uses two coherent sources possessing different frequencies (ω and 2ω) to induce a reversible static polarization inside the medium at room temperature. This last work was performed in the ***Laboratoire des Propriétés Optiques des Matériaux et Applications (POMA)*** at the University of Angers under the supervision of Prof. J.M. Nunzi thanks to the *COST P8* grant. *COST* is an intergovernmental framework for European Co-operation in the field of Scientific and Technical Research.

- *ODEON (design and fabrication of Optoelectronics DEvices based on innovative second order nonlinear Organic Nanomaterials)*
  http://optoweb.fis.uniroma2.it/NewODEON/restricted/index.html
- •• *NeMO (New Material for Optoelectronics)*
  http://optoweb.fis.uniroma2.it/

This thesis is structured as follows:

in Chapter 1 the basics of the nonlinear optics is introduced.

the applications of polymers and hybrid systems are briefly mentioned in Chapter 2 to indicate the desired chemical and physical properties that are required in a useful material.

in Chapter 3 accelerated life tests and fitting models for long-lived decay are discussed.

in Chapter 4 the experimental setup used in accomplishing the work are described, in particular, corona and all-optical poling setup.

in Chapter 5 are presented the measurements performed on organic and hybrid samples using the experimental setup developed by the candidate

in Chapter 6 the measurements performed at the *Laboratoire des Propriétés Optiques des Matériaux et Applications (POMA)*, using the all-optical setup on organic and hybrid materials are shown.

in Appendix 1 the electromagnetic formulation of the nonlinear interaction is discussed while in Appendix 2 the different systems which have been studied are listed and their NLO activity and/or the time stability is shortly summarized.

Abbreviations

3-Glycidoxypropyltrimethoxysilane……Gly

Acetonitrile……...ACN

All-Optical Poling……AOP

Attenuated Reflection Technique..……ATR

Angular Hole Burning ……AHB

Bond Length Alternation……BLA

Bond Order Alternation……..BOA

Decomposition Temperature……...T_d

Difference Frequency Generation……..DFG

Dimethylformamide……DMF

Disperse Red 1……...DR1

Disperse Red 19……...DR19

Disperse Red 1-methacrylate copolymer……DR1-co-PMMA

Electric Field Induced Second Harmonic……...EFISH

Fourier Transform IR spectroscopy……FTIR

Glass Transition Temperature……T_g

Hydroxyethylcarbazole……CbOH

Hyper Rayleigh Scattering……..HRS

Intramolecular Charge Transfer……ITC

Methanol……MeOH

Methoxyethanol……MeOEtOH

N-methyl-2-pyrrolidone……..NMP

NonLinear Optical……...NLO

Optical Rectification……...OR

Polarized Absorption Spectroscopy……PAS

Poling Temperature……T_{poling}

Poling Time……...t_{poling}

Poling Voltage……V_{poling}

Poly(carbonate)……...PC

Poly(methyl methacrylate)……..PMMA

Poly(sulfone)……..PSU

Quasi Phase Matching……QPM

Second Harmonic……SH

Second Harmonic Generation…….SHG

Stimulated Raman Scattering……..SRS

Sum Frequency Generation…….SFG

Tetraethoxysilane……...TEOS

Tetramethoxysilane……..TMOS

Third Harmonic Generation……...THG

Zirconium(IV)propoxide……Zr

Chapter 1

Nonlinear Optics

"MAXWELL'S THEORY of electric and magnetic fields and his idea that light is an electromagnetic wave were some of the great milestones of scientific thought, and unified understanding of a large and diverse set of phenomena. Indeed, by the late nineteenth century, the success of the classical electromagnetic theory of light led some to believe that were few new fundamental discoveries to be made. This smug complacency was soon shattered by the inability of the wave theory to explain several observation: radiation spectra, the photoelectric effect, x-rays, radioactivity. These effects could only be understood by reviving the idea of corpuscular nature of light. Out of this effort, modern quantum theory was born, and optical science settled once again into the complacency of a solved science. Rapid progress was made. The accuracy of the geometrical optics approximations, together with the linearity of the equations, which meant that complicated solution fields could be built by the linear superposition of much simpler solutions (e.g. plane waves), played important roles in this development. The amplitude of the electromagnetic field seemed to matter little.

The discovery of the laser in 1960 (an acronym for Light Amplification by Stimulated Emission of Radiation) changed all that. Now available was a source of highly coherent radiation that could be concentrated and focused to give extremely high local intensities. The nonlinear tiger was released from its cage; a reach stream of fundamental new phenomena, plus several new manifestations of phenomena familiar from other fields, soon followed, and that streams continues to flow, becoming richer by the day. The relatively young subject of nonlinear optics, the study of how high-intensity light interacts with and propagates through matter, is so scientifically fertile and technologically promising that it is destined to be one of the most important areas of science for the next quarter century." (***Newell and Moloney, 1992***)

This Chapter presents an introduction to the field of nonlinear optics from the perspective of the nonlinear susceptibility. This quantity is used to determine the nonlinear polarization of a medium in terms of the strength of an applied optical-frequency electric field. It thus provides a framework for describing nonlinear optical (NLO) phenomena. A description of the anharmonic oscillator model is also given in order to clarify the origin of the NLO coefficients.

1.1 Introduction

Nonlinear optics is the study of phenomena that occur as a consequence of the modification of the optical properties of a material system by the presence of light. Typically, only laser light is sufficiently intense to modify the optical properties of the material system. In fact, the beginning of the field of nonlinear optics is often taken to be the discovery of Second Harmonic Generation (SHG) by **Franken** at al. in **1961**, shortly after the demonstration of the first working laser by **Maiman** in **1960**. Nonlinear optical (NLO) phenomena are "nonlinear" in the sense that they occur when the response of a material system to an applied optical field depends in a nonlinear manner upon the strength of the optical field.

In order to describe more precisely what we mean by an optical nonlinearity, let us consider how the dipole moment per unit volume, or polarization *P(t)*, of a material system depends upon the strength *E(t)* of the applied optical field. In the case of conventional (i.e., linear) optics, the induced polarization depends linearly upon the electric field strength in a manner that can often be described by the relationship

$$P(t) = \chi^{(1)} E(t) \qquad \textbf{(1.1)}$$

where the constant of proportionality $\chi^{(1)}$ is known as the linear susceptibility. In nonlinear optics, the NLO response can often be described by generalizing **Eq. (1.1)** by expressing the polarization *P(t)* as a power series in the field strength *E(t)* as

$$\begin{aligned} P(t) &= \chi^{(1)} E(t) + \chi^{(2)} E^2(t) + \chi^{(3)} E^3(t) + ... \\ &\equiv P^{(1)}(t) + P^{(2)}(t) + P^{(3)}(t) + ... \end{aligned} \qquad \textbf{(1.2)}$$

The quantities $\chi^{(2)}$ and $\chi^{(3)}$ are known as the second and third order NLO susceptibilities , respectively. For simplicity, we have taken the fields *P(t)* and *E(t)* to be scalar quantities in writing **Eq. (1.1)** and **(1.2)**. In **Section 1.3** we show how to treat the vector nature of the fields; in such a case $\chi^{(1)}$ becomes a second rank tensor, $\chi^{(2)}$ becomes a third rank tensor, etc. In writing **Eq. (1.1)** and **(1.2)** in the form shown, we have also assumed that the polarization at time t depends only on the instantaneous value of the electric field strength.

The assumption that the medium responds instantaneously also implies (through the *Kramers-Kroning* relations) that the medium must be lossless and dispersionless. In general, the nonlinear susceptibilities depend on the frequencies of the applied fields, but under our present assumption of instantaneous response we take them to be constants.

We shall refer to $P^{(2)}(t) = \chi^{(2)}E(t)^2$ as the second order nonlinear polarization and to $P^{(3)}(t) = \chi^{(3)}E(t)^3$ as the third order nonlinear polarization. We shall see later in this section that the physical processes that occur as a result of the second order polarization $P^{(2)}$ are distinct from those that occur as a result of the third order polarization $P^{(3)}$. In fact, we shall show that second order NLO interactions can occur only in noncentrosymmetrical materials, that is, in materials that do not display inversion symmetry. Since liquids, gases, amorphous solids (such as glass), and even many crystals do display inversion symmetry, $\chi^{(2)}$ vanishes identically for such media, and consequently they cannot produce second order NLO interactions. On the other hand, third order NLO interactions (i.e., those described by a $\chi^{(3)}$ susceptibility) can occur both for centrosymmetric and noncentrosymmetric media.

In the case in which the nonlinearity is electronic in origin, one might expect that the lowest order correction term $P^{(2)}$ would be comparable to the linear response $P^{(1)}$ when the amplitude of the applied field strength E was of the order of the characteristic atomic electric field strength $E_{at} = e/a_0^2$, where $-e$ is the charge of the electron and a_0 is the Bohr radius of the hydrogen atom. Numerically we find that $E_{at} = 2\times10^7$ *esu*. We thus expect that under conditions of non resonant excitation the second order susceptibility $\chi^{(2)}$ will be of the order of $\chi^{(1)}/E_{at}$. For condensed matter $\chi^{(1)}$ is of the order of unity, and we hence expect that $\chi^{(2)}$ will be of the order of $1/E_{at}$. or that

$$\chi^{(2)} \cong 5\times10^{-8}\,esu \cong 2\frac{pm}{V} \qquad \textbf{(1.3)}$$

Similarly, we expect $\chi^{(3)}$ to be of the order of $\chi^{(1)}/E_{at}^2$, which for condensed matter is of the order of

$$\chi^{(3)} \cong 3\times10^{-15}\,esu \cong 3\frac{pm^2}{V^2} \qquad \textbf{(1.4)}$$

The most common procedure for describing NLO phenomena is based on expressing the polarization $P(t)$ in terms of the applied electric field strength $E(t)$, as we have done in **Eq. (1.2)**. The reason why the polarization plays a key role in the description of NLO phenomena is that a

time varying polarization can act as the source of new components of the electromagnetic field as shown in **Appendix 1**. (**Boyd, 1992**)

1.2 Nonlinear Optical Interactions

In this section, we present a qualitative description of a number of NLO interactions. In addition, for those processes that can occur in a lossless medium, we indicate how they can be described in terms of the nonlinear contributions to the polarization described by **Eq. (1.2)**.

1.2.1 Second Harmonic Generation

As an example of a NLO interaction, let us consider the process of SHG, which is illustrated schematically in **Fig. 1.1**.

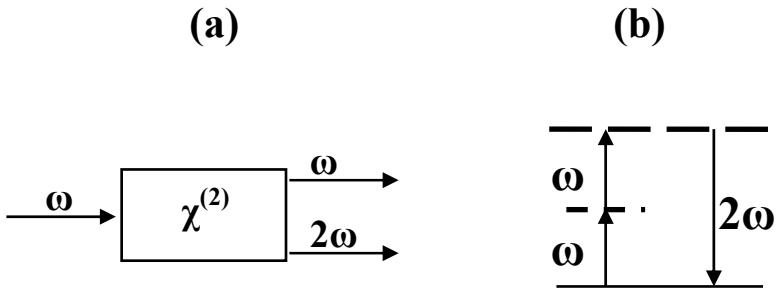

Fig. 1.1 (a) Geometry of SHG; **(b)** Energy-level diagram describing SHG.

Here a laser beam whose electric field strength is represented as

$$E(t) = Ee^{-i\omega t} + c.c. \qquad \textbf{(1.5)}$$

is incident upon a crystal for which the second order susceptibility $\chi^{(2)}$ is nonzero. The nonlinear polarization that is created in such a crystal is given according to **Eq. (1.2)** as $P^{(2)}(t) = \chi^{(2)}E^{(2)}(t)$ or as

$$P^{(2)}(t) = 2\chi^{(2)}EE^{*} + \left(\chi^{(2)}E^{2}e^{-2i\omega t} + c.c.\right) \qquad \textbf{(1.6)}$$

We see that the second order polarization consists of a contribution at zero frequency (the first term) and a contribution at frequency 2ω (the second term).

Under proper experimental conditions, the process of SHG can be so efficient that nearly all of the power in the incident radiation at frequency ω is converted to radiation at the second harmonic frequency 2ω. One common use of SHG is to convert the output of a fixed frequency laser into a different spectral region. For example, the Nd:YAG laser operates in the near infrared at a wavelength of 1064 nm. SHG is routinely used to convert the wavelength of the radiation to 532 nm, in the middle of the visible spectrum.

SHG can also be visualized by considering the interactions in terms of the exchange of photons between the various frequency components of the field. According to this picture, which is illustrated in part **(b)** of **Fig. 1.1**, two photons of frequency ω are destroyed and a photon of frequency 2ω is simultaneously created in a single quantum-mechanical process. The solid line in the figure represents the atomic ground state, and the dashed lines represent what are known as virtual levels. These levels are not energy eigenlevels of the free atom, but rather represent the combined energy of one of the eigenstates of the atom and of one or more photons of the radiation field.

The theory of SHG is developed in **Appendix 1**.

1.2.2 Sum and Difference Frequency Generation

Let us next consider the circumstance in which the optical field incident upon a NLO medium characterized by a nonlinear susceptibility $\chi^{(2)}$ consists of two distinct frequency components, which we represent in the form

$$E(t) = E_1 e^{-i\omega_1 t} + E_2 e^{-i\omega_2 t} + c.c. \qquad \textbf{(1.7)}$$

Then, assuming as in **Eq. (1.2)** that the second order contribution to the nonlinear polarization is of the form

$$P^{(2)}(t) = \chi^{(2)} E(t)^2 \qquad \textbf{(1.8)}$$

we find that the nonlinear polarization is given by

$$P^{(2)}(t)=\chi^{(2)}\begin{bmatrix}E_1^2e^{-2i\omega_1 t}+E_2^2e^{-i2\omega_2 t}+2E_1E_2e^{-(\omega_1+\omega_2)t}\\+2E_1E_2^*e^{-i(\omega_1-\omega_2)t}+c.c.\end{bmatrix}+ \\ +2\chi^{(2)}\left[E_1E_1^*+E_2E_2^*\right] \tag{1.9}$$

It is convenient to express this result using the notation

$$P^{(2)}(t)=\sum_n P(\omega_n)\cdot e^{-i\omega_n t} \tag{1.10}$$

where the summation extends over positive and negative frequencies ω_n. The complex amplitudes of the various frequency components of the nonlinear polarization are hence given by

$$\begin{aligned}
&P(2\omega_1)=\chi^{(2)}E_1^2\,(SHG)\\
&P(2\omega_2)=\chi^{(2)}E_2^2\,(SHG)\\
&P(\omega_1+\omega_2)=2\chi^{(2)}E_1E_2\,(SFG)\\
&P(\omega_1-\omega_2)=2\chi^{(2)}E_1E_2^*\,(DFG)\\
&P(0)=2\chi^{(2)}\left(E_1E_1^*+E_2E_2^*\right)(OR)
\end{aligned} \tag{1.11}$$

Here we have labelled each expression by the name of the physical process that it describes, such as SHG, Sum Frequency Generation (**SFG**), Difference Frequency Generation (**DFG**) and Optical Rectification (**OR**).

Note that, in accordance with our complex notation, there is also a response at the negative of each of the nonzero frequencies given above (i.e., $P(-2\omega_1) = \chi^{(2)}E_1^{*2}$). However, since each of these quantities is simply the complex conjugate of one of the quantities given in **Eq. (1.11)**, it is not necessary to take explicit account of both the positive and the negative frequency components.

We see from **Eq. (1.11)** that four different nonzero frequency components are present in the nonlinear polarization. However, typically no more than one of these frequency components will be present with any appreciable intensity in the radiation generated by the nonlinear interaction. The reason for this behaviour is that the nonlinear polarization can efficiently produce an output signal only if a certain phase-matching condition (discussed in detail in **Appendix 1**) is satisfied. Usually this condition cannot be satisfied for more that one frequency component of the nonlinear polarization at a time. Operationally, one often chooses which frequency component will be

radiated by properly selecting the polarization of the input radiation and orientation of the nonlinear material.

SFG

Let us now consider the process of SFG, which is illustrated in **Fig. 1.2**. According to **Eq. (1.11)**, the complex amplitude of the nonlinear polarization describing this process is given by the expression

$$P(\omega_1 + \omega_2) = 2\chi^{(2)} E_1 E_2 \qquad \textbf{(1.12)}$$

In many ways the process of SFG is analogous to that of SHG, except that in SFG the to input waves are at different frequencies. One application of SFG is to produce tuneable radiation in the UV spectral region by choosing one of the input waves to be the output of a fixed-frequency visible laser and the other to be the output of a frequency-tenable visible laser.

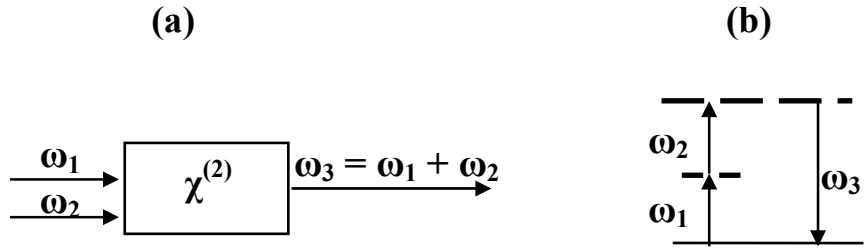

Fig. 1.2 SFG. **(a)** Geometry of the interaction; **(b)** Energy level description.

DFG

The process of DFG is described by a nonlinear polarization of the form

$$P(\omega_1 - \omega_2) = 2\chi^{(2)} E_1 E_2^* \qquad \textbf{(1.13)}$$

and is illustrated in **Fig. 1.3**. Here the frequency of the generated wave is the difference of those of the applied fields. DFG can be used to produce tuneable infrared radiation by mixing the output of a frequency-tuneable visible laser with that of a fixed frequency visible laser.

Superficially, DFG and SFG appear to be very similar processes. However, an important difference between the two processes can be deduced from the description of DFG in terms of a photon energy-level diagram (part **(b)** of **Fig. 1.3**). We see that conservation of energy requires that for every photon that is created at the difference frequency $\omega_3 = \omega_1 - \omega_2$, a photon at the higher input frequency (ω_1) must be destroyed and a photon at the lower input frequency (ω_2) must be created. Thus, the lower-frequency input field is amplified by the process of DFG. For this reason, the process of DFG is also known as optical parametric amplification.

According to the photon energy-level description of DFG, the atom first absorbs a photon of frequency ω_1 and jumps to the highest virtual level. This level decays by a two-photon emission process that is stimulated by the presence of the ω_2 field, which is already present. Two-photon emission can occur even if the ω_2 field is not applied. The generated fields in such a case are very much weaker, since they are created by spontaneous two-photon emission from a virtual level. This process is known as parametric fluorescence and has been observed experimentally **(Harris at al., 1967; Byer and Harris, 1968).**

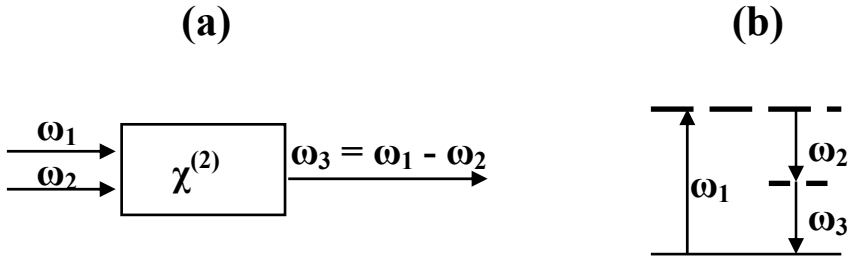

Fig. 1.3 DFG. **(a)** Geometry of the interaction; **(b)** Energy level description.

1.2.3 Optical Parametric Oscillation

We have just seen that in the process of DFG the presence of radiation at frequency ω_2 or ω_3 can stimulate the emission of additional photons at these frequencies. If the nonlinear crystal used in this process is placed inside an optical resonator, as shown in **Fig. 1.4**, the ω_2 and/or ω_3 fields can build up to large values. Such a device is known as an optical parametric oscillator. Optical parametric oscillators are used primarily at infrared wavelengths, where other sources of tuneable

radiation are not readily available. Such a device is tuneable because any frequency ω_2 (that is less then ω_1) can satisfy the condition for some frequency ω_3.

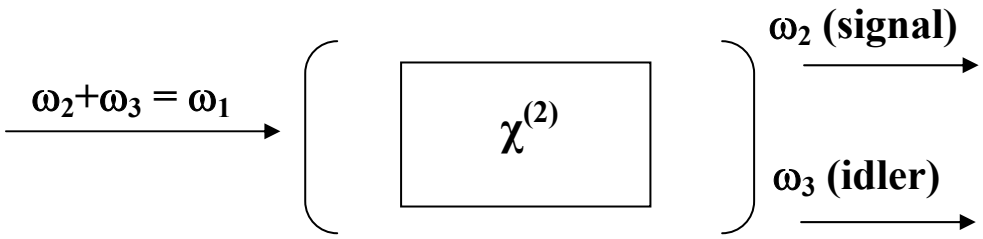

Fig. 1.4 The optical parametric oscillator. The cavity end mirrors have high reflectivity at frequencies ω_2 and/or ω_3.

In practice, one controls the output frequency by adjusting the phase-matching condition, as discussed in **Appendix 1**. The applied field frequency ω_1 is often called the pump frequency, the desired output frequency is called the signal frequency, and the other, unwanted, output frequency is called the idler frequency.

1.2.4 Third Harmonic Generation

We next consider the third order contribution to the nonlinear polarization

$$P^{(3)}(t) = \chi^{(3)} E(t)^3 \qquad \textbf{(1.14)}$$

For the general case in which the field $E(t)$ is made up of several different frequency components, the expression for $P^{(3)}(t)$ is very complicated. For this reason, we first consider the simple case in which the applied field is monochromatic and is given by

$$E(t) = E_0 \cos(\omega t) \qquad \textbf{(1.15)}$$

Then, since $\cos^3(\omega t) = \frac{1}{4}\cos(3\omega t) + \frac{3}{4}\cos(\omega t)$, the nonlinear polarization can be expressed as

$$P^{(3)}(t) = \frac{1}{4}\chi^{(3)} E_0^3 \cos(3\omega t) + \frac{3}{4}\chi^{(3)} E_0^3 \cos(\omega t) \qquad \textbf{(1.16)}$$

The first term in **Eq. (1.16)** describes a response at frequency 3ω that is due to an applied field at frequency ω. This term leads to the process of Third Harmonic Generation (**THG**), which is illustrated in **Fig. 1.5**. According to the photon description of this process shown in part **(b)** of the figure, three photons of frequency ω are destroyed and one photon of frequency 3ω is created in each elementary event.

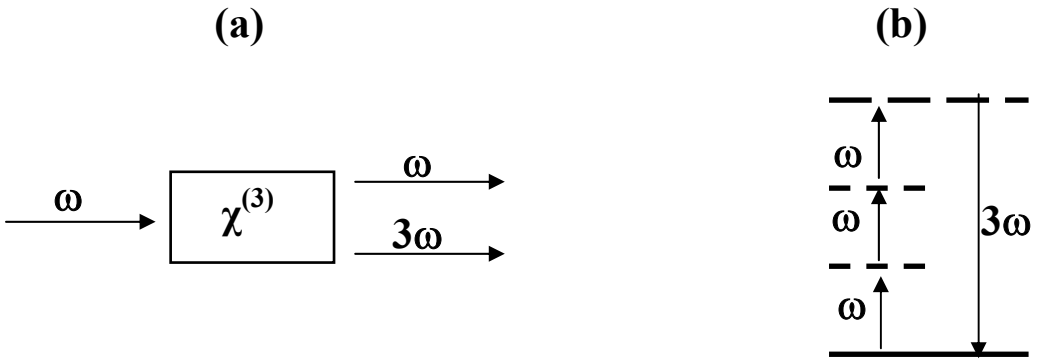

Fig. 1.5 THG. **(a)** Geometry of the interaction; **(b)** Energy level description.

1.3 Nonlinear Susceptibility

NLO interactions can be described in terms of the nonlinear polarization given by **Eq. (1.2)** only for a material system that is lossless and dispersionless. In the present section, we consider the more general case of a material with dispersion and/or loss. In this general case the nonlinear susceptibility becomes a complex quantity relating the complex amplitudes of the electric field and polarization.

We assume that we can represent the electric field vector of the optical wave as the discrete sum of a number of frequency components as

$$\boldsymbol{E}(\boldsymbol{r},t)=\sum_{n}\boldsymbol{E}_{n}(\boldsymbol{r},t) \qquad \textbf{(1.17)}$$

where the summation is to be taken over positive frequencies only. It is often convenient to represent $\boldsymbol{E}_n(\boldsymbol{r},t)$ as the sum of its positive- and negative-frequency parts as

$$\boldsymbol{E}_{n}=\boldsymbol{E}_{n}^{(+)}+\boldsymbol{E}_{n}^{(-)} \qquad \textbf{(1.18)}$$

where

$$\boldsymbol{E}_n^{(+)} = \boldsymbol{E}_n e^{-i\omega_n t} \tag{1.19}$$

and

$$\boldsymbol{E}_n^{(-)} = \boldsymbol{E}_n^{(+)*} = \boldsymbol{E}_n^* e^{i\omega_n t} \tag{1.20}$$

By requiring $\boldsymbol{E}_n^{(-)}$ to be the complex conjugate of $\boldsymbol{E}_n^{(+)}$ we are assured that the quantity $\boldsymbol{E(r,t)}$ of **Eq. (1.17)** will be real, as it must be in order to represent a physical field. It is also convenient to define the spatially slowly varying field amplitude $\boldsymbol{A}_n$ by means of the relation

$$\boldsymbol{E}_n = \boldsymbol{A}_n e^{i\mathbf{k}_n \cdot \boldsymbol{r}} \tag{1.21}$$

The total electric field of **Eq. (1.17)** can thus be represented in terms of these field amplitudes by either of the expressions

$$\begin{aligned} \boldsymbol{E}(\boldsymbol{r},t) &= \sum_n \boldsymbol{E}_n e^{-i\omega_n t} + \boldsymbol{c.c.} \\ &= \sum_n \boldsymbol{A}_n e^{i(\mathbf{k}_n \cdot \mathbf{r} - \omega_n t)} + \boldsymbol{c.c.} \end{aligned} \tag{1.22}$$

On occasion, we shall express these field amplitudes using the alternative notation

$$\boldsymbol{E}_n = \boldsymbol{E}(\omega_n) \text{ and } \boldsymbol{A}_n = \boldsymbol{A}(\omega_n) \tag{1.23}$$

This notation is very convenient, even though ω_n is actually a parameter rather than an argument showing a true functional dependence. In terms of this new notation, the reality condition of **Eq. (1.20)** becomes

$$\boldsymbol{E}(-\omega_n) = \boldsymbol{E}(\omega_n)^* \text{ and } \boldsymbol{A}(-\omega_n) = \boldsymbol{A}(\omega_n)^* \tag{1.24}$$

Using this new notation, we can write the total field in the more compact form

$$\boldsymbol{E}(\boldsymbol{r},t)=\sum_{\boldsymbol{n}}\boldsymbol{E}(\omega_{\boldsymbol{n}})\cdot e^{-i\omega_{\boldsymbol{n}}t}\;= \\ =\sum_{\boldsymbol{n}}\boldsymbol{A}(\omega_{\boldsymbol{n}})\cdot e^{i(\mathbf{k}_{\boldsymbol{n}}\cdot\boldsymbol{r}-\omega_{\boldsymbol{n}}t)} \qquad \textbf{(1.25)}$$

where the summation now is over all frequencies, both positive and negative.

Using a notation similar to that of **Eq. (1.25)**, we can express the nonlinear polarization as

$$\boldsymbol{P}(\boldsymbol{r},t)=\sum_{\boldsymbol{n}}\boldsymbol{P}(\omega_{\boldsymbol{n}})\cdot e^{-i\omega_{\boldsymbol{n}}t} \qquad \textbf{(1.26)}$$

where, as before, the summation extends over all positive- and negative-frequency components.

We now define the components of the second order susceptibility tensor $\chi^{(2)}_{ijk}(\omega_n+\omega_m,\ \omega_n,\ \omega_m)$ as the constants of proportionality relating the amplitude of the nonlinear polarization to the product of field amplitudes according to

$$P_i(\omega_n+\omega_m)=\sum_{jk}\sum_{(nm)}\chi^{(2)}_{ijk}(\omega_n+\omega_m,\omega_n,\omega_m)E_j(\omega_n)E_k(\omega_m) \qquad \textbf{(1.27)}$$

Here the indices *ijk* refer to the Cartesian components of the fields. The notation (*nm*) indicates that, in performing the summation over *n* and *m*, the sum $\omega_n+\omega_m$ is to be held fixed, although ω_n and ω_m are each allowed to vary. Since the amplitude $E(\omega_n)$ is associated with the time dependence $exp(-i\omega_n t)$, and the amplitude $E(\omega_m)$ is associated with the time dependence $exp(-i\omega_m t)$, their product $E(\omega_n)E(\omega_m)$ is associated with the time dependence $exp[-i(\omega_n+\omega_m)t]$. Hence the product $E(\omega_n)E(\omega_m)$ does in fact lead to a contribution to the nonlinear polarization oscillating at frequency $\omega_n+\omega_m$, as the notation of **Eq. (1.27)** suggests. Following convention, we have written $\chi^{(2)}$ as a function of three frequency arguments. This is technically unnecessary in that the first argument is always the sum of the other two. To emphasize this fact, the susceptibility $\chi^{(2)}(\omega_3,\omega_2,\omega_1)$ is sometimes written as $\chi^{(2)}(\omega_3;\omega_2,\omega_1)$ as a remainder that the first argument is different from the other two; or it may be written symbolically as $\chi^{(2)}(\omega_3=\omega_2+\omega_1)$.

Let us examine some of the consequences of the definition of the nonlinear susceptibility as given by **Eq. (1.27)** by considering two simple examples.

SFG

We let the input field frequencies be ω_1 and ω_2 and the sum to be ω_3, so that $\omega_3=\omega_2+\omega_1$. Then, by carrying out the summation over ω_n and ω_m in **Eq. (1.27)**, we find that

$$P_i(\omega_3)=\sum_{jk}\begin{bmatrix}\chi_{ijk}^{(2)}(\omega_3,\omega_1,\omega_2)E_j(\omega_1)E_k(\omega_2)+\\+\chi_{ijk}^{(2)}(\omega_3,\omega_2,\omega_1)E_j(\omega_2)E_k(\omega_1)\end{bmatrix} \tag{1.28}$$

This expression can be simplified by making use of the intrinsic permutation symmetry of the nonlinear susceptibility, which requires that

$$\chi_{ijk}^{(2)}(\omega_m+\omega_n,\omega_m,\omega_n)=\chi_{ikj}^{(2)}(\omega_m+\omega_n,\omega_n,\omega_m) \tag{1.29}$$

Through use of this relation, the expression for the nonlinear polarization becomes

$$P_i(\omega_3)=2\sum_{jk}\chi_{ijk}^{(2)}(\omega_3,\omega_1,\omega_2)E_j(\omega_1)E_k(\omega_2) \tag{1.30}$$

and for the special case in which both input fields are polarized in the x direction, the polarization becomes

$$P_i(\omega_3)=2\chi_{ixx}^{(2)}(\omega_3,\omega_1,\omega_2)E_x(\omega_1)E_x(\omega_2) \tag{1.31}$$

SHG

We take the input frequency as ω_1 and the generated frequency as $\omega_3 = 2\omega_1$. If we again perform the summation over field frequencies in **Eq. (1.27)**, we obtain

$$P_i(\omega_3)=\sum_{jk}\chi_{ijk}^{(2)}(\omega_3,\omega_1,\omega_1)E_j(\omega_1)E_k(\omega_1) \tag{1.32}$$

Again, assuming the special case of an input field polarized along the *x* direction, this result becomes

$$P_i(\omega_3) = \chi^{(2)}_{ixx}(\omega_3, \omega_1, \omega_1)E_x(\omega_1)^2 \qquad \textbf{(1.33)}$$

Note that a factor of two appears in **Eqs. (1.30)** and **(1.31)**, which describes SFG, but not in **Eqs. (1.32)** and **(1.33)**, which describe SHG. The fact that these expressions remain different even as ω_2 approaches ω_1 is at first sight surprising, but is a consequence of our convention that $\chi^{(2)}_{ijk}(\omega_3, \omega_1, \omega_2)$ must approach $\chi^{(2)}_{ijk}(\omega_3, \omega_1, \omega_1)$ as ω_1 approaches ω_2. Note that the expressions for $P(2\omega_1)$ and $P(\omega_1+\omega_2)$ that apply for the case of a dispersionless nonlinear susceptibility [**Eq. (1.11)**] also differ by a factor of two. Moreover, one should expect the nonlinear polarization produced by two distinct fields to be larger than that produced by a single field (all of the same amplitude), because the total light intensity is a larger in the former case.

In general, the summation over field frequencies ($\Sigma_{(nm)}$) in **Eq. (1.27)** can be performed formally to obtain the result

$$P_i(\omega_n + \omega_m) = D\sum_{jk} \chi^{(2)}_{ijk}(\omega_n + \omega_m, \omega_n, \omega_m)E_j(\omega_n)E_k(\omega_m) \qquad \textbf{(1.34)}$$

where D is known as the degeneracy factor and is equal to the number of distinct permutations of the applied field frequencies ω_n and ω_m.

The **Eq. (1.27)** defining the second order susceptibility can readily be generalized to higher order interactions. In particular, the components of the third order susceptibility are defined as the coefficients relating the amplitude of the nonlinear polarization to a product of three electric field amplitudes according to the expression

$$P_i(\omega_o + \omega_n + \omega_m) = \sum_{jkl}\sum_{(mno)} \chi^{(3)}_{ijkl}(\omega_o + \omega_n + \omega_m, \omega_o, \omega_n, \omega_m) \times E_j(\omega_o)E_k(\omega_n)E_l(\omega_m) \qquad \textbf{(1.35)}$$

We can again perform the summation over *m*, *n* and *o* to obtain the result

$$P_i(\omega_o+\omega_n+\omega_m) = D\sum_{jkl} \chi^{(3)}_{ijkl}(\omega_o+\omega_n+\omega_m,\omega_o,\omega_n,\omega_m) \times E_j(\omega_o)E_k(\omega_n)E_l(\omega_m) \qquad \textbf{(1.36)}$$

where the degeneracy factor D represents the number of distinct permutations of the frequencies ω_m, ω_n and ω_o.

1.3.1 Permutation Symmetry

In this section we study some of the formal symmetry properties of the nonlinear susceptibility. Let us first see why it is important that we understand these symmetry properties. We consider the mutual interaction of three waves of frequencies ω_1, ω_2 and $\omega_3 = \omega_1+\omega_2$. A complete description of the interaction of these waves requires that we know the nonlinear polarizations $P(\omega_i)$ influencing each of them. Since these quantities are given in general by the **Eq. (1.27)**, we therefore need to determine the six tensors

$\chi^{(2)}_{ijk}(\omega_1,\omega_3,-\omega_2)$, $\chi^{(2)}_{ijk}(\omega_1,-\omega_2,\omega_3)$, $\chi^{(2)}_{ijk}(\omega_2,\omega_3,-\omega_1)$

$\chi^{(2)}_{ijk}(\omega_2,-\omega_1,\omega_3)$, $\chi^{(2)}_{ijk}(\omega_3,\omega_1,\omega_2)$, $\chi^{(2)}_{ijk}(\omega_3,\omega_2,\omega_1)$

and six additional tensors in which each frequency is replaced by its negative. In these expressions, the indices i, j and k can independently take on the values x, y and z. Since each of these 12 tensors thus consists of 27 cartesian components, as many as 324 different (complex) numbers need to be specified in order to describe the interaction.

Fortunately, there are a number of restrictions resulting from symmetries that relate the various components of $\chi^{(2)}$ and hence far fewer that 324 numbers are usually needed in order to describe the nonlinear coupling. In this section, we shall study some of these formal properties of the nonlinear susceptibility. The discussion will deal primarily with the second order $\chi^{(2)}$ susceptibility, but can readily be extended to $\chi^{(3)}$ and higher order susceptibilities.

According to **Eq. (1.27)**, one of the contributions to the nonlinear polarization $P_i(\omega_n+\omega_m)$ is the product $\chi^{(2)}_{ijk}(\omega_n+\omega_m, \omega_n, \omega_m)E_j(\omega_n)E_k(\omega_m)$. However, since j, k, n and m are dummy indices, we could just as well have written this contribution with n interchanged with m and with j interchanged with k, that is, as $\chi^{(2)}_{ikj}(\omega_n+\omega_m, \omega_m, \omega_n)E_k(\omega_m)E_j(\omega_n)$. These two expressions are numerically equal if

we require that the nonlinear susceptibility be unchanged by the simultaneous interchange of its last two frequency arguments and its last two cartesian indices

$$\chi_{ijk}^{(2)}\left(\omega_n+\omega_m,\omega_n,\omega_m\right)=\chi_{ikj}^{(2)}\left(\omega_n+\omega_m,\omega_m,\omega_n\right) \qquad \textbf{(1.37)}$$

This property is known as intrinsic permutation symmetry. Note that this symmetry condition is introduced purely as a matter of convenience.

This symmetry condition can also be derived from a more general point of view using the concept of the nonlinear response function (**Butcher, 1965; Flytzanis 1975**)

1.3.2 Symmetries for Lossless Media

Two additional symmetries of the nonlinear susceptibility tensor occur for the case of a lossless medium.

The first of these conditions states that for a lossless medium all of the components of $\chi_{ijk}^{(2)}(\omega_n+\omega_m, \omega_n, \omega_m)$ are real. This result is obeyed for the classical anharmonic oscillator, as can be verified by evaluating the expression for $\chi^{(2)}$ in the limit in which all of the applied frequencies and their sums and differences are significantly different from the resonance frequency. The general proof that $\chi^{(2)}$ is real for a lossless medium is obtained by verifying that the quantum-mechanical expression for $\chi^{(2)}$ is also purely real in this limit.

The second of these new symmetries is *full* permutation symmetry. This condition states that *all* of the frequency arguments of the nonlinear susceptibility can be freely interchanged, as long as the corresponding cartesian indices are interchanged simultaneously. In permuting the frequency arguments, it must be recalled that the first argument is always the sum of the latter two, and thus the signs of the frequencies must be inverted when the first frequency is interchanged with either of the latter two. Full permutation symmetry implies, for instance, that

$$\chi_{ijk}^{(2)}\left(\omega_3=\omega_1+\omega_2\right)=\chi_{jki}^{(2)}\left(-\omega_1=\omega_2-\omega_3\right) \qquad \textbf{(1.38)}$$

However, according to the reality of the fields, the positive and negative frequency components of the susceptibility must be relates in the following way

$$\chi_{ijk}^{(2)}\left(-\omega_n-\omega_m,-\omega_n,-\omega_m\right)=\chi_{ikj}^{(2)}\left(\omega_n+\omega_m,\omega_m,\omega_n\right)^* \qquad \textbf{(1.39)}$$

According to **Eq. (1.39)** the right-hand side of **Eq. (1.38)** is equal to $\chi_{jki}^{(2)}(\omega_1 = -\omega_2+\omega_3)^*$. Which, due to the reality of $\chi^{(2)}$ for a lossless medium, is equal to $\chi_{jki}^{(2)}(\omega_1 = -\omega_2+\omega_3)$. We hence conclude that

$$\chi_{ijk}^{(2)}\left(\omega_3=\omega_1+\omega_2\right)=\chi_{jki}^{(2)}\left(\omega_1=-\omega_2+\omega_3\right) \qquad \textbf{(1.40)}$$

By an analogous procedure, one can show that

$$\chi_{ijk}^{(2)}\left(\omega_3=\omega_1+\omega_2\right)=\chi_{kij}^{(2)}\left(\omega_2=\omega_3-\omega_1\right) \qquad \textbf{(1.41)}$$

1.3.3 Kleinman's Symmetry

Quite often NLO interactions involve optical waves whose frequencies ω_i are much smaller that the lowest resonance frequency of the material system. Under these conditions, the nonlinear susceptibility is essentially independent of frequency.

Under conditions of *low-frequency excitation* the system responds essentially instantaneously to the applied field, and under such conditions the nonlinear polarization can be described in the time domain by the relation

$$P(t)=\chi^{(2)}E(t)^2 \qquad \textbf{(1.42)}$$

where $\chi^{(2)}$ can be taken to be a constant.

Since the medium is necessarily lossless whenever the applied field frequencies ω_i are very much smaller that the resonance frequency ω_o, the condition of full permutation symmetry **(1.38)** must be valid under these circumstances. This condition states that the indices can be permuted as long as the frequencies are permuted simultaneously and leads to the conclusion that

$$\begin{aligned}&\chi^{(2)}_{ijk}(\omega_3=\omega_1+\omega_2)=\chi^{(2)}_{jki}(\omega_1=-\omega_2+\omega_3)=\chi^{(2)}_{kij}(\omega_2=\omega_3-\omega_1)\\&=\chi^{(2)}_{ikj}(\omega_3=\omega_2+\omega_1)=\chi^{(2)}_{jik}(\omega_1=\omega_3-\omega_2)\\&=\chi^{(2)}_{kji}(\omega_2=-\omega_1+\omega_3)\end{aligned}\qquad\textbf{(1.43)}$$

However, under the present conditions $\chi^{(2)}$ does not actually depend on the frequencies and we can therefore permute the indices without permuting the frequencies, leading to the result

$$\begin{aligned}&\chi^{(2)}_{ijk}(\omega_3=\omega_1+\omega_2)=\chi^{(2)}_{jki}(\omega_3=\omega_1+\omega_2)=\chi^{(2)}_{kij}(\omega_3=\omega_1+\omega_2)\\&=\chi^{(2)}_{ikj}(\omega_3=\omega_1+\omega_2)=\chi^{(2)}_{jik}(\omega_3=\omega_1+\omega_2)\\&=\chi^{(2)}_{kji}(\omega_3=\omega_1+\omega_2)\end{aligned}\qquad\textbf{(1.44)}$$

This result is known as the *Kleinman* symmetry condition. (**Kleinman, 1962**)

1.3.4 Contracted Notation

We now introduce a notational device that is often used when the *Kleinman* symmetry condition is valid. We introduce the tensor

$$d_{ijk}=\frac{1}{2}\chi^{(2)}_{ijk}\qquad\textbf{(1.45)}$$

and for simplicity suppress the frequency arguments. The nonlinear polarization can then be written as

$$P_i(\omega_n+\omega_m)=\sum_{jk}\sum_{(nm)}2d_{ijk}E_j(\omega_n)E_k(\omega_m)\qquad\textbf{(1.46)}$$

We now assume that d_{ijk} is symmetric in its last two indices. This assumption is valid whenever *Kleinman*'s symmetry condition is valid and in addition is valid in general for SHG, since in this case ω_n and ω_m are equal. We then simplify the notation by introducing a contracted matrix d_{il} according to the prescription

jk:	**11**	**22**	**33**	**23,32**	**31,13**	**12,21**
l:	**1**	**2**	**3**	**4**	**5**	**6**

(1.47)

The nonlinear susceptibility tensor can then be represented as the 3×6 matrix

$$d_{il} = \begin{bmatrix} d_{11} & d_{12} & d_{13} & d_{14} & d_{15} & d_{16} \\ d_{21} & d_{22} & d_{23} & d_{24} & d_{25} & d_{26} \\ d_{31} & d_{32} & d_{33} & d_{34} & d_{35} & d_{36} \end{bmatrix} \tag{1.48}$$

If we now explicitly introduce the *Kleinman* symmetry condition, i.e., that the indices d_{ijk} can be freely permuted, we find that not all of the 18 elements of d_{il} are independent. For instance, we see that

$$d_{12} = d_{122} = d_{212} = d_{26} \tag{1.49}$$

and that

$$d_{14} = d_{123} = d_{213} = d_{25} \tag{1.50}$$

By applying this type of argument systematically, we find that d_{il} has only 10 independent elements when the *Kleinman* symmetry condition is valid; the form of d_{il} under these conditions is

$$d_{il} = \begin{bmatrix} d_{11} & d_{12} & d_{13} & d_{14} & d_{15} & d_{16} \\ d_{16} & d_{22} & d_{23} & d_{24} & d_{14} & d_{12} \\ d_{15} & d_{24} & d_{33} & d_{23} & d_{13} & d_{14} \end{bmatrix} \tag{1.51}$$

We can describe the nonlinear polarization leading to SHG in terms of d_{il} by the matrix equation

$$\begin{bmatrix} P_x(2\omega) \\ P_y(2\omega) \\ P_z(2\omega) \end{bmatrix} = 2 \begin{bmatrix} d_{11} & d_{12} & d_{13} & d_{14} & d_{15} & d_{16} \\ d_{21} & d_{22} & d_{23} & d_{24} & d_{25} & d_{26} \\ d_{31} & d_{32} & d_{33} & d_{34} & d_{35} & d_{36} \end{bmatrix} \begin{bmatrix} E_x(\omega)^2 \\ E_y(\omega)^2 \\ E_z(\omega)^2 \\ 2E_y(\omega)E_z(\omega) \\ 2E_x(\omega)E_z(\omega) \\ 2E_x(\omega)E_y(\omega) \end{bmatrix} \qquad \textbf{(1.52)}$$

When the *Kleinman* symmetry condition is valid, we can describe the nonlinear polarization leading to SFG (with $\omega_3 = \omega_1 + \omega_2$) by the equation

$$\begin{bmatrix} P_x(\omega_3) \\ P_y(\omega_3) \\ P_z(\omega_3) \end{bmatrix} = 4 \begin{bmatrix} d_{11} & d_{12} & d_{13} & d_{14} & d_{15} & d_{16} \\ d_{21} & d_{22} & d_{23} & d_{24} & d_{25} & d_{26} \\ d_{31} & d_{32} & d_{33} & d_{34} & d_{35} & d_{36} \end{bmatrix} \times \begin{bmatrix} E_x(\omega_1)E_x(\omega_2) \\ E_y(\omega_1)E_y(\omega_2) \\ E_z(\omega_1)E_z(\omega_2) \\ E_y(\omega_1)E_z(\omega_2) + E_z(\omega_1)E_y(\omega_2) \\ E_x(\omega_1)E_z(\omega_2) + E_z(\omega_1)E_x(\omega_2) \\ E_x(\omega_1)E_y(\omega_2) + E_y(\omega_2)E_x(\omega_1) \end{bmatrix} \qquad \textbf{(1.53)}$$

As described above in the relation to **Eq. (1.33)**, the extra factor 2 comes from the summation over *n* and *m* in **Eq. (1.27)**.

1.4 On the Physical Origins of the Nonlinear Optical Coefficients

The anharmonic oscillator model assumes that the electronic response to a driving electric field can be simulated by that of an electron in an anharmonic potential well. The equation of motion for the electron is then

$$\ddot{X} + \gamma \dot{X} + \omega_o^2 X + DX^2 = \frac{eE_o}{2m}\left(e^{i\omega t} + e^{-i\omega t}\right) \qquad \textbf{(1.54)}$$

where X is the deviation from the potential minimum, mDX^2 is the anharmonic restoring force [corresponding to the term $(m/3)DX^3$ in the potential], the driving electric field is $E_o cos\omega t$ and γ is the damping term. Since we are looking for the polarization at 2ω, we assume a solution in the form

$$X = \frac{1}{2}\left(q_1 e^{i\omega t} + q_2 e^{2i\omega t} + c.c.\right) \tag{1.55}$$

which, when substituted into **Eq. (1.54)**, yields

$$\begin{aligned}
&-\frac{\omega^2}{2}\left(q_1 e^{i\omega t} + c.c.\right) - 2\omega^2\left(q_2 e^{2i\omega t} + c.c.\right) + \frac{i\omega\gamma}{2}\left(q_1 e^{i\omega t} - c.c.\right) + \\
&+ i\omega\gamma\left(q_2 e^{2i\omega t} - c.c.\right) + \frac{\omega_o^2}{2}\left(q_1 e^{i\omega t} + q_2 e^{2i\omega t} + c.c.\right) + \\
&+ \frac{D}{4}\begin{pmatrix} q_1^2 e^{2i\omega t} + q_2^2 e^{4i\omega t} + q_1 q_1^* + 2q_1 q_2 e^{3i\omega t} + \\ + 2q_1 q_2^* e^{-i\omega t} + q_2 q_2^* + c.c. \end{pmatrix} = \\
&= \frac{eE_o}{2m}\left(e^{i\omega t} + c.c.\right)
\end{aligned} \tag{1.56}$$

By equating the coefficient of $e^{i\omega t}$ on both sides of **Eq. (1.56)** and assuming that $|Dq_2| << [(\omega_o^2 - \omega^2)^2 + \omega^2\gamma^2]^{1/2}$, we obtain

$$q_1 = \left(\frac{eE_o}{m}\right)\frac{1}{\left(\omega_o^2 - \omega^2\right) + i\omega\gamma} \tag{1.57}$$

The linear susceptibility $\chi_L^{(\omega)}$ is defined by

$$P^{(\omega)}(t) = \frac{\varepsilon_o}{2}\left(\chi_L^{(\omega)} E_o e^{i\omega t} + c.c.\right) = \frac{Ne}{2}\left(q_1 e^{i\omega t} + c.c.\right) \tag{1.58}$$

where N is the number of electrons per unit volume that contribute to P. It follows that

$$\chi_L^{\omega} = \frac{Ne^2}{m\varepsilon_o\left[\left(\omega_o^2 - \omega^2\right) + i\omega\gamma\right]} \tag{1.59}$$

In a similar manner, we proceed to solve for q_2. Equating the multipliers of $e^{2i\omega t}$ on both sides of **Eq. (1.56)** leads to

$$q_2\left(-4\omega^2 + 2i\omega\gamma + \omega_o^2\right) = -\frac{1}{2}Dq_1^2 \tag{1.60}$$

that after we use **Eq. (1.57)**, becomes

$$q_2 = \frac{-De^2E_o^2}{2m^2\left[\left(\omega_o^2 - \omega^2\right) + i\omega\gamma\right]^2\left(\omega_o^2 - 4\omega^2 + 2i\omega\gamma\right)} \tag{1.61}$$

Defining the nonlinear susceptibility $d^{(2\omega)}_{NL}$ by

$$P^{(2\omega)}(t) = \frac{1}{2}Ne\left(q_2e^{2i\omega t} + c.c.\right) = \frac{1}{2}\left[d_{NL}^{(2\omega)}E_o^{2i\omega t} + c.c.\right] \tag{1.62}$$

we obtain

$$d_{NL}^{(2\omega)} = \frac{-DNe^3}{2m^2\left[\left(\omega_o^2 - \omega^2\right) + i\omega\gamma\right]^2\left[\left(\omega_o^2 - 4\omega^2\right) + 2i\omega\gamma\right]} \tag{1.63}$$

or, using **Eq. (1.59)**,

$$d_{NL}^{(2\omega)} = \frac{mD\left(\chi_L^{\omega}\right)^2\chi_L^{2\omega}\varepsilon_o^3}{2N^2\left|e^3\right|} \tag{1.64}$$

which is the desired result. If we define a parameter $\delta^{(2\omega)}$ by

$$\delta^{(2\omega)} = \frac{d_{NL}^{(2\omega)}}{\left(\chi_L^{\omega}\right)^2 \chi_L^{2\omega} \varepsilon_o^3} \qquad \textbf{(1.65)}$$

this parameter has a value

$$\delta^{(2\omega)} = \frac{mD}{2\left|e^3\right|N^2} \qquad \textbf{(1.66)}$$

This result was first given by **Garret and Robinson** (**1961**). **Miller** (**1964**) has observed that the three-dimensional analogue of δ, which is defined by

$$\delta_{ijk} = \frac{d_{ijk}^{(2\omega)}}{\chi_{ii}^{2\omega} \chi_{jj}^{\omega} \chi_{kk}^{\omega} \varepsilon_o^3} \qquad \textbf{(1.67)}$$

is remarkably constant ($\delta_{mean} \sim 2\times10^9$) over a large variety of crystals.

The observed constancy of δ, when examined in light of **Eq. (1.66)**, suggests that the nonlinear term D is nearly a constant in various materials and that the large variation in the observed values of d_{ijk} reflect the dependence of the latter on the linear susceptibilities. A more sophisticated approach to the derivation of the NLO constants is via a quantum mechanical formalism. Such a treatment, at this point, will constitute a considerable diversion and can be found elsewhere. (**Yariv, 1975**)

Chapter 2

Second Order NLO Properties of Non-Crystalline Media

Over the past years the NLO properties of organic and hybrid materials have gained an increasing interest for both applied physics and optical engineering. The reason of this arises from the possible use of such materials for photonic and telecommunication devices. In principle ***, organic*** *and* ***hybrid*** *optoelectronics can supersede the traditional* ***inorganic*** *optoelectronics in communication technology, with low cost.*

Optoelectronics revolution, based on the replacement of electron transport by conduction and manipulation of light pulses, has allowed a growth of telecommunications with the increasing of data transfer rate and signal-to-noise ratio together with miniaturization of devices. This technology is based, in particular, on the use of second order NLO phenomena for electrooptical modulation. To date, such modulators are based on expensive inorganic crystals ($LiNbO_3$ or similar). Moreover they have poor optical quality and posses only marginal NLO activity.

The alternative approach to overcome difficulties related to production of large monocrystals is the use of organic molecules with high second order NLO activity, dispersed in or covalently bonded to inert polymeric or glassy matrix. Organic and hybrid materials allow, generally speaking, a great flexibility in synthesis and have physical properties that can be tailored for specific applications. A fundamental advantage in electrooptic applications of organic materials is their low value of refractive index with respect to $LiNbO_3$. This means that optical and electrical waves can propagate with similar velocities in such materials allowing longer interaction length. Bandwidth up to 150 GHz has been obtained for polymeric integrated devices. The advantage of easy fabrication and low-cost of such materials is however connected to some drawbacks: first, the need of active molecules orientation to achieve an overall noncentrosymmetric system, mandatory for attaining large electrooptic coefficient; second, a high time stability of the macroscopic NLO properties necessary for the fabrication of practical devices. The former can be achieved by means of the so called ***poling techniques****, while the latter needs a careful control of the physical and chemical properties of host matrix. (****Sarcinelli and Casalboni, 2003****)*

In this Chapter the applications of the NLO phenomena are described, paying particular attention to electrooptic modulators (EOM). Systems identified as promising second order materials are showed, together with the poling techniques used to obtain non-centrosymmetric media.

2.1 Pockels and Kerr Effect

The refractive index of an electrooptic medium is a function $n(E)$ of the applied electric field E. This function varies only slightly with E so that it can be expanded in a Taylor's series about $E = 0$

$$n(E) = n + a_1 E + \frac{1}{2} a_2 E^2 + \ldots \qquad \textbf{(2.1)}$$

where the coefficients of expansion are $n = n(0)$, $a_1 = (dn/dE)|_{E=0}$, and $a_2 = (d^2n/dE^2)|_{E=0}$. For reasons that will become apparent subsequently, it is conventional to write **Eq. (2.1)** in terms of two new coefficients $r = -2a_1/n^3$ and $\xi = -a_2/n^3$, known as the electrooptic coefficients, so that

$$n(E) = n - \frac{1}{2} r n^3 E - \frac{1}{2} \xi n^3 E^2 + \ldots \qquad \textbf{(2.2)}$$

Pockels Effect

In many materials the third term of **Eq. (2.2)** is negligible in comparison with the second, whereupon

$$n(E) \approx n - \frac{1}{2} r n^3 E \qquad \textbf{(2.3)}$$

The medium is then known as a *Pockels medium* (or a *Pockels cell*). The coefficient r is called also as the *Pockels coefficient*. Typical values of r lie in the range 1 to 100 pm/V. For $E = 10^6$ V/m (10 kV applied across a cell of thickness 1 cm), for example, the term $1/2rn^3E$ in **Eq. (2.3)** is on the order of 10^{-6} to 10^{-4}. Changes in the refractive index induced by electric fields are indeed very small. The most common crystals used as Pockels cells include $NH_4H_2PO_4$ (ADP), KH_2PO_4, $LiNbO_3$, $LiTaO_3$ and CdTe.

Kerr Effect

If the material is centrosymmetric, as is the case for gases, liquids and certain crystals, *n(E)* must be an even symmetric function since it must be invariant to the reversal of *E*. Its first derivative then vanishes, so that the coefficient *r* must be zero, whereupon

$$n(E) \approx n - \frac{1}{2}\xi n^3 E^2 \qquad \textbf{(2.4)}$$

The material is then known as a *Kerr medium* (or a *Kerr cell*). The parameter ξ is called the *Kerr coefficient* or the quadratic electrooptic coefficient. Typical values of ξ are 10^{-18} to 10^{-14} m^2/V^2 in crystals and 10^{-22} to 10^{-19} m^2/V^2 in liquids. For $E = 10^6$ V/m the term $1/2\xi n^3 E^2$ in **Eq. (2.4)** is on the order of 10^{-6} to 10^{-2} in crystals and 10^{-10} to 10^{-7} in liquids.

2.2 Electrooptic Modulators

EOM's are key devices in telecommunication and information systems. They encode signals on the light beams to carry data along optical fibers. EOM's are essentially based on the second order nonlinearity of some materials.

A class of materials, intrinsically lacking of the center of symmetry, necessary feature for second order nonlinearity, is represented by noncentrosymmetric crystals. Lithium Niobate ($LiNbO_3$) is the most exploited electrooptic material. In the last years a lot of effort have been done to improve overall performance, especially with regards to the transmission speed and bandwidth, but intrinsic limitations exist, due to high value of the refractive index of $LiNbO_3$. This produces a mismatch between optical and electrical signals that travel in the material with different speed.

At present, in front of the need for new and faster devices able to send large amount of information at high bit rates, the well established technology of $LiNbO_3$ modulators seems to have reached their performance plateau and low-cost polymer or glassy-based modulators can be envisaged as suitable alternatives. (**Lee, 2002**)

Phase Modulators

When a beam of light traverses a Pockels cell of length L to which an electric field E is applied, it undergoes a phase shift $\varphi = n(E)k_oL = 2\pi n(E)L/\lambda_o$, where λ_o is the free-space wavelength. Using **Eq. (2.3)**, we have

$$\varphi \approx \varphi_o - \pi \frac{rn^3 EL}{\lambda_o} \qquad \textbf{(2.5)}$$

where $\varphi_o = 2\pi nL/\lambda_o$. If the electric field is obtained by applying a voltage V across to faces of the cell separated by distance d, then $E = V/d$ and **Eq. (2.5)** gives

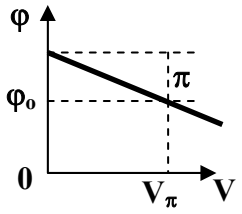

$$\varphi = \varphi_o - \pi \frac{V}{V_\pi} \qquad \textbf{(2.6)}$$

where

$$V_\pi = \frac{d}{L}\frac{\lambda_o}{rn^3} \qquad \textbf{(2.7)}$$

The parameter V_π, known as the half-wave voltage, is the applied voltage at which the phase shift changes by π. One can therefore modulate the phase of an optical wave by varying the voltage V that is applied across a material through which the light passes. The parameter V_π is an important characteristic of the modulator. It depends on the material properties (n and r), on the wavelength λ_o and on the aspect ratio d/L.

The electric field may be applied in a direction perpendicular to the direction of light propagation (*transverse modulator*) or parallel to that direction (*longitudinal modulator*), in which case $d = L$ (**Fig. 2.1**). Typical values of V_π are in the vicinity of 1 to a few kV for longitudinal modulators and hundred of Volts for transverse modulators.

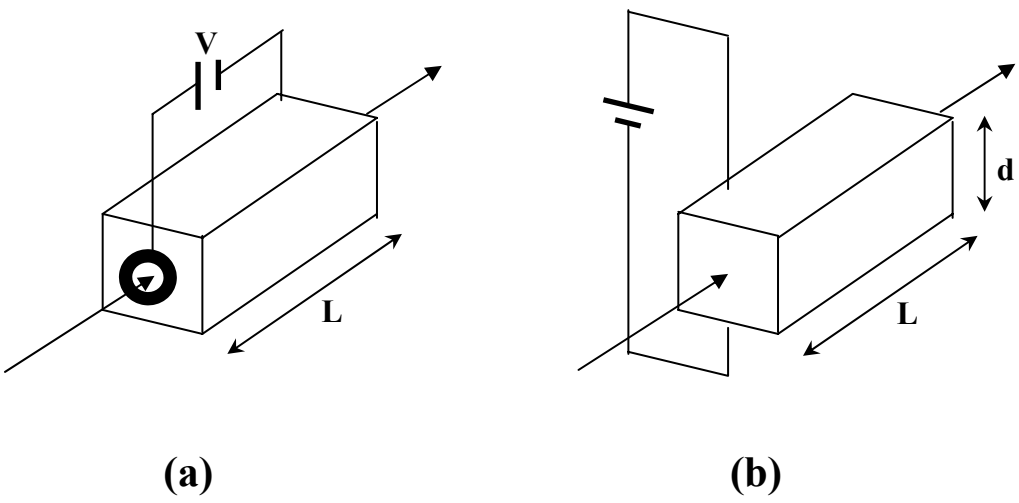

Fig. 2.1 (a) Longitudinal modulator. The electrodes may take the shape of washers or bands or may be transparent conductors. **(b)** Transverse modulator

Intensity Modulators

Phase delay (or retardation) alone does not affect the intensity of a light beam. However, a phase modulator placed in one branch of an interferometer can function as an intensity modulator. Consider, for example, the *Mach-Zehnder interferometer* illustrated in **Fig. 2.2**. If the beamsplitters divide the optical power equally, the transmitted intensity I_0 is related to the incident intensity I_i by

$$I_o = \frac{1}{2} I_i + \frac{1}{2} I_i \cos\varphi = I_i \cos^2 \frac{\varphi}{2} \qquad \textbf{(2.8)}$$

where $\varphi = \varphi_1 - \varphi_2$ is the difference between the phase shifts encountered by light as it travels through the two branches. The transmittance of the interferometer is $T = I_0/I_i = \cos^2(\varphi/2)$.

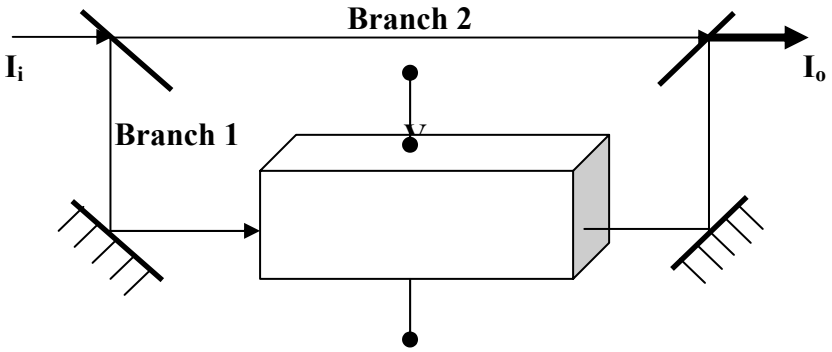

Fig.2.2 A phase modulator placed in one branch of a *Mach-Zehnder* interferometer can serve as an intensity modulator

Because of the presence of the phase modulator in branch 1, according to **Eq. 2.6** we have $\varphi_1 = \varphi_{10} - \pi V/V_\pi$, so that φ is controlled by the applied voltage V in accordance with the linear relation $\varphi = \varphi_1 - \varphi_2$ depends on the optical path difference. The transmittance of the device is therefore a function of the applied voltage V

$$T(V) = \cos^2\left(\frac{\varphi_o}{2} - \frac{\pi}{2}\frac{V}{V_\pi}\right) \qquad \textbf{(2.9)}$$

A *Mach-Zehnder* intensity modulator may also be constructed in the form of an integrated-optical device. Waveguides are placed on a substrate in the geometry shown in **Fig. 2.3**. The beamsplitters are implemented by the use of waveguide *Y*'s. The optical input and output may be carried by optical fibers. (**Saleh and Teich, 1991**)

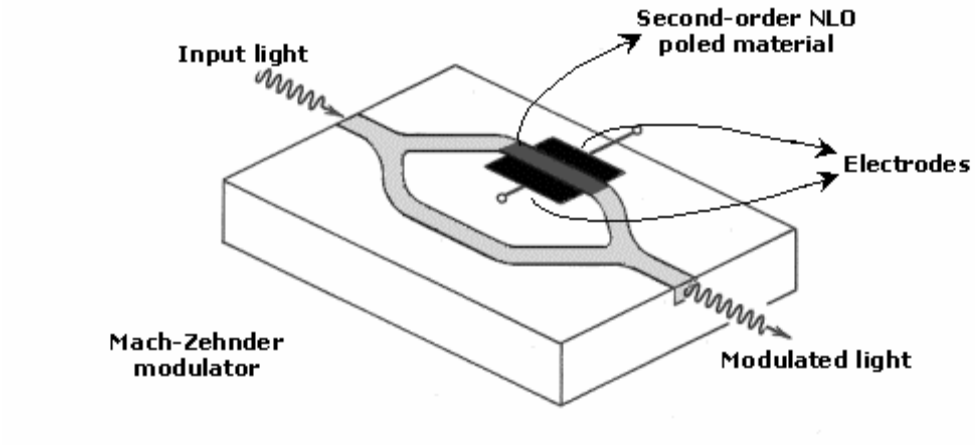

Fig. 2.3 An integrated-optical intensity modulator (or *optical switch*).

Today the best $LiNbO_3$ modulators operate at 40 Gb/s with a bandwidth of 30-35 GHz (**Wong, 2002**)

Existing technologies show various limitations. Dielectric constant of materials are quite high, as it is the case of $LiNbO_3$. Dispersion of the dielectric constant from microwave to optical frequency makes harder to fulfil the need of velocity matching between RF and optical signal. The necessity of achieving, in spite of the above stated limitations, velocity and impedance matching, requires the use of low dielectric constant thick buffer layer, which, laid as it is between electrodes and substrates, reduces electrooptic efficiency of the device as a whole.

For both modulators type, high production costs due to vacuum based deposition and crystal growth techniques such as *MBE* or *MOCVD* constitutes a severe limitation. Growth and patterning of $LiNbO_3$ devices also involves expensive and time consuming methods.

An alternative approach consists in the using of polymeric and hybrid modulator materials: single molecules, endowed with very high second order nonlinearity embedded in a inert matrix. The need of macroscopic effect is reached with a post-synthesis alignment procedure. This strategy allows to decouple the two well distinct problems: on one side the necessity of high optical quality matrix suitable for low cost processing and waveguide fabrication; on the other side, the synthesis of high hyperpolarizability active molecules.

2.2 Chromophore Design

An applied electric field (0-120 GHz) perturbs the electron distribution of a material affecting the transit of light through the material. The result is an electric field dependent change in the index of refraction of the material with the subsequent phase shift of light passing through the material.

For a significant perturbation of light (e.g., a phase shift of one-half a wavelength, π) to be realized with the application of small applied voltages, the electrons of the material must be weakly confined by the nuclei (i.e., the electrons must be highly polarizable). For organic materials, π-electrons are much less tightly bound by nuclei than σ-electrons as is easily understood from considering their relative positioning with respect to the nuclei. Thus, more than 2 decades ago, π-electron organic materials were identified as promising candidates for NLO applications.

Organic molecules that exhibit second order NLO properties usually consist of a frame with a delocalized π-system, end-capped with either an electron donor and acceptor substituent as shown in **Figs. 2.4-2.5-2.6**. This asymmetry results in a high degree of intramolecular charge-transfer (ICT) interaction from the donor to acceptor, which seems to be a prerequisite for a large second order nonlinearity. (**Oudar, 1977**)

The nonlinear part of the induced molecular polarization is the result of the polarizability of the π-electron system. Because of the low mass of the electrons compared to that of ions in inorganic crystals, organic molecules can respond to the electromagnetic fields with much higher frequencies (up to 10^{14} Hz). (**Möhlmann, 1987**) This faster optical response is particularly interesting for applications that depend on the speed of information processing, such as optical switching.

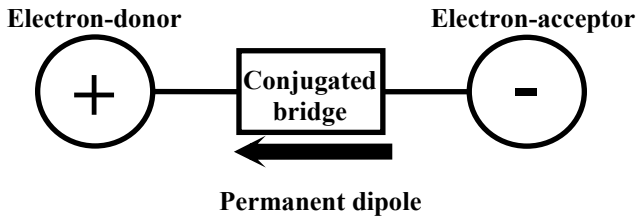

Fig. 2.4 Sketch of a *push-pull* charge transfer molecule

Organic chemists have been very successful in producing ever-improved chromophores, with different polar symmetry, as can be seen from a consideration of **Fig. 2.6**, from which *p*-nitroaniline (***p*NA**) is prototypical example and 4,4'-aminonitroazobenzene (**DR1**) is the most used reference in tests and comparisons (**Fig. 2.5**).

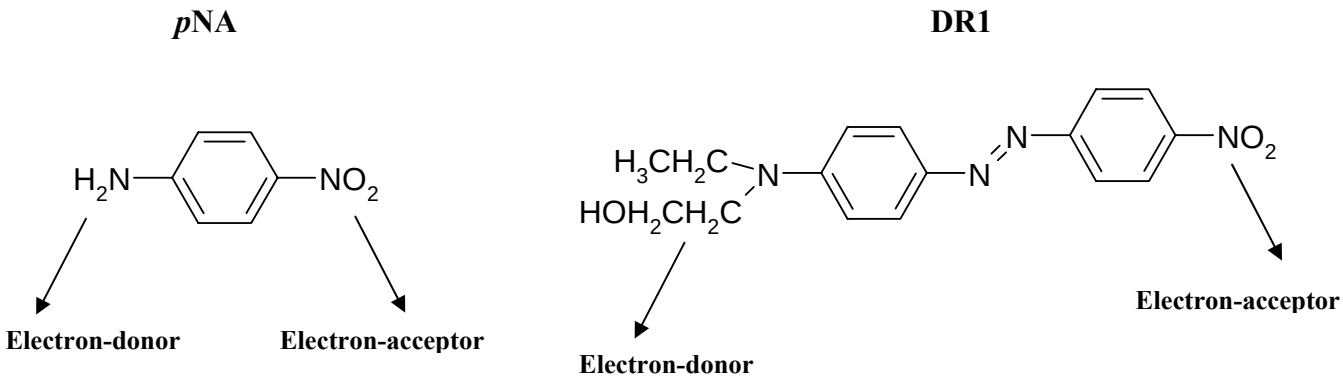

Fig.2.5 Prototypical examples of NLO molecules

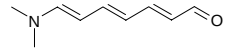 **POLYENES**	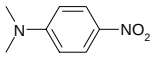 **AROMATIC MOLECULES**	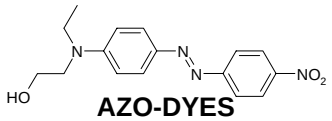 **AZO-DYES**
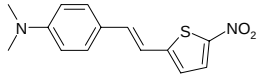 **HETEROCYCLIC DYES**	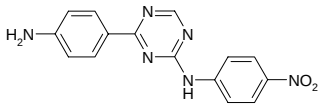 **TRIAZINE DERIVATIVES**	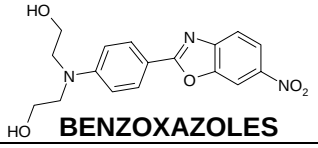 **BENZOXAZOLES**
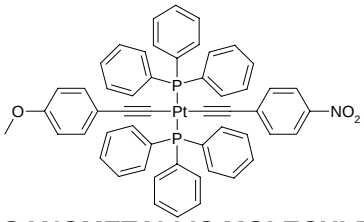 **ORGANOMETALLIC MOLECULES**	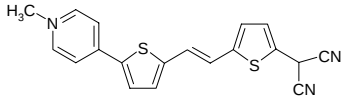 **ZWITTERIONIC MOLECULES**	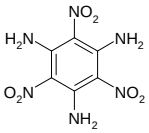 **OCTUPOLAR MOLECULES**
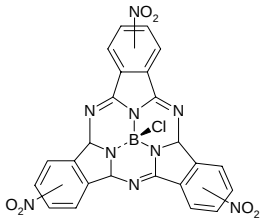 **CYANINES**	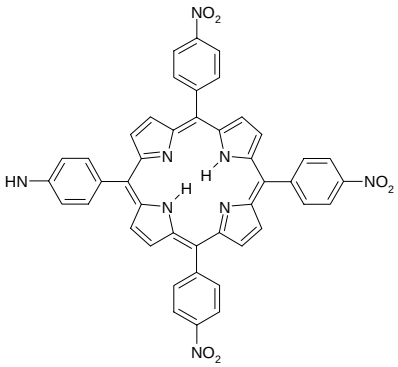 **PORPHIRINS**	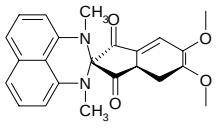 **SPYROCONJUGATED DYES**
 **CARBORANES**	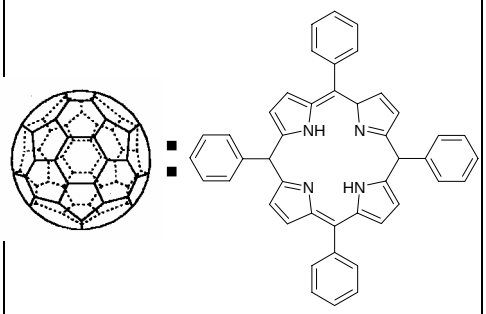 **FULLERENE DERIVATIVES**	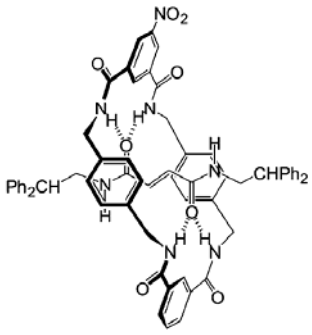 **ROTAXANES**

Fig. 2.6 Some of the classes of second order NLO organic molecules.

NLO materials owe their bulk nonlinearity to the optical nonlinearity of their constituents. Thus, bulk properties can be thought of as being built up from the corresponding properties of individual molecules. By direct analogy of **Eq. (1.2)**, the component in the *i-th* molecule fixed-coordinate direction of the electric field induced dipole moment for an isolate molecule can be written:

$$p_i(\omega) = \alpha_{ij}(\omega)E_j(\omega) + \beta_{ijk}(-\omega;\omega_1,\omega_2)E_j(\omega_1)E_k(\omega_2) + \\ + \gamma_{ijkl}(-\omega;\omega'_1,\omega'_2,\omega_3')E_j(\omega'_1)E_k(\omega'_2)E_l(\omega'_3) \qquad \textbf{(2.10)}$$

where $\alpha_{ij}(\omega)$ is the linear molecular polarizability and $\beta_{ijk}(-\omega;\omega 1,\ \omega 2)$ and $\gamma_{ijkl}(-\omega;\omega_1',\omega_2',\omega_3')$ are the *frequency-dependent* first and second hyperpolarizabilities, respectively. Here *Ej* is the local field at the site of the molecule and is, in general, different with respect to the external field **E**. For the case of SHG, one obtains

$$p_i^{(2)}(2\omega) = \frac{1}{2}\beta_{ijj}(-2\omega;\omega,\omega)E_j(\omega)^2 \qquad \textbf{(2.11)}$$

Quantum mechanical calculations, including two state calculations (**Williams, 1984**) predict that, far from the absorption edge ($\omega << \frac{E_{ge}}{\hbar}$), β is given by

$$\beta = \frac{(\mu_{ee} - \mu_{gg})(\mu_{ge})^2}{(E_{ge})^2} \qquad \textbf{(2.12)}$$

where μ_{ee}-μ_{gg} is the difference between excited and ground-state dipole moments, μ_{ge} is the transition dipole moment and E_{ge} is the optical (HOMO-LUMO) gap. In this so-called two-level model, the hyperpolarizability is assumed to be only the result of an excitation from the ground to the first excited state, which is usually, in the case of DπA-molecules, the charge-transfer excitation. Although β is a figure of merit of second order NLO molecules, it has to be noted an intrinsic difficulty in determining it experimentally. β can be measured by techniques such as Electric Field Induced SH (EFISH) and Hyper-Rayleigh Scattering (HRS). However EFISH measures $\mu\beta$ rather than β and caution must be exercised with HRS as two-photon effects can lead to artificially high

values of β. Results of HRS and EFISH measurements are given in **Table 2.1**, for a representative high $\mu\beta$ chromophores.

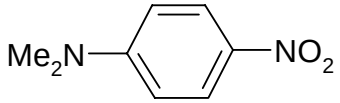	80
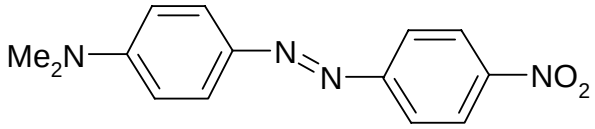	580
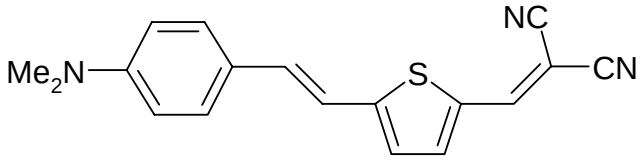	1300
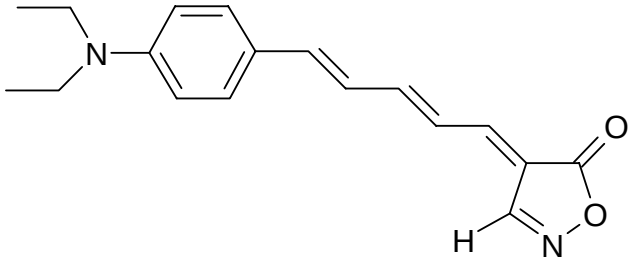	4000
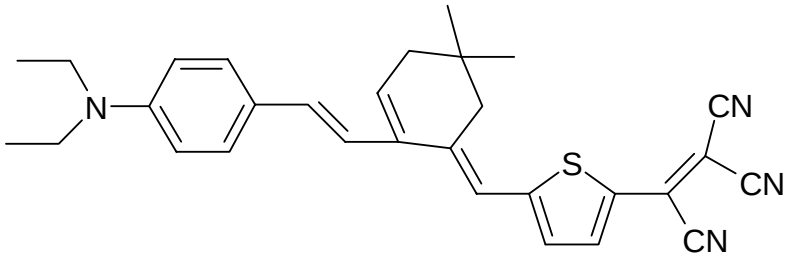	13000
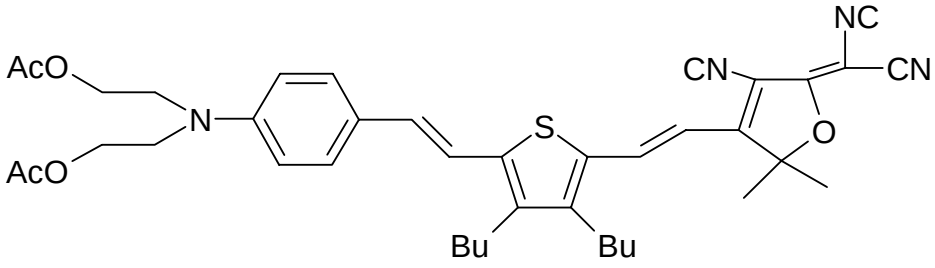	18000

Table 2.1 Representative electrooptic chromophores with $\mu\beta$ values (x10^{-48} esu, @ 1,9 μm,) obtained by EFISH (**Dalton, 1999**)

Starting from a certain "base molecule" second order nonlinearity can be enhanced by using a proper choice of donor and acceptor substituents to tune the electronic asymmetry or by changing the conjugation length between the substituents. **Dulcic** and **Sauteret** (1978) were the first to study the substituent effect in p-disubstituted benzene derivatives and **Oudar** and **LePerson** (1975) reported about the effect of the conjugation length by using a stilbene instead of a benzene π-system. Since then, many systematic studies have been performed on the structure-property relationship of NLO chromophores. Compounds with conjugating bridges such as tolans, diazo-stilbenes, polyenes, polyphenylenes and with bridges containing heteroaromatic 5- or 6-membered rings such as thiophenes and (thi)azoles have been investigated. From all these investigations, some general features can be summarized:

1) the NLO effect increases with chain length; e.g., β of polyenes increases with a quadratic to cubic dependency on the number of double bonds (n), levelling off at a value of n = 10. (**Morley, 1987**)

2) a trade-off exists between nonlinearity and transparency: an increase in β is accompanied by a red shift in the absorption spectrum due to a larger conjugation length and/or stronger donor and acceptor substituents.

3) instead of optimizing β, it is more efficient to optimize the hyperpolarizability density ρ ($\rho = \beta$/molecular volume) which has been shown to level off at a certain maximum when lengthening the conjugation. (**Morley, 1989**)

4) β is strongly correlated to the Bond Length Alternation (*BLA*) and Bond Order Alternation (*BOA*) which are parameters related to the molecular structure. The *BLA* is usually defined as the difference between the average single and double bond distances in the conjugated pathway. In the case of DπA-systems, the value of *BLA* can be tuned by D/A strength. On the other hand, in real materials (i.e., condensed phases), the *BLA* parameter and the NLO properties are controlled by intermolecular interactions effects. The relationships between molecular structure (*BLA* and/or *BOA*) and nonlinear polarizability for several DπA-molecules are relatively well investigated. β exhibit minima and maxima as a function of *BOA* (**Fig. 2.7**). (**Bartkowiak, 2003**)

Of course, other requirements such as low optical absorption at operating wavelengths (e.g., 980, 1300 and 1550 nm) and stability (thermal, chemical and photochemical) must be satisfied by a chromophore before it can be considered as promising for electrooptic applications.

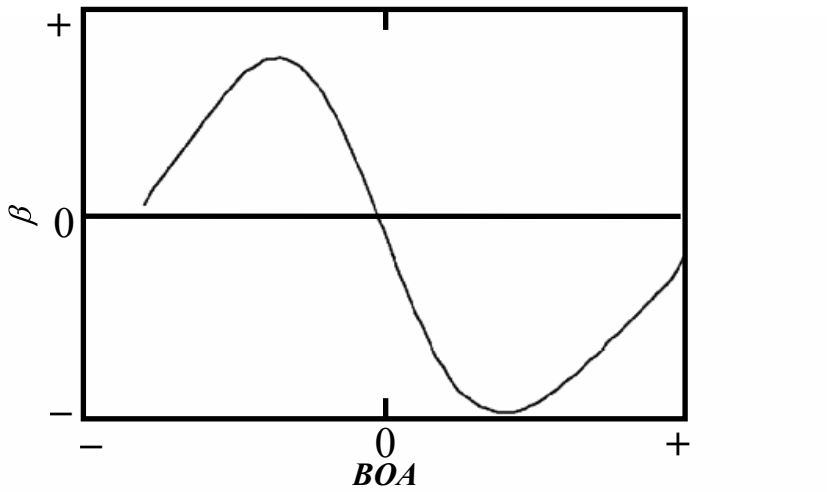

Fig. 2.7 Dependence of β on *BOA* (**Marder, 1991**)

2.4 Polymeric Systems

Our daily life can be scarcely envisaged without polymers, as nearly all the products that we use contain polymers in some form. Approximately forty years ago polymers were exclusively used as textile fibers, films, coatings and inexpensive disposable plastics. Today we have a large variety of high technology applications for polymers and **Table 2.2** will summarize shortly high technology polymers together with their main fields of applications. (**Bauer, 1996**)

In order to incorporate the molecular dipoles into the polymer matrix, a variety of different molecular design approaches has been identified by polymer chemists (**Fig. 2.8**).

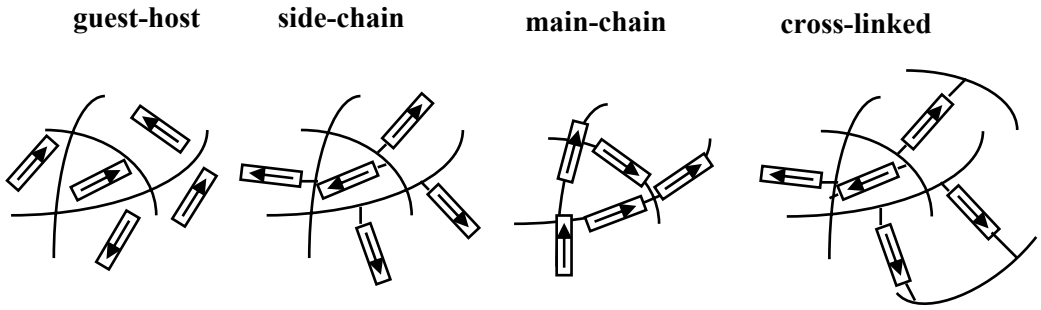

Fig. 2.8 Schematic representation of different ways of making functionalized polymers for second order NLO applications.

In *guest/host* systems the NLO dipoles are simply dissolved in the host polymer, in *side-chain* polymers they are chemically bonded to the backbone polymer via flexible spacers and in *main-chain* polymers the dipoles are part of the main polymers chain. In addition, various *cross-linkable* polymers have been synthesized in which the thermal stability of the oriented dipoles is hoped to be increased by chemical cross-linking during electric-field poling. (**Burland, 1994**)

The initially reported polymethylmethacrylate (**Fig. 2.9 (a))** based guest-host showed insufficient nonlinearities and thermal stability of the dipole orientation (**Singer, 1986**), in the meantime polyimide (**Fig. 2.9 (b))** based guest-host polymers systems (**Ermer, 1992**) with a remarkable thermal stability of the dipole orientation have been identified.

(a)

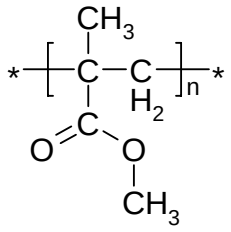

(b)

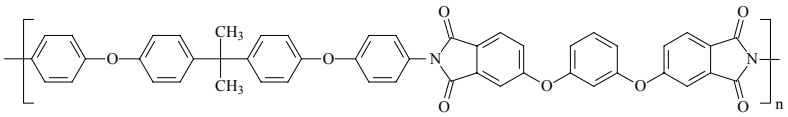

Fig.2.9 Chemical structure of the amorphous PMMA **(a)** and Polyimide **(b)**

However, the amount of dipoles that can be incorporated into the polymer matrix is restricted because of the limited solubility of the dye dipoles in the polymer matrix. Side-chain polymers seem to be very attractive, as they usually exhibit good thermal stabilities together with large nonlinearities. (**Matsumoto, 1987**) In main-chain polymers, the orientation of dipoles is difficult, as whole main-chain segments must rotate. In cross-linking polymers (**Liang, 1994**), at least one additional process step is required. Today it is still not clear which of the different approaches is best suited to fulfil all the simultaneously required demands of low absorption and scattering, strong nonlinearities and good thermal stability of the oriented chromophores as dictated by the applications.

High technology polymers	*Area(s) of application*
Photoresists	lithography
Dielectric polymers	Packaging, high voltage insulation
Conductive polymers	Batteries
Photoconductive polymers	Laser printing
Piezo- and pyroelectric polymers	Sensors and actuators, electro-acoustic, thermal imaging
Optical polymers	Fibers, lenses, passive and thermo-optical switching elements
NLO polymers	Light modulation, frequency conversion
Photochromic and/or photorefractive polymers	Optical data storage
Hole burning polymers	Optical multiplex data storage
Electroluminescent polymers	Large area displays

Table 2.2 High technology polymers and their main areas of applications

2.5 Sol-Gel Systems

In order to find materials endowed of higher rigidity with respect to polymers and with good optical transparency, chemical endurance and mechanical stability, organic-inorganic hybrid materials synthesized by sol-gel method was proposed and tested since early ’90. Like in main-chain polymers, however, the intrinsic rigidity of the matrix increases the difficulty of the orientational process and a trade-off has to be reached.

The sol-gel process, as the name implies, involves the evolution of inorganic networks through the formation of a colloidal suspension (*sol*) and gelation of the sol to form a network in a continuous liquid phase (*gel*). The precursors for synthesizing these colloids consist of a metal or metalloid element surrounded by various reactive ligands. Metal alkoxides are most popular because they react readily with water. The most widely used metal alkoxides are the alkoxysilanes, such as tetramethoxysilane (TMOS) and tetraethoxysilane (TEOS). However, other alkoxides such as aluminates, titanates, and borates are also commonly used in the sol-gel process, often mixed with TEOS.

At the functional group level, three reactions are generally used to describe the sol-gel process: hydrolysis, alcohol condensation, and water condensation. This general reaction scheme can be seen in **Fig. 2.10**.

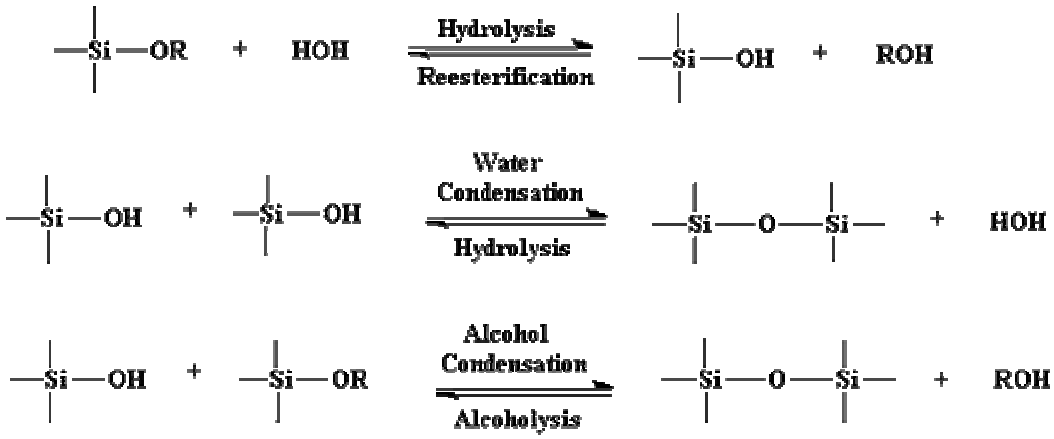

Fig. 2.10 Sol-gel process

However, the characteristics and properties of a particular inorganic sol-gel network are related to a number of factors that affect the rate of hydrolysis and condensation reactions, such as, pH, temperature and time of reaction, reagent concentrations, catalyst nature and concentration, H_2O/Si molar ratio (R), aging temperature and time, and drying as shown in **Fig. 2.11**. Among the factors listed above, pH, nature and concentration of catalyst, H_2O/Si molar ratio (R), and temperature have been identified as most important. Thus, by controlling these factors, it is possible to vary the structure and properties of the sol-gel-derived inorganic network over a wide range.

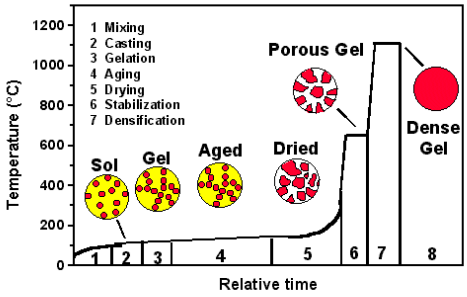

Fig. 2.11 Gel glass process sequence

Generally speaking, the hydrolysis reaction, through the addition of water, replaces alkoxide groups (OR) with hydroxyl groups (OH). Subsequent condensation reactions involving the silanol groups (Si-OH) produce siloxane bonds (Si-O-Si) plus the by-products water or alcohol. Under most conditions, condensation commences before hydrolysis is complete. However, conditions such

as, pH, H_2O/Si molar ratio (R), and catalyst can force completion of hydrolysis before condensation begins. Additionally, because water and alkoxides are immiscible, a mutual solvent such as an alcohol is utilized. With the presence of this homogenizing agent, alcohol, hydrolysis is facilitated due to the miscibility of the alkoxide and water. As the number of siloxane bonds increases, the individual molecules are bridged and jointly aggregate in the sol. When the sol particles aggregate, or inter-knit into a network, a gel is formed. Upon drying, trapped volatiles (water, alcohol, etc.) are driven off and the network shrinks as further condensation can occur.

The fundamental property of the sol-gel process is that it is possible to generate ceramic material at a temperature close to room temperature. Therefore such a procedure opened the possibility of incorporating in these glasses soft dopants, such as fluorescent dye molecules and organic cromophores. (**Brinker, 1990**)

2.6 Symmetry Requirements

Once a chromophore characterized by an acceptable optical nonlinearity and adequate stability has been identified, it must be organized in a noncentrosymmetric material. In fact, for a centrosymmetric material system (i.e., endowed with a center of inversion) the $\chi^{(2)}$ nonlinear susceptibility must vanish identically. While the result that $\chi^{(2)}$ vanishes for a centrosymmetric medium is general in nature, we will demonstrate this fact only for the special case of SHG in a medium that responds instantaneously to the applied optical field. We assume that the nonlinear polarization is given by

$$P(t) = \chi^{(2)} E^2(t) \qquad \textbf{(2.13)}$$

where the applied field is given by

$$E(t) = E_o \cos \omega t \qquad \textbf{(2.14)}$$

If we now change the sign of the applied electric field *E(t)*, the sign of the induced polarization *P(t)* must also change, because we have assumed that the medium possesses inversion symmetry. Hence, the **Eq. (2.13)** must be replaced by

$$-P(t) = \chi^{(2)}[-E(t)]^2 \tag{2.15}$$

which shows that

$$-P(t) = \chi^{(2)}E^2(t) \tag{2.16}$$

By comparison of this result with **Eq. (2.13)**, we see that *P(t)* must equal *–P(t)*, which can occur only if *P(t)* vanishes identically. This result shows that

$$\chi^{(2)} = 0 \tag{2.17}$$

In other words, "$\chi^{(2)}$ materials" must lack a center of inversion: this can be a structural feature, as in some inorganic crystals or can be achieved using non-centrosymmetric molecular units. However, in this case suitable strategies have to be taken in place for inducing at least a partial ordering into these otherwise amorphous systems.

2.7 From Microscopic to Macroscopic Nonlinearity

Relationship between microscopic hyperpolarizability β of the active molecules and NLO macroscopic properties of the materials ($\chi^{(2)}$) can be established. It can be set up under the assumption that intermolecular interaction could be considered weak. This approximation is known as the *oriented gas model.* (**Williams, 1984**) In this condition the bulk susceptibility, defined in **Eq. (1.32)** can be regarded as the statistical average of individual, molecular hyperpolarizabilities

$$\chi^{(2)}_{ijk} = Nf_i f_j f_k \langle \beta_{IJK} \rangle_{ijk} \tag{2.18}$$

where subscripts IJK refer to a molecule-based coordinate system, ijk refer to the coordinate system of the bulk material, *N* is the number density of NLO molecules, f_i, f_j, f_k represent local field factors and the brackets denote the statistical average over all orientations of NLO molecules. Local field factors depend in a dielectric medium by the sum of the dipole fields from all the polarizable particles. NLO molecules are assumed to be imbedded within a cavity inside a uniformly polarized medium. For a spherical cavity appropriate local field corrections are *Lorentz-Lorenz* (for optical

frequencies) or *Onsager* (for dc and low frequency fields) ones. More general corrections are to be considered for no spherical cavities or for interacting molecules. Local fields factors do not include all the effects of surrounding medium. However, solvent environment for a NLO molecule is in general different from solid one and measurements of β in solution, as in *EFISH* technique, could not give an appropriate description for their behaviour in a solid.

In order to have a high NLO response with organic materials, molecules with large β have to be used with high concentration. However generally these molecules have large permanent dipole moments, and dipole-dipole interactions needs to be included in the analysis. Intermolecular interactions between spherical shaped molecules can be modelled by means of *London theory* and the poling-induced NLO coefficient d_{33} (where subscripts 3 indicate the poling direction) can be calculated (**Harper, 1998**)

$$d_{33} \propto \frac{\mu\beta}{\mathrm{M_W}}\left[1 - L^2\left(\frac{W}{kT}\right)\right]E_P \qquad \textbf{(2.19)}$$

where μ is the permanent dipole of molecule, $\mathrm{M_W}$ is its molecular weight, E_p is the poling field, k is the Boltzmann constant, T is temperature at which poling is performed, $L(x)=\coth(x)-1/x$ is the first-order *Langevin* function and W is the potential energy molecular dipolar moment, that can be written as the sum of three terms, the orientation force (interaction between *permanent* dipoles), the induction force (interaction between *induced* dipoles) and the dispersion force: W results proportional to R^{-6}, where R is the average distance between NLO molecules. Even if this analysis can be applied, at a first approximation, also to non-spherical particles, other models have to be developed for more general cases. Taking into account intermolecular interactions involves a variation of NLO coefficient with respect to molecule loading (**Fig. 2.12**). Dipole-dipole interactions introduce a limitation to the maximum NLO molecule concentration.

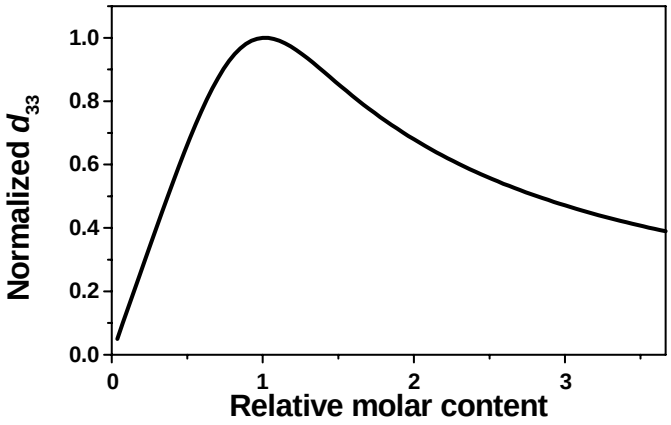

Fig.2.12 Normalized second order nonlinear coefficient d_{33} as a function of molecule loading according to **Eq. (2.19)**. Molecular concentration is normalized to the value corresponding to maximum of d_{33}. Intermolecular interactions are taken into account.

To produce an ordering in an otherwise isotropic dispersion of molecules, even endowed of high hyperpolarizability and related dipole momenta, two main strategies have been developed: autoassembling and forced alignment.

In the first are non-centrosymmetric crystals, *Langmuir-Blodgett* films, ionically self-assembled monolayers, intermolecular charge transfer complexes. Non-centrosymmetric organic crystals have been the first bulk organic materials to be investigated for second order NLO. This approach has two fundamental disadvantages: only a small part of NLO organic molecules tends to crystallize in non-centrosymmetric system and it is difficult to achieve crystals of the required size, stability and transparency for applications. Some interesting results have been obtained throughout the years. Adopted strategies to favour crystallization are the incorporation of chiral substituents, the use of organic salts and the designing of species with specific intermolecular interactions, such as hydrogen bonding .Langmuir-Blodgett technique is another way which has been investigated to achieve organic macroscopic NLO materials. The main disadvantages of this technique are the poor orientational stability of NLO layers and the difficulty to achieve thick oriented films.

In the second class are poling techniques where the orientation of active molecules in solid matrices of polymers or sol-gel derived materials is performed with application of external forces. This class of techniques will be discusses in detail because of their extensive use during the work of this thesis.

2.8 Poling Techniques

Poling, i.e. the orientation of the molecular dipoles, is mandatory in order to break the centrosymmetry of the starting materials. Although poling represents an additional processing step, it also introduces a new degree of freedom in the design of devices. By poling, the dipoles can be oriented parallel or perpendicular to the film plane. In addition to the global orientation, selective orientation in the film-plane and across the film thickness are possible, as required for applications in high density data storage or photonic devices. A summary of all the poling techniques is shown in **Table 2.3**. No other competing materials, such as ferroelectric crystals or semiconductors, offer this variability in device design.

Orientation method	***Electric field poling***	***Photoassisted poling***	***All-optical poling***
Excitation factor	thermal	optic	optic
Orienting factor	electric	electric	optic
Working temperature	~10 degrees below T_g	room temperature	room temperature
Material	solid state or solution	solid state	
Temporal stability	potentially high	potentially high	low

Table 2.3. Summary of the existing poling techniques and their main features.

2.8.1 Static Field Techniques

Application of a static field to dipolar molecules leads to the alignment of their dipolar moments in the external electric field direction. The idea of using solid solutions and large electric fields in order to orient imbedded dipolar chromophores is relatively old. (**Havinga, 1979**) Classically the

required orientation of active molecules is obtained by heating polymers to the glass transition temperature, at which they can rotate and by applying a sufficiently large external dc field (typically 100÷200V/μm). The obtained orientation is frozen by cooling down sample to room temperature under the applied external field (**Fig. 2.13**). An additional chemical modification of the matrix network could be performed, through thermal or photo-crosslinking, in order to further increase the temporal stability of induced orientation.

The following techniques of dc poling have been developed:

(i) contact (electrode) poling

(ii) corona poling

(iii) photothermal poling

(iv) electron beam poling

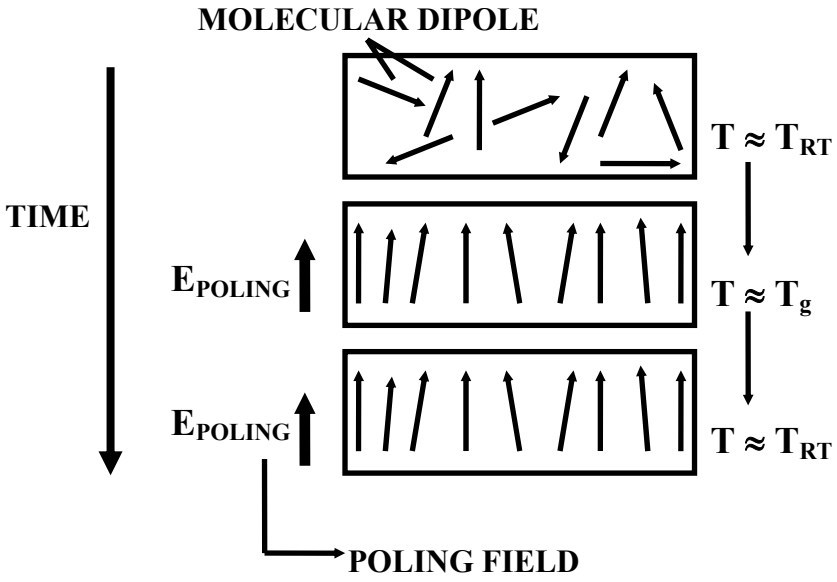

Fig. 2.13 Scheme of dc poling technique for polymeric materials

In the first case a large poling field is created through electrodes with the polymer thin film placed in between. The film is heated up to the glass transition temperature and the poling voltage is applied between electrodes. Interdigitated and coplanar electrodes are used when one wants to obtain orientation in the plane of the film, while a sandwich (electrode-film-electrode) configuration (parallel plate electrodes) can be used to achieve perpendicular poling.

Corona poling is surely the most used electric field poling technique. With such technique can be achieved electric fields up to 4 MV/cm, obtained by depositing on the film surface the charges created by ionization of the surrounding atmosphere. The gas ionization is caused by a sharp needle, a wire or a grid placed at high potential (kV) with respect to the ground. Because of

the reduced dimension of the needle or wires, the extremely high field near the electrode is able to ionize molecule of the gas and accelerate them toward the film. A constant voltage grid is often interposed between electrode and film to control more accurately the poling field. (**Dao, 1993**)

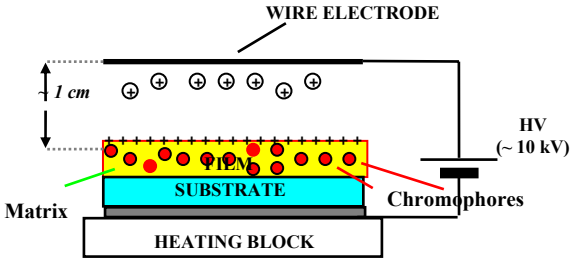

Fig. 2.14 A typical setup for corona poling

A typical setup for corona poling of polymer and hybrid films is shown in **Fig. 2.14**. Corona poling is a threshold phenomenon and requires application of high voltages, around 5-7 kV, with the electrode distant 1 cm from the film surface.

The efficiency of corona poling depends upon several factors: voltage, distance of electrode from the film surface, temperature, type pf atmosphere. Depending on the polarity of the electrode, so called *positive* or *negative* poling can be achieved. In positive corona poling, electrons are directly responsible for the ionization of molecules or atoms of the gas, while in negative corona poling, the electrode is involved in sustaining the discharge avalanche, providing a source of electrons by secondary emission, ion impact or photoelectric effect: the result is that negative corona poling is less stable and very dependent on the chemical composition of the surrounding atmosphere, as it has been demonstrated experimentally. (**Mortazavi, 1989**)

Photothermal poling is a simple modification of the main electrode poling technique. The only difference consists in the use of a laser beam, with wavelength lying in the material absorption band, to heat thin film. The main advantage of this technique consists in a very localized poling. It has been used for fabrication of bi-directionally poled polymer films. (**Yilmaz, 1994**)

In the electron beam poling technique the constant current, created in material by a monoenergetic electron beam with energy ranging between 2 and 40 KeV is used to orient chromophores. The dipoles are oriented by the polarization field, created by trapped in bulk decelerated electrons. In this sense the technique is very similar to the corona poling technique, with the difference that in the former the poling is due to the field created by surface while in the latter to the bulk charges. The technique allows also poling very small areas and has been used for fabrication of periodical structures for Quasi Phase Matched (QPM) SHG applications. (**Houe, 1995**)

In all techniques the chromophore orientation is frozen by cooling poled film to the room temperature under the applied external field or by thermal or photo-crosslinking during the poling procedure.

2.8.2 Photoassisted Poling

Dumont and co-workers (**1995**) have observed that shining in the chromophore absorption band, doped (or functionalized) with noncentrosymmetric dipolar molecules, polymer thin films, induces a significant increase of electrooptic coefficient, corresponding to a better polar orientation of chromophores. The measurements have been done using the Attenuated Total Reflection technique (ATR) and the optical field polarization was perpendicular to the applied low frequency external electric field to the thin film. A better stability of induced orientation was observed in the case of functionalized polymers than in guest-host systems, as usual in static field poled polymers. The chromophores orient with dipolar moments perpendicular to the optical field (and parallel to the applied static (or low frequency) field. As it will be discussed later, the chromophore orientation is going through *trans-cis isomerization* process (**Fig. 2.15**).

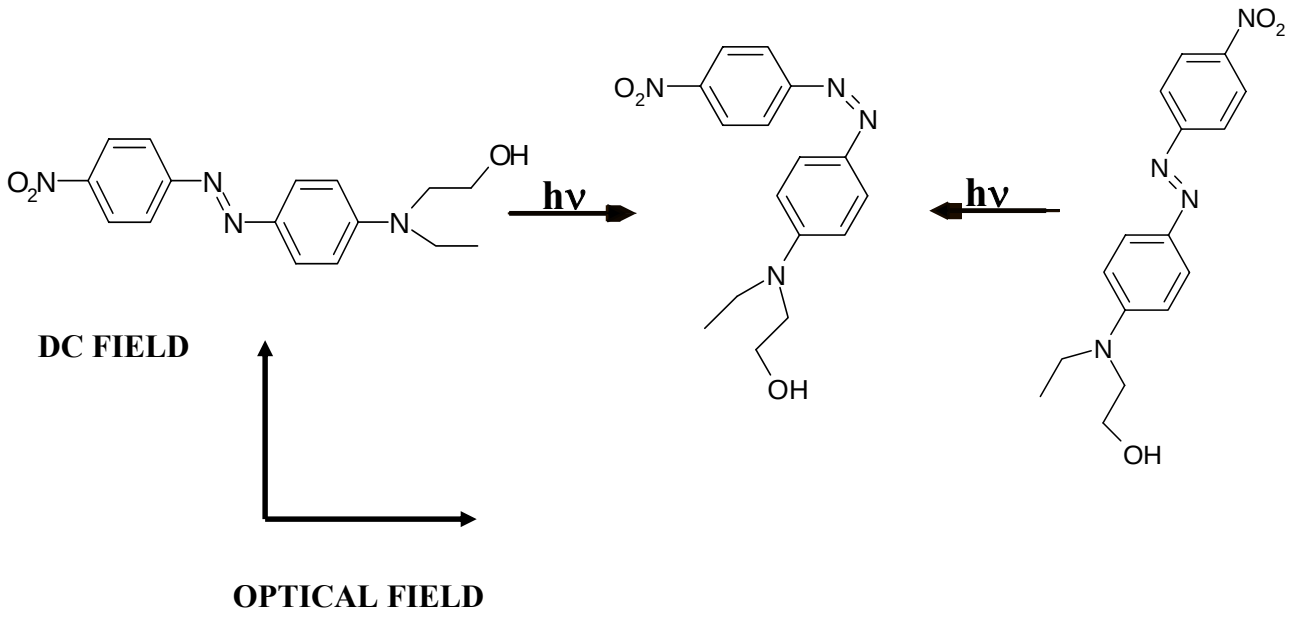

Fig. 2.15 Light induced orientation of DR1 molecule in the presence of the static field and photoisomerization process.

The *trans-cis* isomerization under light illumination (**Fig. 2.16**) is more efficient in azo-dye based systems (**Fig. 2.17**). The double N=N bond is flexible at excited state and through rotation or translation, molecule may change configuration from trans to cis form. This process is very fast in liquids and is significantly slower in solid state (about 150 ns, **Kajzar, 1995**). The inverse transformation from cis to trans form, may go only through non-radiative channels and is very slow (of the order of few seconds in solids). Molecules can return to the previous configuration, but will be again excited by incoming light. Thus the only stable position will be obtained if molecule orients with the dipole moment perpendicular to the incident light polarization, that is parallel to the applied electric field. As a consequence, the light induced molecular re-orientation will lead to an increase of the electrooptic coefficient as it was observed experimentally. (**Sekkat, 1992**)

(a)

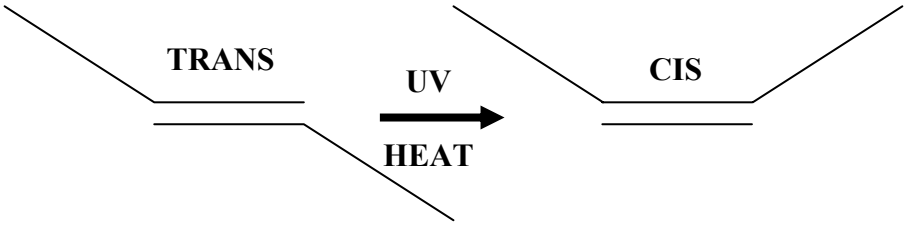

(b)

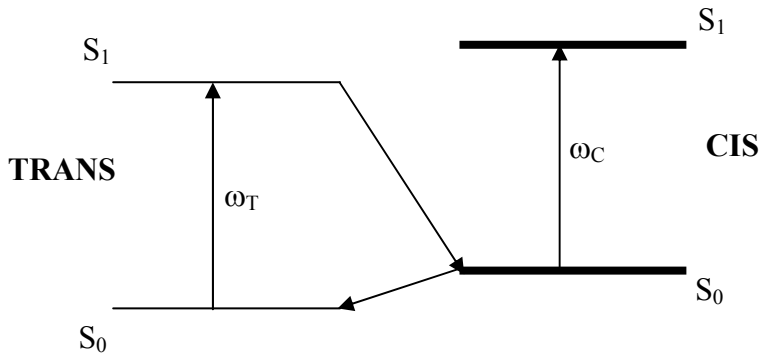

Fig. 2.16 Light (or heat) induced photoisomerization process **(a)** and electron transitions between fundamental and excited singlet states diagram **(b)** with $\omega_C > \omega_T$

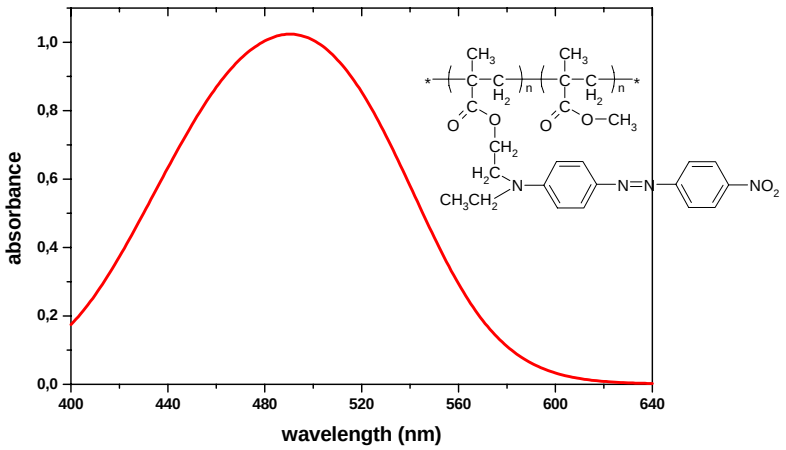

Fig. 2.17 Chemical structure of azo-dye-containing polymer film (DR1-co-PMMA) with 35% molar content and its optical absorption spectrum.

Fig. 2.18 shows the experimental setup used by **Dumont** and co-workers. The studied poled film is placed between two electrodes, one of them being a silver electrode deposited on the side of a prism. The condition to excite surface polaritons in thin films depends on its refractive index and thickness as well as on the refractive indices of electrode material and prism. By varying incidence angle it is possible to satisfy this condition, what is observed as a dip in the intensity of reflected beam. By varying refractive index of thin film with applied voltage one changes the resonance conditions. The technique is very sensitive to film thickness and refractive index variation. As the variation of refractive index depends on the electrooptic coefficient (**Eq. 2.20**)

$$\Delta\left(\frac{1}{n^2}\right) = \sum_I r_{IJ} E_J \qquad \textbf{(2.20)}$$

the technique serves to determine it with high precision.

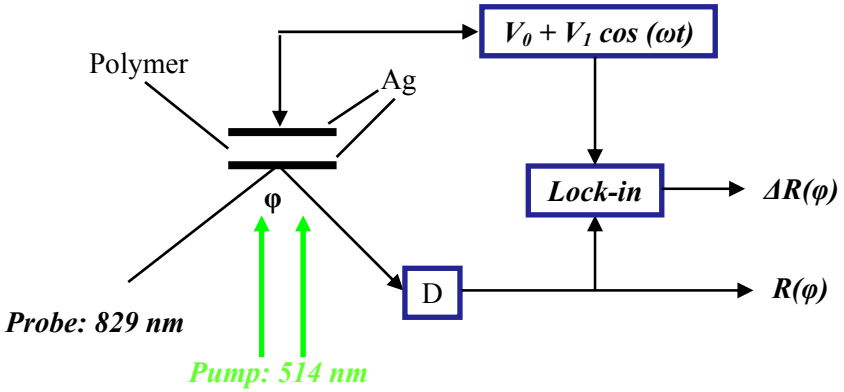

Fig. 2.18 ATR setup

2.8.3 All-Optical Poling

The first observation of an induced orientation of chromophores in a grafted DR1-doped PMMA polymer in a four wave mixing geometry with two picosecond pump beams at 1064 nm and a probe beam at double frequency (**Fig. 2.19**) has been done by **Charra** et al. (**1993**). The observed signal at 532 nm rose slowly with time, up to a saturation value. A spontaneous SHG was observed after switching off the probe beam. This experiment has shown that using a purely optical fields one can obtain an orientation of chromophores in a functionalized or doped film.

Significantly larger $\chi^{(2)}$ value was obtained in seeding geometry using two collinear picosecond beams at 1064 nm and 532 nm. (**Kajzar and Nunzi, 1998**) For more details see **Chapter 4**.

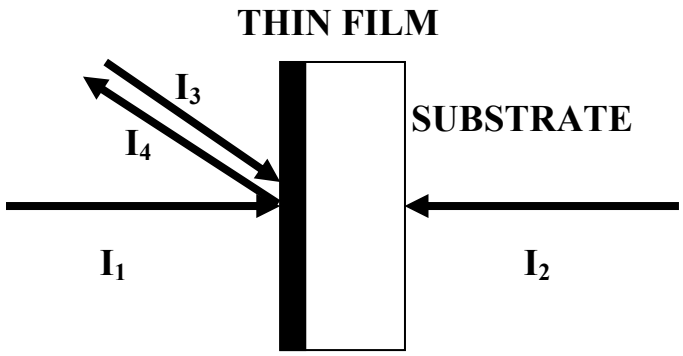

Fig. 2.19 Four wave mixing geometry. Pump beams I_1 and I_2 are at 1064 nm while probe I_3 and signal I_4 beams at 532 nm.

2.9 An Open Problem: Long-Term Time Stability

Temporal stability of NLO properties is the most important requirement for these materials and here is the main challenge. Two main phenomena influence stability: disorientation of active molecules and their decomposition. The first phenomenon decreases the effective number of active molecules able to generate macroscopic second order effect, the second one reduces the overall molecules concentration. A number of strategies can be set up. The more direct one is the use of matrices with higher rigidity, that means higher glass transition temperature (T_g).

However the price to pay is often too high: in the poling phase, when the sample has to be held at temperatures near the T_g the active species, sensitive to thermal treatment, can decompose.

An alternative approach for a more rigid matrix consists in the use of sol-gel materials. Their rigidity can be attained with moderate thermal treatment and moreover sol-gel reaction is irreversible. The challenge here is to promote the network formation of the active molecules after orientation. (**Casalboni, 2004)**

In order to have a better insight on this crucial point, many attempts were settled both for quantify and monitor the orientation stability and for developing new strategies for make more rigid materials. The first aspect will be discussed in **Chapter 3**.

Chapter 3

Accelerated Life Test

Life testing of materials which exhibit high reliability requires a long time to obtain test data when tested under use condition. Accelerated tests consist in exposing specimen of tested material to higher stress levels and observing the time to failure. The data acquired in these tests have to be extrapolated to nominal conditions to obtain an estimate of the life distribution function under nominal condition.

By definition, an accelerated test requires that the degrading agent or agents is present at a level higher than that to be seen in service. The general procedure is to measure the degree of degradation by change in selected properties of interest as a function of time of exposure to the degrading agent, it is necessary to carry out tests at several levels of the agent. There are two stages to modelling the degradation process:

(1) obtaining a function for the change of parameter(s) of interest with time

(2) obtaining a function for the rate of change of the parameter(s) with the level of the degrading agent.

*Using these relationships, the change in the property for longer times and lower levels of the degrading agent can be predicted. Clearly, the success of the prediction is critically dependent on the validity of the models used. (**Brown, 1995**)*

The purpose of this Chapter is to review the models which have been applied to NLO materials.

3.1 What is Accelerated Life Test?

Traditional life data analysis involves analyzing *times-to-failure* data (of a system, product or component) obtained under normal operating conditions in order to quantify the life characteristics of the system. In many cases and for many reasons, such life data is very difficult, if not impossible, to obtain. The reasons for this difficulty can include the long life times of today's systems, the small time period between design and release and the challenge of testing systems that are used continuously under normal conditions. Given this difficulty and the need to observe failures of products to better understand their failure modes and their life characteristics, reliability practitioners have attempted to devise methods to force these products to fail more quickly than they would do under normal use conditions. In other words, they have attempted to accelerate their failures. Over the years, the term accelerated life testing has been used to describe all such practices. As we use the term in this work, accelerated life test involves acceleration of failures with the single purpose of quantification of the life characteristics of the system at normal use conditions.

More specifically, accelerated life test can be divided into two areas: *qualitative* accelerated test and *quantitative* accelerated life test. The first one gives failure information (or failure mode) only and is performed on small samples with the specimens subjected to a single severe level of stress, to a number of stresses or a time-varying stress (i.e., stress cycling, cold to hot, etc.). If the specimen survives, it passes the test. Otherwise, appropriate actions will be taken to improve the product's design in order to eliminate the cause(s) of failure.

The second one consists of tests designed to quantify the life characteristics of the product under normal use conditions. This procedure involves making assumptions about:

(1) the type of life distribution at each test level

(2) stress-life relationship (known also as aging model). (**Reliasoft Corporation, 2002**)

3.2 Life Distributions

As observed above, for application in practical devices, second order NLO materials must retain at least 80% of its initial nonlinear activity at an operating temperature of 70°C for a period of 5 years. They must also withstand brief excursions to device processing temperatures of 250°C and higher. For these reasons, it is common to chose temperature as degrading agent.

Compared with crystals, poled polymers have various advantages, however they present the main disadvantage that their nonlinearities disappear gradually with the time, due to rotation of nonlinear active units after the poling procedure. Relaxation in poled systems arises from thermal

re-orientational effects whose rate is governed by the mobility of the molecules in the glass. The mobility is in turn determined by a number of parameters including glass transition temperature (T_g) and the level of free volume. SHG is a diagnostic tool for studying relaxation mechanisms primarily below the T_g of these materials (in timescale of the order of hours up to months). However, it was shown that SHG can serve as a probe for the entire range of relaxation times above and below the T_g. (**Dhinojwala, 1993**)

Therefore, by examination and analysis of the bulk NLO response of a poled chromophore-functionalized polymer, information can be obtained on the orientational distribution of the NLO-active chromophore units. In samples where a polar axis has been induced, the relationship between macroscopic and microscopic SH properties for quasi-one-dimensional molecules (i.e., in which the dipole moment is directed along the symmetry axis such that the β_{zzz} component dominates) is given by only two independent non-vanishing components of d_{ijk}.

$$d_{33} = \frac{1}{2} N \beta_{zzz} f^{2\omega} f^{\omega} f^{\omega} \left\langle \cos^3 \vartheta \right\rangle \qquad \textbf{(3.1)}$$

$$d_{31} = \frac{1}{2} N \beta_{zzz} f^{2\omega} f^{\omega} f^{\omega} \left[\left\langle \cos \vartheta \right\rangle - \left\langle \cos^3 \vartheta \right\rangle \right] \qquad \textbf{(3.2)}$$

In the above equations, N is the chromophore number density, β_{zzz} is a component of the molecular hyperpolarizability tensor, β, $\langle \cos\theta \rangle$ and $\langle \cos^3\theta \rangle$ are angular averages which describe the degree of polar order achieved during poling, $f^{\omega,2\omega}$ are the local field correction factors at ω and 2ω respectively. They are given by the *Lorentz-Lorenz* expression. (**Burland, 1994**)

$$f^{\omega} = \left\{ \frac{n^2(\omega) + 2}{3} \right\} \qquad \textbf{(3.3)}$$

Thus, to model SHG in poled materials, the first and third moments, $\langle \cos\theta \rangle$ and $\langle \cos^3\theta \rangle$, must be evaluated. A static theoretical description of dipolar alignment in the presence of a field can be used to calculate these orientational order parameters at equilibrium.

The molecular statistical model describes the interaction of an isolated, uniaxial molecule with its environment. The permanent dipole, μ, is at an angle, θ, with respect to the applied field and its energy in the field is given by

$$V(\vartheta) = -\mu E \cos\vartheta \tag{3.4}$$

Using the Boltzmann distribution, the net moment is given as

$$\langle z(\theta)\rangle_{eq} = \frac{\int_0^{\pi} e^{(u\cos\vartheta)} z(\vartheta)\sin\vartheta \cdot d\vartheta}{\int_0^{\pi} e^{(u\cos\vartheta)} \sin\vartheta \cdot d\vartheta} \tag{3.5}$$

Here $u = \mu E/kT$, k is the Boltzmann constant, T is the thermodynamic temperature, μ is the dipole moment of the uniaxial molecule, E is the strength of the applied field, θ is the spherical polar angle between the molecular dipole axis and the direction of the field (**Fig. 3.1**) and $z(\theta)$ is either $\cos\theta$ or $\cos^3\theta$.

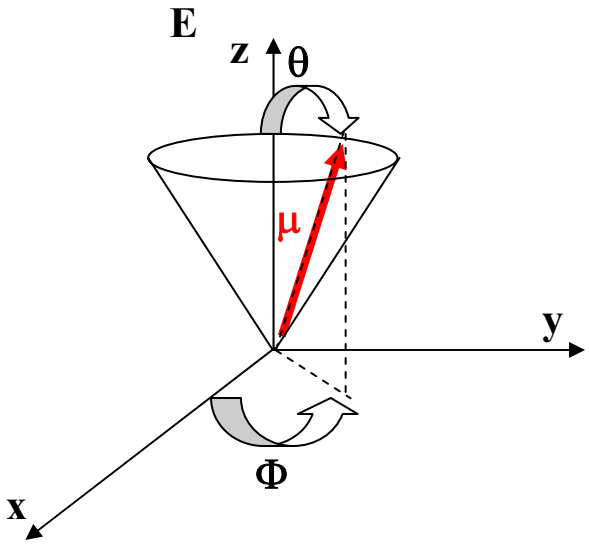

Fig. 3.1 Three-dimensional rotational diffusion model of a polar molecule in the presence of an external field.

The rotational diffusion of a rigid rod is described by (**McConell, 1980**)

$$\frac{1}{D_R}\frac{\partial f(\vartheta,t)}{\partial t} = \frac{1}{\sin\vartheta}\frac{\partial}{\partial\vartheta}\left\{\sin\vartheta\left[\frac{\partial f(\vartheta,t)}{\partial\vartheta} + \frac{f(\vartheta,t)}{kT}\frac{\partial V}{\partial\vartheta}\right]\right\} \tag{3.6}$$

Here, $f(\theta,t)$ is the probability of obtaining the dipole vector in an orientation θ at time t. The hydrodynamic parameter of interest is D_R, the rotational diffusion coefficient. The potential energy $V(\theta)$ is described in **Eq. (3.4).**

An analytic solution to the rotational diffusion equation can be found by expansion in orthogonal functions. The appropriate eigenfunctions for a three-dimensional system of axial symmetry are the Legendre polynomials. By substituting both Legendre's equation expressed in terms of differentiation with respect to θ (**Arfken, 1985**)

$$\frac{1}{\sin\vartheta}\frac{\partial}{\partial\vartheta}\left(\sin\vartheta\frac{\partial P_m(\cos\vartheta)}{\partial\vartheta}\right) = -m(m+1)P_m(\cos\vartheta) \tag{3.7}$$

and the expression for the time-dependent probability of θ

$$f(\vartheta,t) = \sum_m f_m(t)P_m(\cos\vartheta) \tag{3.8}$$

back into the rotational diffusion equation, the following expression is obtained

$$\sum_m f_m(t)\left[\begin{array}{l} -m(m+1)P_m(\cos\vartheta)+ \\ +\dfrac{\mu E}{kT}\left(\left(\cos^2\vartheta-1\right)\dfrac{\partial P_m(\cos\vartheta)}{\partial\cos\vartheta}+2\cos\vartheta P_m(\cos\vartheta)\right)\end{array}\right] \tag{3.9}$$

Re-expressing the first derivative of a Legendre polynomial as

$$\frac{\partial P_m(\cos\vartheta)}{\partial\vartheta} = \frac{-m\cos\vartheta P_m(\cos\vartheta)+mP_{m-1}(\cos\vartheta)}{1-\cos^2\vartheta} \tag{3.10}$$

Multiplying both sides by $P_m(\cos\theta)$ and applying the orthogonality condition

$$\int_{-1}^{1} P_m(\cos\vartheta)P_{m'}(\cos\vartheta)d\cos\vartheta = \frac{2\delta_{mm'}}{2m+1} \tag{3.11}$$

where $m = 0, 1, 2, 3, \ldots$

results in a diffusion equation of the following form

$$\frac{1}{D_R}\frac{df_{m'}(t)}{dt}\frac{2}{2m'+1} = -m'(m'+1)\frac{2}{2m'+1}f(t)_{m'} - \frac{\mu E}{kT}\frac{2(m'+1)}{2m'+3}f(t)_{m'+1} + \frac{\mu E}{kT}(m'+2)\sum_m f(t)_{m'}\int_{-1}^{1} P_m P_l P_{m'} d\cos\vartheta \qquad \textbf{(3.12)}$$

The solution to the remaining integral over the triple product of Legendre polynomials can be evaluated through the use of 3-*j* symbols. From this, the following recursion formula may be derived, from which the time-dependent coefficients, $f_m(t)$, are found

$$\frac{df_{m'}(t)}{dt} = \frac{5D_R\mu E}{kT}\left(\frac{m'+1}{2m'+3}\right)f_{m'+1}(t) - D_R m'(m'+1)f_{m'}(t) + \frac{2D_R\mu E}{kT}\left(\frac{m'(m'+1)}{2m'-1}\right)f_{m'-1}(t) \qquad \textbf{(3.13)}$$

Once the differential equation for the time-dependent coefficient (**Eq. (3.13)**) is solved, the temporal behavior of the pertinent SH coefficients, d_{33} and d_{31}, may be determined through the orientational order parameters $\langle\cos^3\theta\rangle$ and $1/2[\langle\cos\theta\rangle - \langle\cos^3\theta\rangle]$. The first and third moments of $\cos\theta$ can be found by employing an average

$$\langle z(\theta)\rangle_{3D} = \frac{\int_{-1}^{1} f(\vartheta,t)z(\vartheta)\cdot d\cos\vartheta}{\int_{-1}^{1} f(\vartheta,t)\cdot d\cos\vartheta} \qquad \textbf{(3.14)}$$

The third moment, $\langle\cos^3\theta\rangle$, can be found by substitution of the rearranged third-order Legendre polynomial, $P_3(\cos\theta)$

$$\cos^3 \vartheta = \frac{2P_3(\cos\vartheta) + 3P_1(\cos\vartheta)}{5} \qquad \textbf{(3.15)}$$

and the expression for the time-dependent probabilities of θ, **Eq. (3.8)** into **Eq. (3.14).** After application of the orthogonality relationship, **Eq. (3.11)**, the third moment can be written in terms of the calculated probabilities

$$\left\langle \cos^3 \vartheta \right\rangle = \frac{2f_3 + 7f_1}{35f_0} \qquad \textbf{(3.16)}$$

By using a similar procedure, $\langle \cos\theta \rangle$ can be written in the following term

$$\left\langle \cos\vartheta \right\rangle = \frac{f_1}{3f_0} \qquad \textbf{(3.17)}$$

Upon sudden removal of the orienting field, the dipolar chromophores disorient by Brownian motion and the second order NLO signal decays. Since the chromophores are released from the aligned state, the diffusion equation reduces to

$$\frac{df_{m'}}{dt} = -D_R m'(m'+1) f_{m'} \qquad \textbf{(3.18)}$$

Integration yields

$$f_{m'}(t) = f_{m'}(0) \cdot e^{-D_R m'(m'+1)t} \qquad \textbf{(3.19)}$$

where $f_{m'}(0)$ is the initial value of the probabilities. The integrated rate law describes the decay process for each m' as a simple exponential, with each Legendre polynomial processing a characteristic relaxation constant, k_r, equal to $D_R m'(m'+1)$. Substitution of the required time-dependent probabilities into **Eq. (3.16)** and **Eq. (3.17)** yields an expression for the $\langle \cos^3\theta \rangle$ ($\propto d_{33}$) depolarization dynamics.

$$\frac{\langle \cos^3 \vartheta \rangle(t)}{\langle \cos^3 \vartheta \rangle(0)} = \frac{d_{33}(t)}{d_{33}(0)} = \frac{7f_1(0)}{2f_3(0)+7f_1(0)} e^{-2D_R t} + \\ + \frac{2f_3(0)}{2f_3(0)+7f_1(0)} e^{-12D_R t} \tag{3.20}$$

Re-casting the pre-exponential coefficients in **Eq. (3.20)**

$$W_1 = \frac{7f_1(0)}{2f_3(0)+7f_1(0)} \tag{3.21}$$

and

$$W_2 = \frac{2f_3(0)}{2f_3(0)+7f_1(0)} \tag{3.22}$$

The pre-exponential coefficients W_1 and W_2 can be viewed as the fractional contributions of the fast and slow components of the total decay. We found for the *3-D* rotational diffusion

$$\frac{d_{33}(t)}{d_{33}(0)} = W_1 e^{-2D_R t} + W_2 e^{-12D_R t} \tag{3.23}$$

Eq. (3.23) resembles the empirical bi-exponential function frequently discussed in studies of NLO polymer dynamics and thus provides some theoretical justification for fitting the chromophore randomization process after finishing the poling procedure to a sum of exponentials even if, experimentally, one doesn't find an exact correlation between the two time constants. Presumably the increasing complexity of the chromophore microenvironment (the matrix) is the main contribution to the breakdown of the rotational diffusion dynamics. Consideration must also be given to specific interactions both of the NLO chromophore dipole with the matrix and between the NLO chromophores themselves.

Often, a relaxation mechanism of greater complexity is invoked, leading to more accurate modelling of the dynamics by the empirical *Kohlrausch-Williams-Watts* (KWW) stretched exponential function. (**Hodge, 1982**)

$$\frac{d_{33}(t)}{d_{33}(0)} = e^{\left(-\frac{t}{\tau}\right)^{\beta}} \qquad \textbf{(3.24)}$$

The KWW function corresponds to a continuous distribution of single exponential decays, with the width of the distribution characterized by β which assumes values between 0 and 1. The average relaxation time is given by $\langle\tau\rangle = \left(\frac{\tau}{\beta}\right)\Gamma\left(\frac{1}{\beta}\right)$, where the Γ function is a well-known numerically tabulate integral. Examining **Fig. 3.2**, we note that this decay (**Eq. (3.24)**) is slower than exponential ($\beta = 1$). A value of β in the range from 0.5 to 0.7 is common in glasses; values around 0.3 have been observed in polymers, but can be as low as 0.1. In general, however, it is best not to over interpret the significance of **Eq. (3.24)**. It should perhaps simply be viewed as a means of characterizing non-exponential decay with only two adjustable parameters.

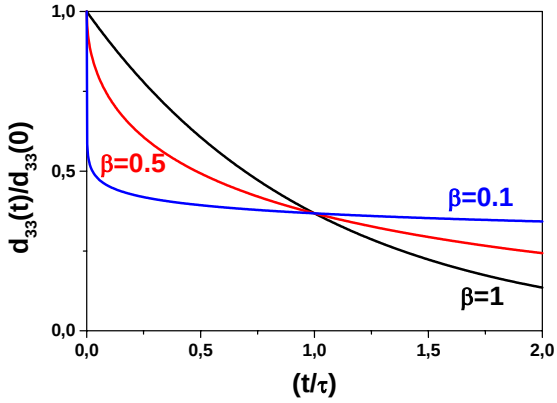

Fig. 3.2 normalized d_{33} for various values of β

Data are sometimes expressed in terms of a distribution of relaxation times

$$\frac{d_{33}(t)}{d_{33}(0)} = \int_0^{\infty} e^{\left(-\frac{t}{\tau}\right)} \xi(\tau) \cdot d\tau \qquad \textbf{(3.25)}$$

Eq. (3.25), along with the normalization condition,

$$\int_0^{\infty} \xi(\tau) \cdot d\tau = 1 \qquad \textbf{(3.26)}$$

defines the relaxation-time distribution function $\xi(\tau)$. For a single relaxation-time process, $\xi(\tau) = \delta(\tau-\tau')$.

3.3 Stress-Life Relationships

In the case of the conventional decay time evaluation method, a sample is kept at room temperature and its decay is evaluated from the observed SH intensities; however, for materials with long decay times it is difficult to evaluate the decay time with sufficient accuracy within a practical experimental period of time. (**Suzuki, 1995**) For this reason, it is common to study the NLO relaxation of polymeric systems at elevated temperatures. Once the decay times are evaluated using an appropriate life distribution, a stress-life relationship has to be chosen.

Below the T_g, the relaxation behavior of the poled NLO materials can be described using the *Arrhenius* relation (**Eq. (3.27)**) which is the first choice to apply to the effects of temperature.

$$\frac{1}{\tau} = A \cdot e^{\left(-\frac{E}{kT}\right)} \qquad \textbf{(3.27)}$$

Here τ is the slower time constant of the relaxation process, E is the activation energy, usually identified as the energy barrier (or threshold) that must be surmounted, A is the frequency factor and provides a measure of the frequency of occurrence of the reaction situation, usually envisaged as incorporating the vibration frequency in the reaction co-ordinate. A survey of published E and A showed a spread of activation energies mainly between 100 and 230 $kJmol^{-1}$, with no dominant values and a slight predominance of A values between 10^{11} and 10^{13} s^{-1}. From this equation, it follows that the process proceeds really faster under increased temperature. There are similar ideas about the influence of other factors of external environment (such as light, loading, etc.) on the process of aging.

For temperature above T_g, the *Williams-Landel-Ferry* (WLF) (or the equivalent *Vogel-Tamann-Fulcher*-VTF) equation describes accurately the relaxation process. (**Rong-Ho-Lee, 1998**) This relation is derived from the free-volume theory which assumes a linear dependence of the fractional free volume on temperature. Free volume can be described from a theoretical point of view as that portion of total unoccupied volume in an amorphous system that can be redistributed without a change in the free energy. Polymer glasses are composed by local free-volume elements whose sizes are in the range of $Å^3$. The WLF equation is shown in **Eq. (3.28)**, where τ is the

relaxation time, T_0 is empirically found to be about 50°C the T_g, B and C are constants more or less independently of the system. This equation has been found to be valid in many systems above T_g.

$$\tau = Be^{\left[-\frac{C}{(T_0-T)}\right]} \qquad \textbf{(3.28)}$$

Chapter 4

Experimental Section

Poling, i.e. the orientation of the molecular dipoles in an electric field, is necessary in order to break the centrosymmetry in the polymer or hybrid film. Although poling represents an additional processing step, it also introduces a new degree of freedom in the design of nonlinear devices. By poling, the dipoles can be oriented parallel or perpendicular to the film plane. No other competing materials, such as ferroelectric crystals or semiconductors, offer this variability in device design.

Poling procedure produces in the system changes in the linear and NLO properties that can be followed in order to monitor the process and to measure its efficiency. Techniques sensitive to linear optical properties like birefringence and Polarized Absorption Spectroscopy (PAS) are related to the order parameter Φ that in turn can be related to the permanent dipole of NLO molecules μ. Linear changes can be obtained in a easier way but are affected by systematic errors. They are often used in preliminary evaluations.

Among the NLO techniques, SHG is certainly the most used method able to characterize NLO properties of second order materials. This characterization can be accomplished by means of the Maker fringes technique. All these procedures are described in this Chapter, together with the description of the experimental setup.

4.1 Samples Preparation

All the samples were prepared by means of the following procedure. We used standard BK7 microscope glasses as substrates. The substrates were rinsed in acetone ,refluxed in distilled H_2O and dried using a flux of N_2. Appropriate amounts of the second order materials were dissolved in a fixed solvent and the solutions were stirred until it became homogeneous. Then it was filtered through a 0.2 μm membrane filter to remove undissolved contaminants directly onto the substrate surface. The solution was spun at 1000-2000 rpm depending on the desired thickness (**Fig. 4.1**) for a variable time at room temperature and, in general, baked in a vacuum oven to remove all the solvent. The spin coating parameters (speed, acceleration, time, etc.) were calibrated for each system depending on its nature, used solvent, etc.. The film thickness was measured with an Alphastep 200 profilometer. Both the spin coater and the profilometer are placed in a clean room (class 10000) in a laminar flow cabin.

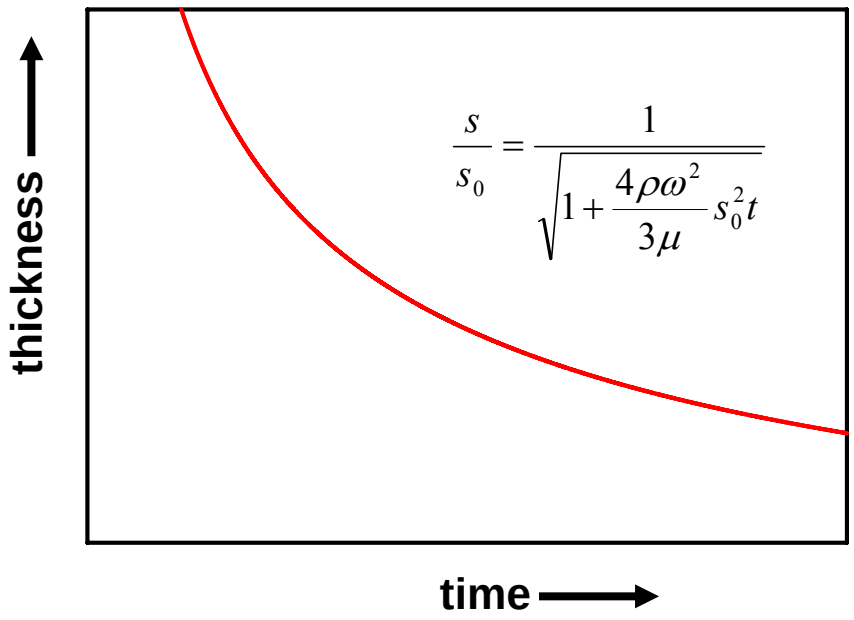

Fig. 4.1 Film thickness as a function of material and process parameters (fluid viscosity μ, fluid density ρ, initial thickness s_0, spinning time t, rotation speed ω) (**Middleman, 1993**)

4.2 Corona Poling Setup

The experimental arrangement for corona poling setup is schematically shown in **Fig. 4.2**. Our corona poling setup used a 20–μm diameter gold wire biased with high static potential (typically

+5÷7 kV) placed at about 1 cm from the film surface. The HV generator and the heating plate were connected to a common ground and the whole apparatus was held in a controlled atmosphere (dry-nitrogen) box. Poling current was carefully monitored to allow the comparison of measurements for different samples.

The intense electric field generated at the wire during the corona process accelerates nearby free electrons to velocities high enough to impact-ionize gas molecules in their path, creating ions with the same polarity as the wire. The ions generated are a function of the atmosphere and most often of the type and amount of impurities present in the gas. We used a positive corona poling setup, where positive ions are deposited on the film surface. The reactive ions accelerate toward the grounded film and accumulate near the surface region, generating a very high magnitude electric field across the film. This field orients the dopants thereby inducing second order nonlinear activity. If poling is performed under conditions where a visible strong corona glow can be seen, an irreversible change is observed in the film surface. All the poling performed in the experiments presented in this thesis were done at voltage levels low enough to prevent such damages.

As mentioned before, the typical poling procedure consisted in heating the samples at a temperature near T_g, with the electric field on. The films were then cooled down to room temperature at 1°C/min rate and then the electric field was switched off.

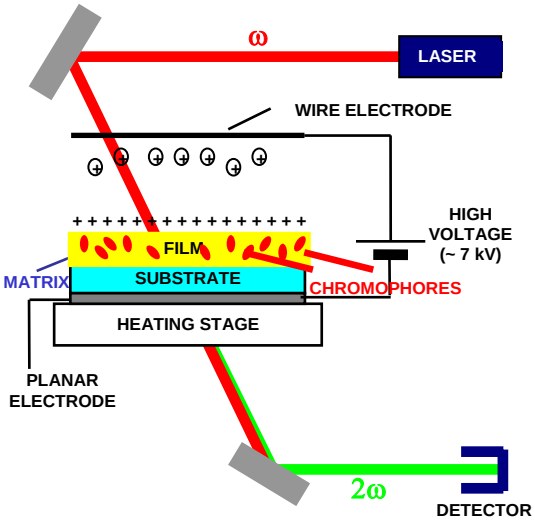

Fig. 4.2 Positive corona poling setup

During the PhD time, we built a new corona poling setup made of Macor® (**Fig. 4.3**), a pyroceramic which can tolerate high temperatures (> 300°C). By means of appropriate resistors (200 W), we were able to reach higher poling temperatures. Moreover, the horizontal position of the

sample holder permitted to orient dopants in sol-gel samples immediately after the deposition, when the condensation is still in progress.

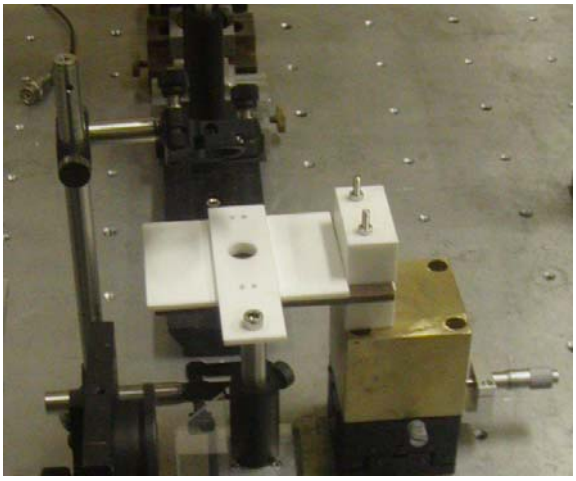

Fig. 4.3 Horizontal corona poling setup built for the measurements reported in this work

4.3 Linear Optical Characterization: Polarized Absorption Spectroscopy (PAS)

With the poling field applied perpendicularly to the thin film surface, the dipolar moments of NLO chromophores will orient preferentially parallel to the field. This can be easily evidenced by observing UV-Vis absorption spectrum after poling.

At the normal incidence, with electric field of the light parallel to the thin film surface a net decrease of the linear absorption is observed as it is seen in **Fig. 4.5** for a DR1-doped polyimide film. This variation may be used to calculate the order parameter Φ as it will be described below.

To examine the effect of poling on linear optical properties let's consider the dependence of macroscopic induced polarization in the direction (3) of poling by molecular linear polarizability

$$P_3(\omega) = \int \left[p_z(\omega)\cos(z,3) + p_x(\omega)\cos(x,3) + p_y(\omega)\cos(y,3) \right] \cdot G(\Omega) d\Omega = \chi_{33}^{(1)}(\omega) E_3(\omega) \quad \textbf{(4.1)}$$

where $G(\Omega)$ is a normalized distribution function of molecules over the solid angle Ω (being $G(\Omega)=1/(8\pi^2)$ for an isotropic distribution) and $cos(z,3) = cos(\theta)$ is the angle between molecular axis and poling direction (**Fig. 4.4**).

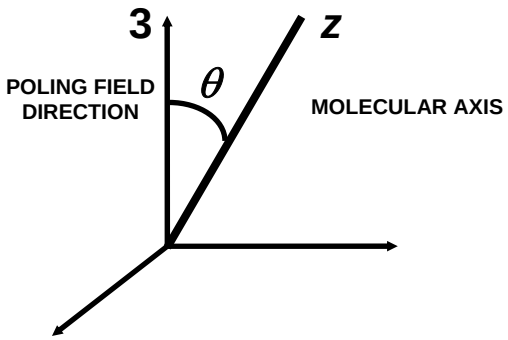

Fig. 4.4 Molecular dipole orientation with respect to the poling direction

For materials submitted to a poling field, having uniaxial symmetry in first approximation, $G(\Omega)$ becomes a function of the polar angle θ only. Then, for a system at thermal equilibrium, one can write

$$G(\theta) = \frac{e^{-\frac{A(\theta)}{kT}}}{\int_0^{\pi} e^{-\frac{A(\theta)}{kT}} \sin\theta \, \mathrm{d}\theta}. \qquad \textbf{(4.2)}$$

where $A(\theta)=U-TS$ is thermodynamic free energy. For molecules with large permanent dipole μ, and neglecting the influence of polarizability, energy is only function of angle θ, namely $U(\theta)=U_i(\theta)-\mu E^l \cos\theta$. Averaged value of $\cos^n\theta$ can be calculated

$$\left\langle \cos^n \theta \right\rangle = \frac{\int_0^{\pi} e^{-\frac{\mu E^l \cos\theta}{kT}} \cos^n\theta \sin\theta \, \mathrm{d}\theta}{\int_0^{\pi} e^{-\frac{\mu E^l \cos\theta}{kT}} \sin\theta \, \mathrm{d}\theta} \equiv L_n\left(\frac{\mu E^l}{kT}\right), \qquad \textbf{(4.3)}$$

where E^l is the local field and $L_n(u)$ the *Langevin functions*. $L_2(u)$, being $u=\mu E^l/(kT)$, is expressed by the following equation

$$L_2(u) = \frac{1}{3}\left(2\langle P_2 \cos\theta \rangle + 1\right) \qquad \textbf{(4.4)}$$

where $P_2(x)$ is the second order *Legendre polynomial* and the averaged value of $P_2(\cos\theta)$ is referred as *order parameter*

$$\Phi = \langle P_2(\cos\theta) \rangle \qquad \textbf{(4.5)}$$

Φ is zero for a completely disordered (isotropic) system and unity in a system in which all molecules have their dipole axes along the same direction. Has to be noted that, because of its dependence on $\cos^2\theta$, the order parameter is not able to distinguish between axial and polar ordering. The degree of orientation can be studied by measuring the absorbance of the sample. If the sample is illuminated in the direction of the orientating electric field, the absorbance will be minimum (null in the ideal case when the orientation is total), because the component of the dipolar moment of the molecules will be reduced or will not exist, in the direction of the electromagnetic field of the probing light as shown in **Fig. 4.5**.

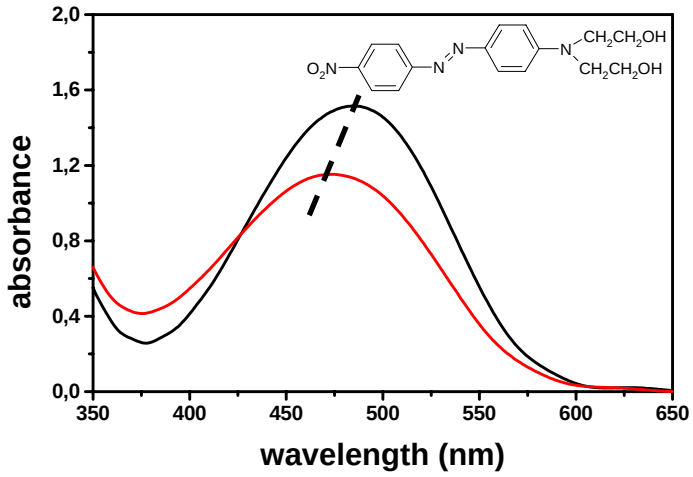

Fig. 4.5 Linear absorption spectrum of a DR19-doped polyimide film, before (**black line**), after (**red line**) poling. The spectra are measured with light polarized perpendicular to the poling field.

The decrease of absorbance is due to the alignment of the dipole of molecules parallel to the ***k*** vector of the incident radiation used in these absorption measurements. If one assumes that the molecular electronic transition moment is parallel to the permanent dipole moment (reasonable for a

plane molecule), the order parameter can be obtained by measures of absorbance changes before and after poling, with light polarized perpendicular to the poling direction

$$\Phi = 1 - \frac{A_{\perp}}{A_0} \qquad \textbf{(4.6)}$$

where $A_{\perp}$ and A_0 are absorbance measured at the peak wavelength with light polarized perpendicular to the poling direction after and before poling respectively. In this work, values of Φ in the range of **0.2-0.4** have been obtained after poling for different systems.

Another phenomena which can be noted in the linear absorption spectrum is the shift of the maximum absorption wavelength towards larger (red shift) or smaller (blue shift) wavelengths (**Fig. 4.5**). This shift can be ascribed to *dc Stark effect* due to the high dc field experienced by molecules. It can be related to the difference $\Delta\mu = \mu_{11} - \mu_{00}$ between molecule dipole moment in excited (1) and fundamental (0) states

$$\frac{\Delta\lambda}{\lambda} \cong -\frac{\lambda}{c}\frac{\Delta\mu}{\hbar c}E \qquad \textbf{(4.7)}$$

where $\hbar$ is the Planck constant, c the light velocity and E the poling field. (**Burland, 1994**) Depending on sign of $\Delta\mu$ one can observe a red or a blue shift.

Changes of absorbance spectrum can be caused by effects other than molecules orientation: sublimation of molecules in guest-host systems when they are not chemically bonded and thermal decomposition of the molecules being the poling procedure usually performed at temperature between 80 °C and 200°C . Besides, the measure of order parameter can be related to an orientation different from poling one, such as axial orientation, in the case of systems having an intrinsic preferred direction different from the poling one. In general in these cases a direct estimate of the poling induced second-order NLO properties is needed. This can be achieved by means of electrooptic effect and SHG described in the following paragraph.

4.4 Nonlinear Optical Characterization: SHG

SHG is certainly the most direct technique able to characterize NLO properties of second order materials. The SHG coefficients d_{ij} can be determined with the *Maker fringe* technique.

(**Jerphagnon, 1970**) By varying the incidence angle of a laser beam on a plane parallel sample of NLO material, the intensity of the SH generated and transmitted is found to oscillate in a periodic way. This technique is presented in **Fig. 4.6**.

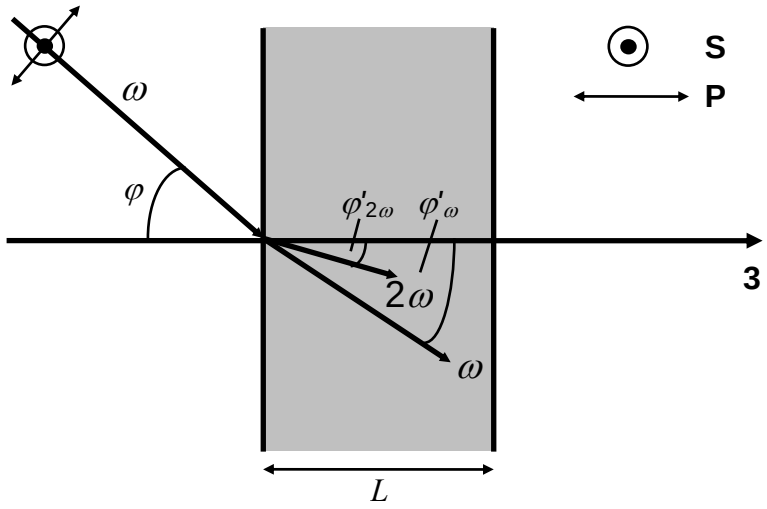

Fig. 4.6 *Maker fringe* technique for poled materials. The fundamental beam is incident at angle φ on a film thickness L. The angles of fundamental and SH beams are $\varphi'_{2\omega}$ and φ'_{ω} respectively.

By using polarized radiation incident on a poled film, being the poling direction orthogonal to the film surface, it can be shown that SH intensity for the two polarizations (S and P) is

$$I_{2\omega}^{S} \propto d_{31}^{2} \sin^{2} \varphi_{2\omega}^{'} I_{\omega}^{2} \sin^{2}\left(\pi \frac{L}{2l_C} \right)$$
$$I_{2\omega}^{P} \propto d_{eff}^{2} I_{\omega}^{2} \sin^{2}\left(\pi \frac{L}{2l_C} \right) \qquad \textbf{(4.8)}$$

where the effective coefficient d_{eff} is

$$d_{eff} = d_{33} \sin^{2} \varphi_{\omega}^{'} \sin \varphi_{2\omega}^{'} + d_{31} \cos^{2} \varphi_{2\omega}^{'} \sin \varphi_{2\omega}^{'} + \\ + 2d_{15} \sin \varphi_{\omega}^{'} \cos \varphi_{\omega}^{'} \cos \varphi_{2\omega}^{'} \qquad \textbf{(4.9)}$$

$I^{S}_{2\omega}$ refers to the SH intensity measured with intensity I_{ω} of the fundamental beam polarized perpendicular to the plane formed by the direction of the incident fundamental beam and the NLO

film surface normal (S-polarized). $I^{P}_{2\omega}$ is the SH intensity with the fundamental beam polarized in this plane (P-polarized).

In **Eqs. (4.8)** l_C represents the so called *coherence length*: SH radiation generated at a point x is 180° out of phase with SH radiation generated at $x \pm 2l_C\ (2j+1)$, being j an integer. Coherence length is given in terms of refractive indices n_ω and $n_{2\omega}$ respectively at ω and 2ω frequency and of the wavelength λ of the fundamental radiation

$$l_C = \frac{\lambda}{4\left|n_\omega \cos\varphi'_\omega - n_{2\omega}\cos\varphi'_{2\omega}\right|} \qquad \textbf{(4.10)}$$

By rotating the sample, the coherence length and path length of the light through the sample change. This results in an oscillating variation of the SHG intensity according to **Eq. (4.8)**. If the film thickness is greater than l_C *Maker fringes* must be taken into account. Nevertheless, for polymeric and glassy materials coherence length is of the order of tens of microns and for film thickness of 1÷2 μm *Maker fringes* don't occur. They are to be taken into account in the measure in crystalline Quartz that is usually employed as reference in quantitative determination (see below). In general, the coherence length can be determined from the spacing between the minima (or maxima) of the *Maker fringes* while the NLO coefficient is correlated with the peak amplitudes of the oscillations.

For P-polarized incident radiation, which is the case of this work, SHG intensity for polymeric and glassy micron-thick film is

$$\boldsymbol{I_{2\omega} = \frac{512\pi^3}{A} d^2_{eff} t^4_\omega T_{2\omega} p^2 I^2_\omega \frac{sin^2\left[\Psi(\varphi)\right]}{\left(n^2_\omega - n^2_{2\omega}\right)^2}} \qquad \textbf{(4.11)}$$

where A is the laser beam area, t_ω and $T_{2\omega}$ are *Fresnel* coefficients and p a form factor, while the term $sin^2(\Psi(\varphi))$, for thickness negligible with respect to l_C, is (**K. Singer, 1986**)

$$\sin^2\left[\Psi(\varphi)\right] \cong \left[\frac{\pi}{2}\frac{L}{l_C}\frac{n'}{\left(n''^2 - \sin^2\varphi\right)^{1/2}}\right]^2 \qquad \textbf{(4.12)}$$

where

$$n' = \frac{n_\omega + n_{2\omega}}{2} \; and \cdot n''^2 = n'^2 + \left(\frac{n_\omega - n_{2\omega}}{2} \right)^2 \qquad \textbf{(4.13)}$$

Away from resonance, *Kleinman* symmetry can be assumed yielding the identity $d_{31} = d_{15}$ in **Eq. (4.9)**. By considering that $d_{31} < d_{33}/3$ (**L. Hayden, 1990**), informations on d_{33} value can be obtained from **Eq. (4.11)**, once d_{31} is estimated from **Eq. (4.8)** and the $I^P_{2\omega}$, the refractive indices at ω and 2ω and the *Fresnel* factors are known.

4.4.1 Experimental Arrangement

Fig. 4.7 shows schematically the basic setup we used for the observation of SHG by a Quantel Brilliant Q-switched Nd:YAG laser (frequency up to 10 Hz, 5 ns pulse duration, 400 mJ per pulse) which provides the fundamental beam output at 1064 nm. This source feeds a *Solid State Raman Shifter* (Moltech CRS-14) which shifts the beam output to 1194, 1368 and 1598 nm. Its operation is based on Stimulated Raman Scattering (SRS) of laser radiation in Barium Nitrate ($Ba(NO_3)_2$) crystal. The incident power and polarization was controlled through half wave plate (λ/2) and appropriate polarizers. In the present work we used both 1064 and 1368 nm fundamental beam. This wavelength shift was done by selecting the appropriate output window of the Raman Shifter.

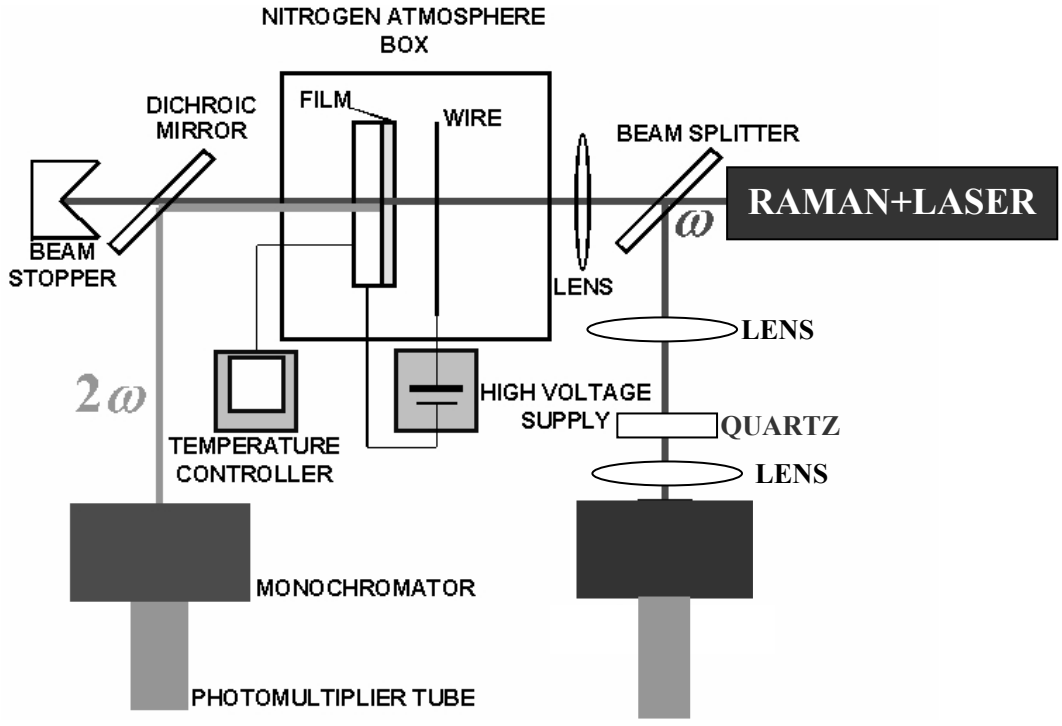

Fig. 4.7 Setup for *in-situ* SHG measurements

All the positioning adjustments were made using a 632.8 nm He-Ne laser, which is collinear with the YAG laser.

The P-polarized laser beam was split into two parts, one of which is focused by a 100 mm lens into the quartz crystal (or sample holder) positioned on a turntable and its power was measured by a power meter. The lens was mounted on a micrometric adjustment stage so that the focus of the laser beam could be tracked through the crystal (or the sample). The other one was focused onto another reference Quartz under a fixed angle in order to correct for laser power fluctuations.

The SHG was detected by Hamamatsu 1P28 photomultiplier tube through a monochromator settled at 532 and 684 nm, according to the incident wavelength and a dichroic mirror was used to reject the incident laser beam. The signal was sufficiently strong for making quantitative measurements by means of an oscilloscope which collected the SH coming from the samples, the incident laser and the trigger signal. The output signal was statistically averaged over 64 pulses to increase the signal/noise ratio.

To make sure of the selected incident laser light, we made a wavelength scan, using the selected window at 1368 nm. The emission spectra is shown in **Fig. 4.8,** with an indication of the other components' percentages.

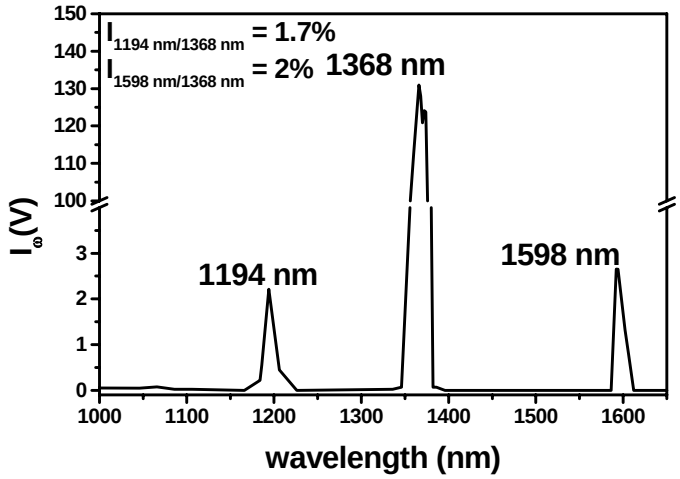

Fig. 4.8 Emission spectra of the Raman Shifter when the window at 1368 nm was selected

4.4.2 Calibration Measurements

Since SHG is mediated by the second component $\chi^{(2)}$ ($\propto d_{33}$), in the expansion of the susceptibility, the intensity of the SH signal is proportional to the square of the fundamental intensity. If, as is usually the case, the beam cross sectional area is kept constant, then the signal is proportional to the

square of the laser power. Half wave plate was used to vary laser power incident on the crystal. The SH power generated by a 2 mm thick Quartz crystal slab cut in the direction (010) as a function of the incident laser power (**Fig. 4.9)** was detected in order to check the phototube linearity. The parabolic nature of the curve is evident plotting the data in a *log-log* graph and performing a linear fit.

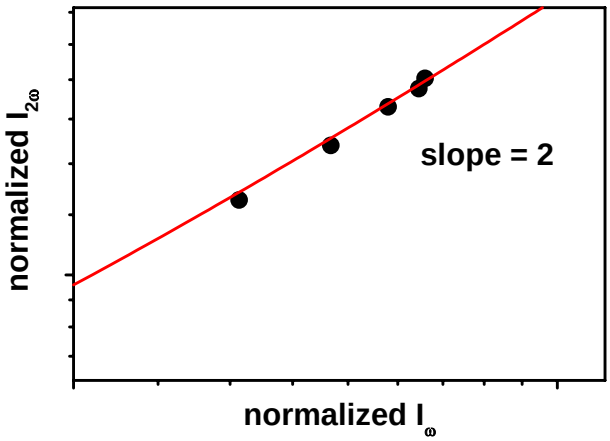

Fig. 4.9 Dependence of the SH signal on the fundamental power

In order to obtain second order nonlinear macroscopic coefficients, SHG intensities for poled NLO materials were measured relatively to the intensity of the reference Quartz at a fixed angle resulting in an indirect determination of the parameter d_{33}. Indirect measurements are normally affected by a number of errors. In order to check the validity of the procedure and to estimate this source of errors, we performed a *Maker fringe* experiment on two crystals, $LiNbO_3$ and Quartz, using the second one as reference.

Starting from **Eq. (4.11)** we calculated the nonlinear coefficient of the sample as follows

$$d_s = d_q \frac{1}{\rho_\omega} \frac{n_{\omega_S}^2 - n_{2\omega_S}^2}{n_{\omega_q}^2 - n_{2\omega_q}^2} \left[\frac{F_q}{F_s} \cdot \rho_{2\omega} \right]^{1/2} \left| \frac{\sin \Psi_q}{\sin \Psi_s} \right| \qquad \textbf{(4.14)}$$

with

s	**sample (or $LiNbO_3$)**
q	**quartz**
d	**second order nonlinear coefficient**
$\rho = I_s/I_q$	**power ratio**
$\Psi = 2\pi \frac{L}{\lambda}\left(n_\omega cos\varphi_\omega' - n_{2\omega} cos\varphi_{2\omega}'\right)$	**phase mismatch function**
L	**path length through the sample**
λ	**fundamental wavelength**
$F_q = t^4_{\omega q}\, T_{2\omega q}$	
$F_s = t^4_{\omega s}\, T^{FS}_{2\omega s}\, T^{SA}_{2\omega s}$	***Fresnel* transmission coefficients (F = film, S= substrate, A = air)** and for P-polarized light

$$t_\omega = \frac{2n_\omega cos\varphi}{n_\omega cos\varphi_\omega' + n_\omega' cos\varphi}$$

$$T_{2\omega} = 2n_{2\omega}' cos\varphi_{2\omega}, \frac{\left(n_\omega cos\varphi + n_\omega' cos\varphi_\omega'\right)\left(n_\omega' cos\varphi_\omega' + n_{2\omega}' cos\varphi_{2\omega}'\right)}{\left(n_{2\omega}' cos\varphi_{2\omega}' + n_{2\omega} cos\varphi\right)^3}$$

where n' is derived by the *Snell law* $\sin\varphi' = \frac{n}{n'}\sin\varphi$.

The crystals were mounted on a rotating stage for varying the angle of incidence of the light. The angular resolution was 0.5°. The experiment was performed at 1368 nm as fundamental wavelength. An oscillating variation of the SHG intensity vs the incident angle according to **Eq. (4.9)** was observed **(Fig. 4.10)**.

(a)

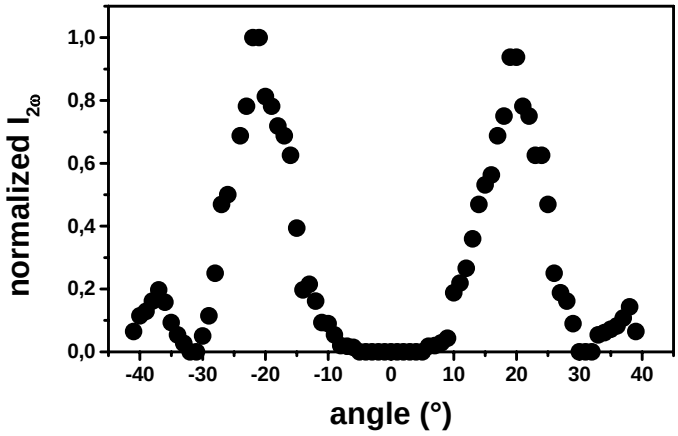

(b)

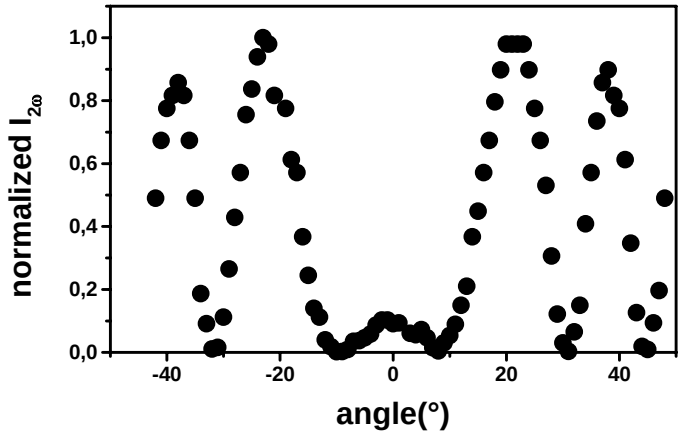

Fig. 4.10 *Maker fringes* for Quartz (010) **(a)** and $LiNbO_3$ **(b)** crystal slabs

Using the value of the refractive index for the ordinary wave at 1368 nm, n_ω = 1.530 and $n_{2\omega}$ = 1.513 for the Quartz and n_ω = 2.220 and $n_{2\omega}$ = 2.276 for $LiNbO_3$, we found for $LiNbO_3$ a nonlinear coefficient d_{22} = 6.7 pm/V (7.6 pm/V from literature). (**Saleh, 1991**) It turns out that the experimental value of nonlinear coefficient of $LiNbO_3$ agrees with *this literature value*, within 14%.

4.4.3 Poling Parameters

As previously mentioned, the films were poled at selected temperatures and times, using a wire-electrode configuration shown in **Figs. 4.2-4.3**. Poling efficiency (measured by means of *in-situ* SHG signal intensity) depends upon many parameters. Once the film was prepared, we varied all these parameters in order to obtain the best poling conditions which lead to a maximum value for SHG. As an example, we report some tests performed for each parameters on different systems, that summarize typical behavior of polymers.

Poling time

The results for polymers based on polyvinylpyridine and NLO active chromophore CuL_1 (35%), $PVPyCuL_1$35, synthesized by the chemistry group of Prof. Roviello and Prof. Centore at the University of Naples Federico II, are shown in **Fig. (4.11)** and shows an increase of SHG with time in the first 120 minutes, afterwards, the SH intensity approached a constant value, indicating that almost all chromophores in the polymer are poled to the maximum degree possible in that conditions.

(a)

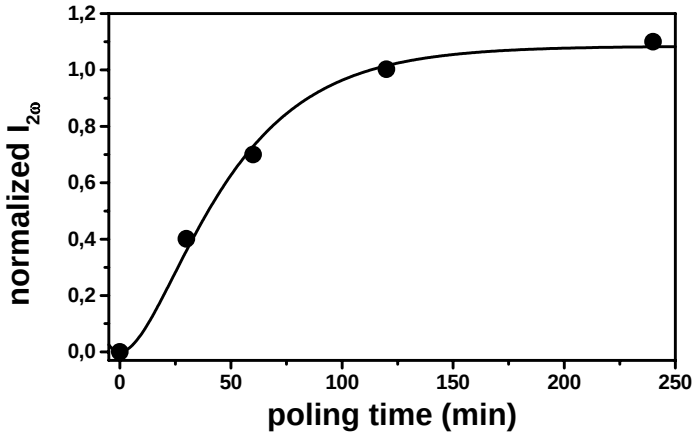

(b)

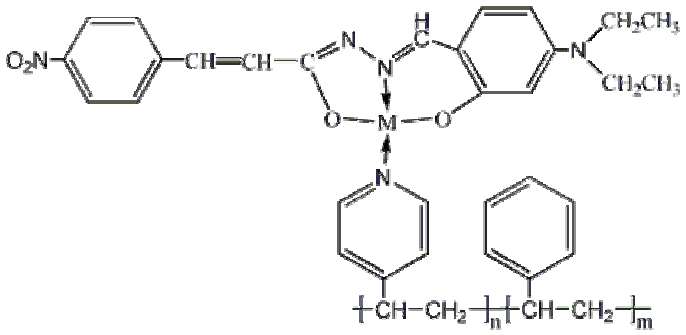

Fig. 4.11 Relationship between SH intensity and poling time **(a)** for PVPyCuL$_1$35 film **(b)**

Poling temperature

DR1-doped polysulfone (PSU) was poled at different poling temperatures (5kV/cm for 30 min), after which the films were cooled to room temperature and the SHG was measured. The results are shown in **Fig. (4.12)** and indicate that the SHG reaches a maximum value when poling temperature is close to the T_g (190°C, for PSU). Indeed, if the poling is performed at T_g or higher temperature, the efficiency of the poling strongly decreases due to the enhanced conductivity of the polymer.

(a)

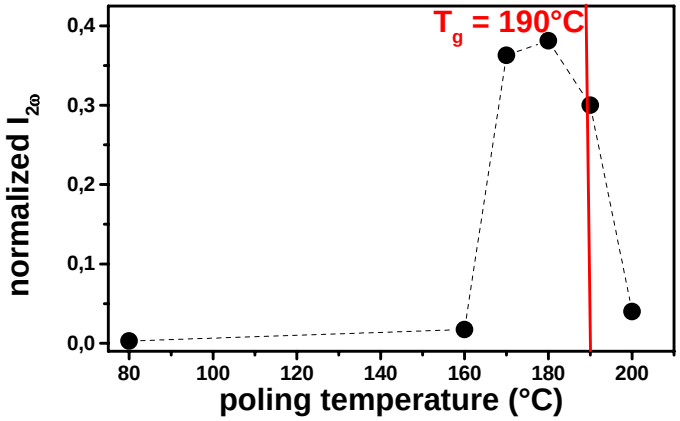

(b)

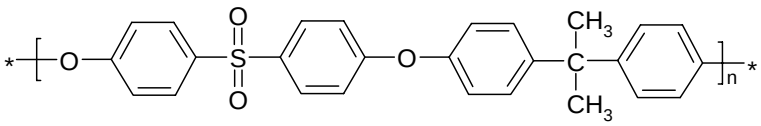

Fig. 4.12 Relationship between SHG and poling temperature **(a)** for DR1-doped PSU **(b)**

Poling electric field

Polymers based on NLO active chromophore 2-[4-(4-N,N-dihydroxyethylamino)phenylazo]-4,5-dicyanoimidazole (IMI) films, synthesized by the chemistry group of Prof. Roviello and Prof. Centore at the University of Naples Federico II, were poled at 128°C for 30 min with the applied electric field being varied from 5 to 7 kV/cm. The results are shown in **Fig. 4.13**, which indicates that the SHG intensity increases with increasing poling electric field across the film. This is due to the more chromophores aligning for the NLO activity under the applied stronger electric field. Since the films are easily damaged under too strong electric fields, in general in our experiments, it didn't exceed 7 kV/cm.

(a)

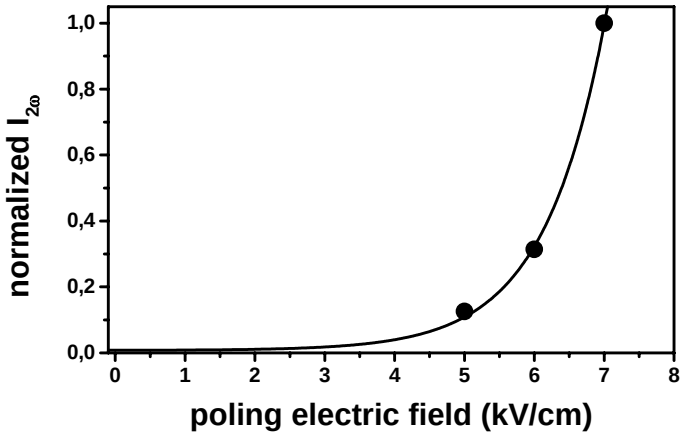

(b)

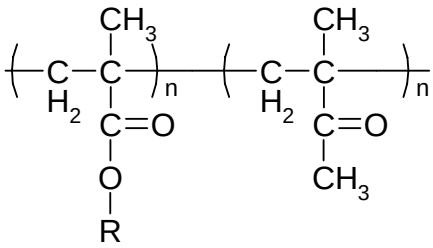

with R

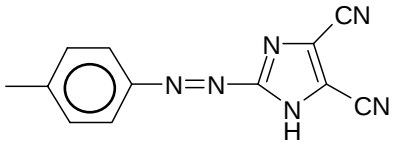

Fig. 4.13 Relationship between SHG and poling electric field **(a)** for polymer based on IMI chromophore **(b)**

4.5 All-Optical Setup

Since its first demonstration (**Osterberg, 1986**), light-induced SHG, is attracting great interest. The method consists of a seeding-type experiment. Indeed, the interference between a light wave and its coherent SH leads to a polar optical field. Owing to a nonlinear interaction, it results in the recording of a quadratic optical susceptibility $\chi^{(2)}$.

If the medium is exposed to a sum of mutually coherent optical waves with frequencies ω and 2ω, E_ω and $E_{2\omega}$, then the probability of excitation of a given molecule $P(\theta)$ is contributed from the following three terms: $a_1|E_{2\omega}|^2\cos^2\theta$, associated with one-photon absorption of SH, $a_2|E_\omega|^4\cos^4\theta$, associated with two-photon absorption of fundamental and an interference term

$a_3 | E^2_\omega E^*_{2\omega} | cos(\Delta kz+(\varphi_{2\omega}-2\varphi_\omega))Xcos^3\theta$. Here E_ω and $E_{2\omega}$ are electric fields of the optical waves. Coefficients a_1, a_2, a_3 depend on the transition dipole moment and the difference between the dipole moments in the excited and ground states. θ is the angle between polar axis and the dipole moment of the molecule, z is the propagation direction, $\Delta k = k_{2\omega}-2k_\omega$ is a wave vector mismatch and φ_ω, $\varphi_{2\omega}$ are initial phases for the fundament al and SH waves, respectively. The last term possesses a polar asymmetry and is responsible for creation of the noncentrosymmetry in an originally isotropic medium. Under polar-asymmetrical optical field $E_\omega+E_{2\omega}$ (fundamental beam plus coherent SH), the molecules with dipole moments nearly parallel to the polar axis experience *trans-cis* isomerization, that results in the *Angular Hole Burning* (AHB) and short-lived $\chi^{(2)}$ in first few seconds of poling process. However, the subsequent behavior of $\chi^{(2)}$ depends on whether the thermal *cis-trans* relaxation exists or not. In azo-systems, the reverse *cis-trans* transition results in molecular reorientation and, consequently, in the further increase of $\chi^{(2)}$ to some saturated value, comparable with that obtained with the corona method. This is because, under optimized poling conditions, there is no considerable decrease of the number of *trans* molecules, but there is only their angular redistribution. If the *trans-cis* isomerization is almost irreversible, the further pumping reduces the total number of *trans* molecules without their reorientation, so the decrease of $\chi^{(2)}$ occurs during the rest of time.

In the following model, a simplified four-level scheme of the molecular photoisomerization (**Fig. 4.14**) is applied. We suppose that the $\chi^{(2)}$ is contributed only by *trans* molecules and the first hyperpolarizability of *trans* molecule has only one nonzero component $\beta = \beta_{\Delta\Delta\Delta}$, where Δ is a given direction in the (x, y) plane of the film.

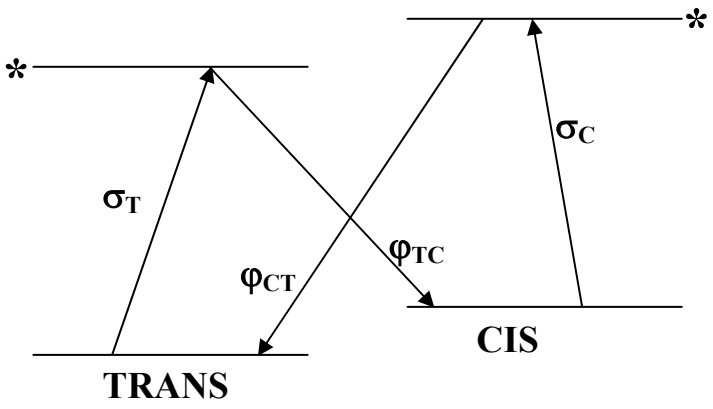

Fig. 4.14 Simplified scheme of *trans-cis* and *cis-trans* photoisomerization in the absence of thermal *cis* to *trans* relaxation. Here σ_T and σ_C are the absorption cross section of *trans* and *cis* molecules and φ_{TC} and φ_{CT} are the quantum yields for *trans-cis* and *cis-trans* transitions, respectively.

If the interaction between molecules is neglected, the general expression for $\chi^{(2)}_{\Delta\Delta\Delta}$ is then

$$\chi^{(2)}_{\Delta\Delta\Delta} = f^3 \beta \int N_T(\Omega)\cos^3\theta d\Omega \qquad \textbf{(4.14)}$$

where $f^3 = f^2_{\omega} f_{2\omega}$ is a collection of the local field factors, $N_T(\Omega)$ is a number density of *trans* molecules oriented in the direction Ω and θ is the angle between the polar axis of the poling optical field and the molecular direction Ω. In the absence of thermal *cis-trans* relaxation and the molecular reorientation, the dynamics of the *trans* population is described by the following equation

$$\frac{dN_T(\Omega)}{dt} = -N_T(\Omega)\varphi_{TC}P_T(\theta) + N_C(\Omega)\varphi_{CT}P_C(\theta) \qquad \textbf{(4.15)}$$

where $N_T(\Omega)$ and $N_C(\Omega)$ are the number densities of *trans* and *cis* molecules oriented in the Ω direction. $P_T(\theta)$ and $P_C(\theta)$ are the excitation probabilities for *trans* and *cis* molecule oriented at the angle θ, and φ_{TC} and φ_{CT} are quantum efficiencies for the *trans-cis* and *cis-trans* transitions, respectively. Taking into account that in the absence of molecular rotation $N_T(\Omega)+N_C(\Omega) = N/(4\pi)$, where N is the number density of dye molecules in original isotropic distribution, one has the following solution of **Eq. (4.15)**

$$N_T(\theta,t) = N_T(\theta,\infty) + \left(\frac{1}{2}N\sin\theta - N_T(\theta,\infty)\right)\cdot e^{\left(-\frac{t}{\tau(\theta)}\right)} \qquad \textbf{(4.16)}$$

with $N_T(\theta,\infty)=(1/2)N\sin\theta[1+\varphi_{TC}P_T(\theta)/\varphi_{CT}P_C(\theta)]^{1}$ and $\tau(\theta)=[\varphi_{CT}P_C(\theta)+\varphi_{TC}P_T(\theta)]^{1}$.

Substituting **Eq. (4.16)** into **Eq. (4.14)**, one has the temporal dependence of $\chi^{(2)}_{\Delta\Delta\Delta}$. However, the accurate integration of **Eq. (4.14)** is difficult, because the exact forms of excitation probability functions $P_T(\theta)$ and $P_C(\theta)$ are unknown. For simplicity, we suppose the polarizations of the seeding beams are parallel and seeding intensities are optimized, so $P_T(\theta) = a(\cos^2\theta+\cos^4\theta+2\cos^3\theta)$, where a is a constant which can be interpreted as one-photon excitation rate, σ_T is the absorption cross section of trans molecules parallel to the pump field at the 2ω frequency. The *cis* conformation possesses a smaller excitation probability $P_C(\theta)$ in comparison with *trans* one and, after excitation, the *cis* molecule can rotate respect to the direction of initial *trans* molecule, with a random azimuthal angle. Therefore, the absorption anisotropy for *cis* state is

reduced and we assume $P_C(\theta) = b = const$ and $b<<a$. Since the excitation probability $P_T(\theta)$ for a *trans* molecule is very different for $\theta<\pi/2$ and $\pi/2<\theta<\pi$ angles (**Fig. 4.15**), it is possible to introduce average probabilities P_{TA} and P_{TO}, for acute and obtuse angles θ, respectively.

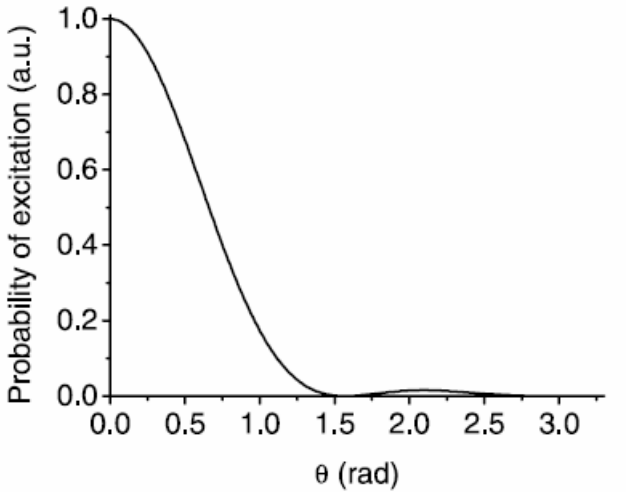

Fig. 4.15 Probability of excitation as a function of the polar angle θ under optimized poling conditions. Optimal poling conditions mean the equality of one-two-photon excitation rates and maximum value of the phase factor in the interference term if the thickness of the sample is much smaller than the coherent length l_C

In this case, the integral in **Eq. (4.14)** can be divided in two parts for acute and obtuse angle θ and the following equation can be obtained

$$\chi^{(2)}_{\Delta\Delta\Delta} = \left(f^3\beta N/8\right)\cdot\left[\left(1-B_A\right)e^{-\frac{t}{\tau_A}}+B_A\right]-\left(f^3\beta N/8\right)\cdot\left[\left(1-B_o\right)e^{-\frac{t}{\tau_o}}+B_o\right] \quad \textbf{(4.17)}$$

Here $Bj = [1+\varphi_{TC}P_{Tj}(\theta)/\varphi_{CT}b]^{-1}$ and $\tau_j = [\varphi_{CT}b+\varphi_{TC}P_{Tj}]^{-1}$ where $j = A, O$.

Eq. (4.17) approximately describes dynamics of optically induced $\chi^{(2)}$ due to the AHB mechanism in the absence of molecular reorientation. The analysis of **Eq. (4.17)** shows that in the absence of reverse *cis-trans* photoisomerization (i.e. $b = 0$) the $\chi^{(2)}$ disappears at $t = \infty$. So, the reverse *cis-trans* photoisomerization is of crucial importance for the final $\chi^{(2)}$value.

The AOP technique opens prospects that are not permitted with corona poling. In particular, orientation of molecules without a permanent dipole moment in the ground state, such as octupolar molecules has been demonstrated. (**Nunzi, 1994**)

4.5.1 Experimental Arrangement

These experiments have been performed by the candidate in the *Laboratoire POMA* at the *University of Angers*", under the supervision of Prof. J.M. Nunzi, during a two months stage in the framework of *COST P8 Action*. (**COST P8 Mission Report 2003**)

The scheme of the experimental setup is presented in **Fig.4.16**. The beam source was the Q-switched Nd:YAG laser (YG 580, Quantel) delivering 7 ns pulses at 1064 nm with 10 Hz repetition rate. A type II KDP crystal was used as frequency doubler. An half-wave plate was used to turn the polarization of the fundamental beam. A polarizer assured linear and parallel polarization of the two beams. The beams diameter was about 3.5 mm at the sample location. The experiment consisted in two alternating phases: seeding (writing) and probing (reading) (**Fig. 4.17**)

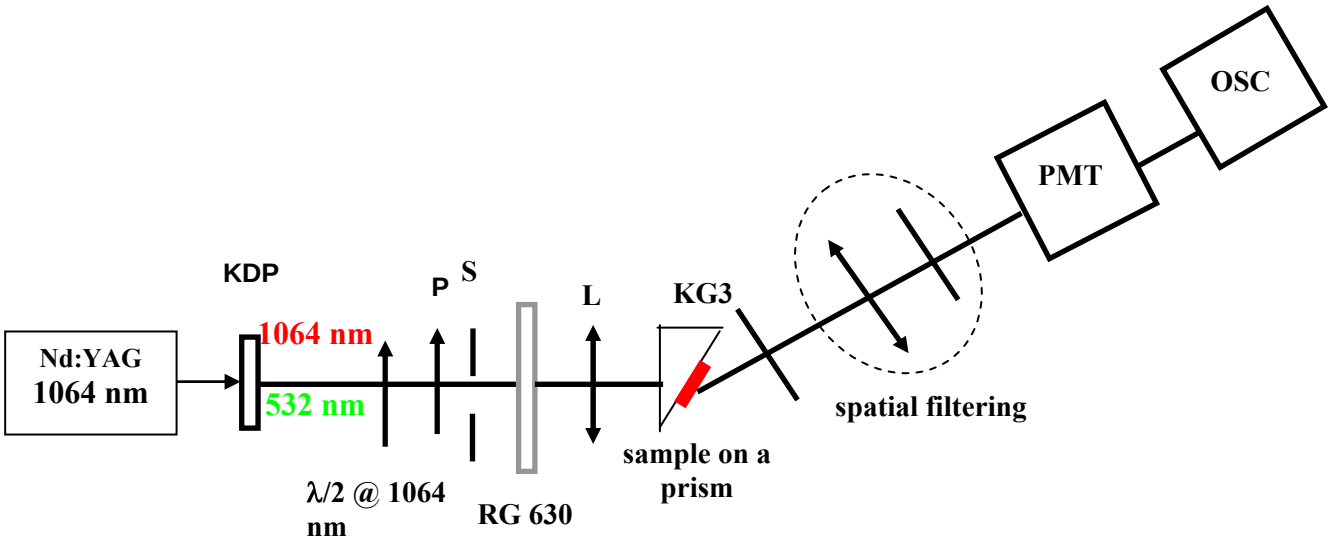

Fig. 4.16 Experimental setup for AOP. **P**-polarizer, λ/2 for 1064 nm-half wave plate at 1064 nm, RG 630-Schott green blocking filter, 3 mm thick, KG3-Schott heat blocking filter, shutter (S) was synchronized with the insertion of the red filter (Shott RG 630) which cut the 2ω beam during $\chi^{(2)}$ readout process, F spatial filter for 532 nm. The signal was detected by a photomultiplier tube (PMT) and registered on a digital oscilloscope (OSC).

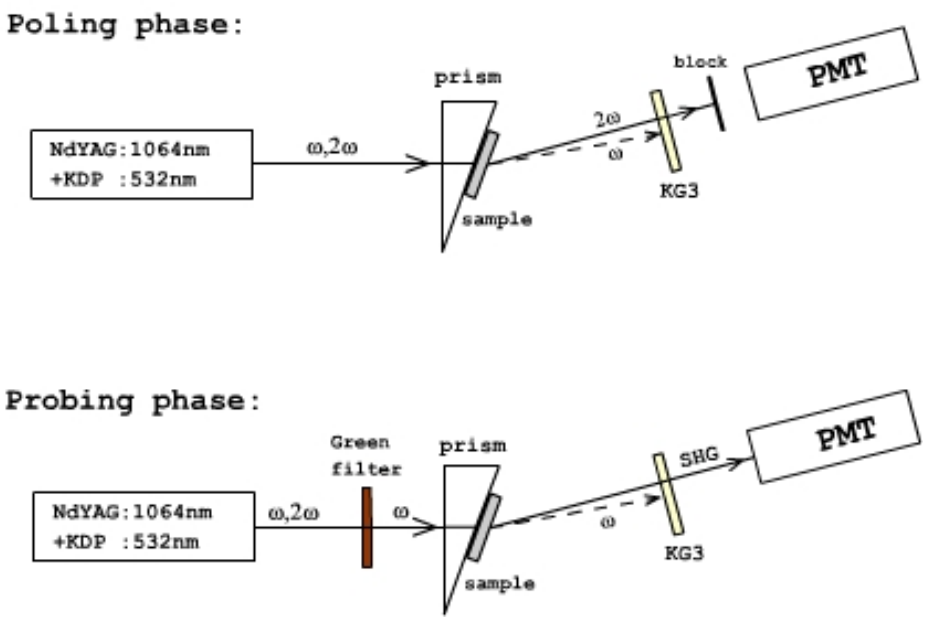

Fig. 4.17 Experimental setup. During the poling phase, fundamental and SH beams were introduced to the sample for breaking the centrosymmetry of (or inscribing $\chi^{(2)}$ to) the NLO systems. After finishing AOP, during the probing phase, only fundamental beam was introduced to the sample for reading the inscribed $\chi^{(2)}$ by SHG.

In the writing phase, both beams (**Fig. 4.17**) were co-propagating and weakly focused by a lens (**L**) onto the sample at a spot of 3.5 mm diameter. A polarizer (P) was used to ensure parallel polarization of the two beams. The photoinduced second-order susceptibility $\chi^{(2)}$ was probed by SHG inside the sample and was detected by a photomultiplier tube (PMT).

During the readout phase a red-glass filter could be inserted just after the laser output to block the 532 nm light. An interferential filter was placed in front of the photomultiplier tube to stop the infrared beam. A set of calibrated filters was used to ensure the correct scaling of the SH signal. The signal from the photomultiplier tube was measured with a digital oscilloscope (OSC). Moreover, an electronically controlled shutter was placed in front of the PMT in order to avoid the possible saturation due to the strong green seeding beam during seeding step. The fundamental beam served both as seeding and probing beam, while the SH beam was used as a seeding beam only. The influence on the efficiency of AOP of such seeding parameters as the relative phase between writing beams, their relative intensities and the beam polarization states as well as the temperature dependence has been studied by several groups. The relative phase is an important factor, particularly when the writing beams are linearly polarized. Efficient SHG requires phase matching, so the harmonic fields generated in different regions along the material interfere

constructively at the output. Experimentally, the phase difference was tuned placing the samples on an isosceles glass prism. (**Apostoluk, 2002**)

Chapter 5

Characterization of NLO Materials Oriented by Corona Poling

In this Chapter nonlinear d_{33} coefficients are evaluated and their relation with chromophore concentration are discussed for polymers and sol-gel based NLO materials. .The relaxation of poled films containing different NLO chromophores has been investigated by measuring the isothermal decay of the macroscopic nonlinear coefficient d_{33} at different temperatures below T_g, upon removal of the poling electric field. All the decay curves can be fitted by a double-exponential function. Below T_g, the slower relaxation time, τ_2, shows an Arrhenius temperature dependence. An extrapolation to room temperature allows to predict the time stability. In addition, the relationship between the stability of polar order and the T_g is discussed.

Particular care is paid in the study of hybrid sol-gel materials doped with push-pull chromophores. The microstructure modification of the matrices are investigated during the thermal treatment and the poling procedure, together with the stability of the aligned dopants.

5.1 Introduction

This thesis is mainly concerning on relaxation processes in poled composite materials. In order to study the orientational stability is important to start with a second order NLO activity as high as possible; for this reason, a preliminary study of d_{33} vs concentration was performed.

To present some general rules, we report the NLO property characterization of some methacrylate polymers containing 2-[4-(N-methyl,N-hydroxyethylamino)phenylazo]-phenyl-6-nitrobenzoxazole chromophore at different concentration (**Fig. 5.1**). The spacer between the chromophoric segment and the polymer chain was kept constant and short to reduce the number of structural differences among the polymers, excluding long and exceedingly flexible spacers that may lead to materials with low glass-transition temperatures and low short-time stability of the poled structure. (**Persico, 2003**)

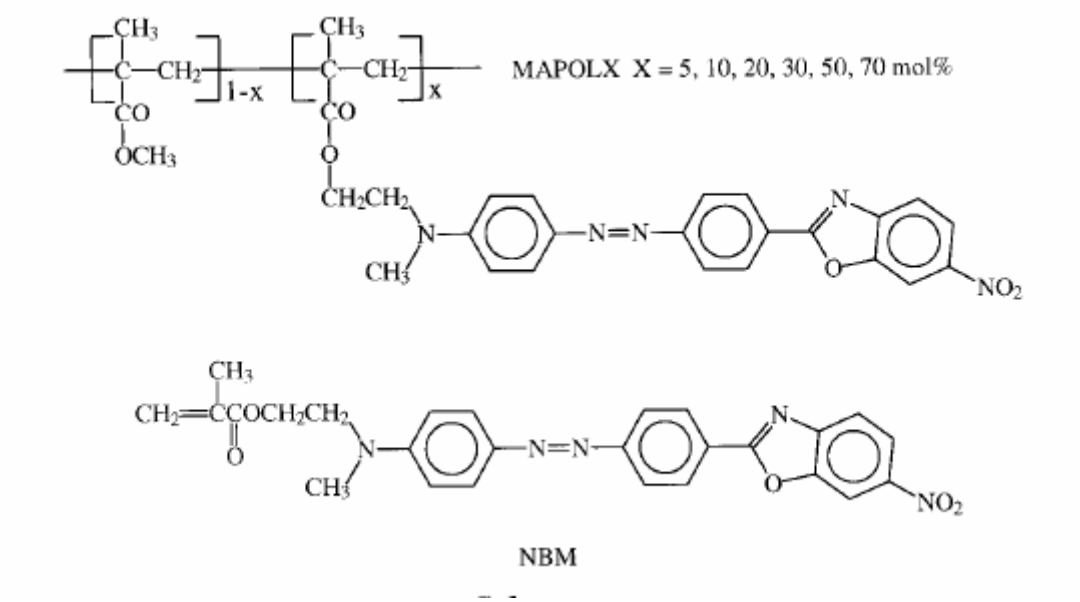

Fig. 5.1 Chromophores structures

The NLO characterization was carried out by the performance of SHG measurements on 0,3 μm-thick films. The SHG experimental setup, described in detail in **Chapter 4**, involved the fundamental beam output at λ = 1064 nm and a *Maker fringes* reference experiment was run to compare the NLO activity of the films (kept at a constant angle ≈ 27° with respect to the incidence of light) with that of a quartz crystal in order to obtain the d_{33} values of the samples.

The poling procedure was performed in nitrogen atmosphere with the gold wire biased with +7.0 kV and the poling current (≈ μA) was carefully monitored to control the efficiency of the procedure and to allow the comparison of measurements between different samples. Moreover,

using 1064 nm as fundamental wavelength, the SH is localized around 532 nm. Such wavelength is in the main chromophore absorption band as shown in the following figures. According to the two-level model, a correction was made by multiplying the SH intensity for $10^{O.D.532}$, where $O.D._{532}$ is the absorbance at 532 nm. The poling experiments were performed by the measurements of the SHG growth while the samples were first heated and held for 30 min at 100°C with the electric field on. The films were then cooled to room temperature at about 1°C/min and the electric field was switched off.

The thermal stability of all the investigated polymers is largely sufficient to safely submit films to poling conditions at temperatures close to or greater than T_g. Absorbance spectra before and after poling are reported in **Fig. 5.2** for MAPOL5 and MAPOL30. In all the spectra, the absorbance decrease after poling can be explained as a result of a partially successful orientation of the chromophore moiety.

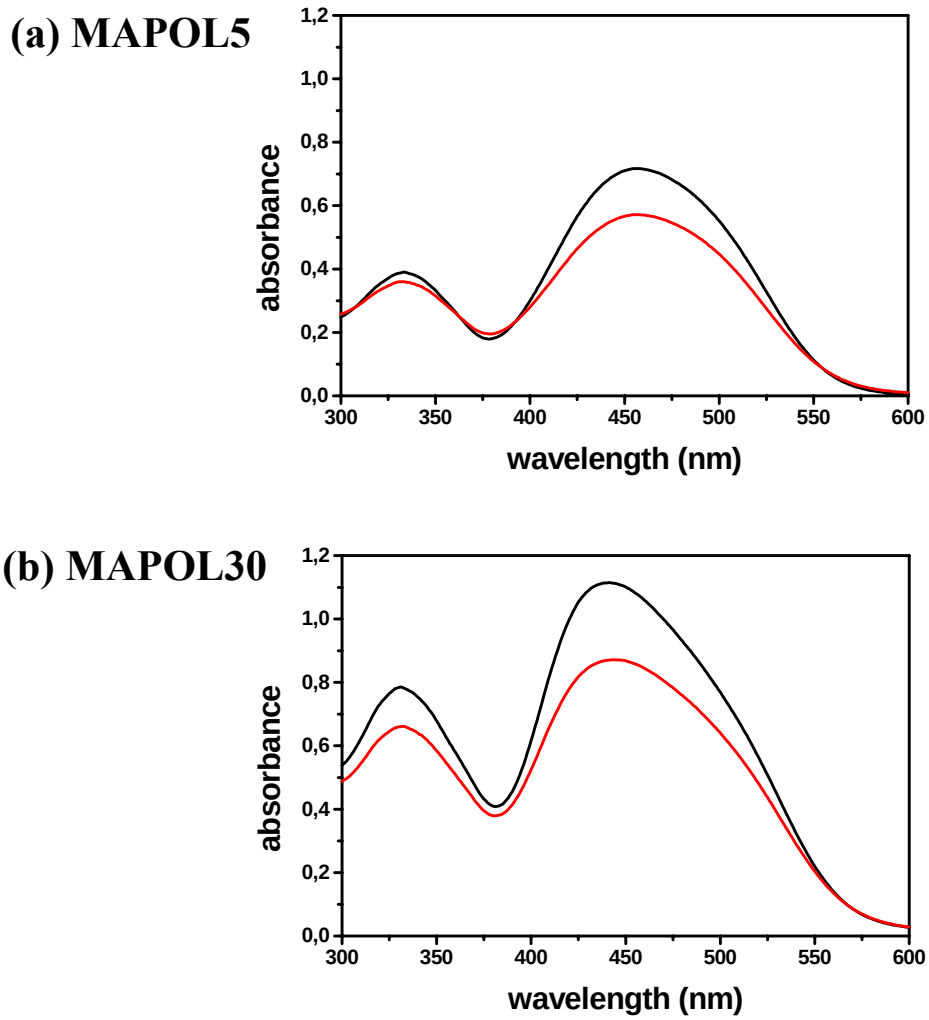

Fig. 5.2 Absorbance spectra for polymer films before poling (**black line**) and after poling (**red line**): **(a)** MAPOL5 and **(b)** MAPOL30

Some basic data concerning polymers whose NLO properties have been investigated, namely, MAPOLX (X = 5, 10, 20 or 30) are shown in **Table 5.1**, together with the obtained values of d_{33}.

Polymer	***Chromophore (experimental mol%)***	***T_d (°C)****	***T_g (°C)***	***d_{33} (pm/V)***
MAPOL5	6	300	128	40
MAPOL10	9	299	130	50
MAPOL20	17	300	130	60
MAPOL30	33	299	133	50

Table 5.1 Polymer characterization data. T_d is the chromophore decomposition temperature.

NLO coefficients increase with increasing molar contents up to X = 20. A significant decrease is measurable for X = 30. This feature has previously been observed in NLO side-chain polymers (**Harper, 1998**) and sol-gel materials (**Reyes-Esqueda, 2001**). It can be explained qualitatively by the competition of the chromophore electric field and chromophore-chromophore electrostatic interaction: the macroscopic NLO activity will increase with the number of active molecules, that is, with the molar content, but so will chromophore-chromophore interactions, leading to saturation. A simple model (**Harper, 1998**) can be derived for this behaviour; a fit of the d_{33} coefficient versus the molar content is shown in **Fig. 5.3**. This may be a case in which structural peculiarities of the polymer chain play a significant role in simplifying or hindering the chromophore poling process.

In this thesis we followed these considerations to optimize the intensity of the SH signal (i.e. d_{33}), choosing the best concentration for each material.

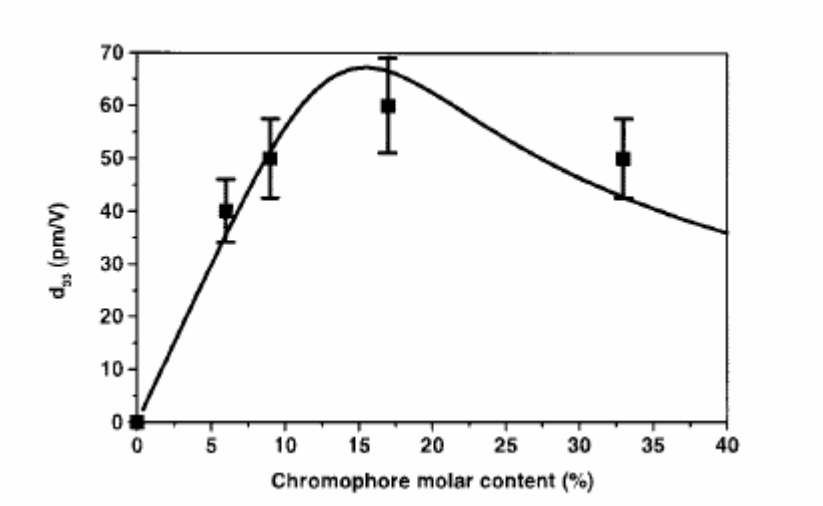

Fig. 5.3 MAPOL X d_{33} coefficient as a function of the chromophore molar content for MAPOLX

5.2 Relaxation Processes in Guest-Host Polymeric Systems

5.2.1 DR1-doped Polymer Films

Optically transparent polymers, poly(methyl methacrylate) (PMMA), poly(carbonate) (PC), polysulfone (PSU) were used as hosts. Guest molecule was Disperse Red 1 (DR1) (Aldrich Chemical Company, Inc.). Polymers and guest molecule were dissolved in chloroform at a certain concentration. The glass transition temperature T_g of the azo-dye-doped PMMA is ~114°C, that of PC is ~149°C, that of PSU is ~190°C. Polymers and chromophore structures are shown in **Fig. 5.4**. The as received polymers were dissolved in $ChCl_3$ at a concentration such to obtain samples absorbing about 1 O.D. at 532 nm. Each solution was cast by spin coating at 1200 rpm for 30 seconds and the thickness of the films was in the range of 1 μm.

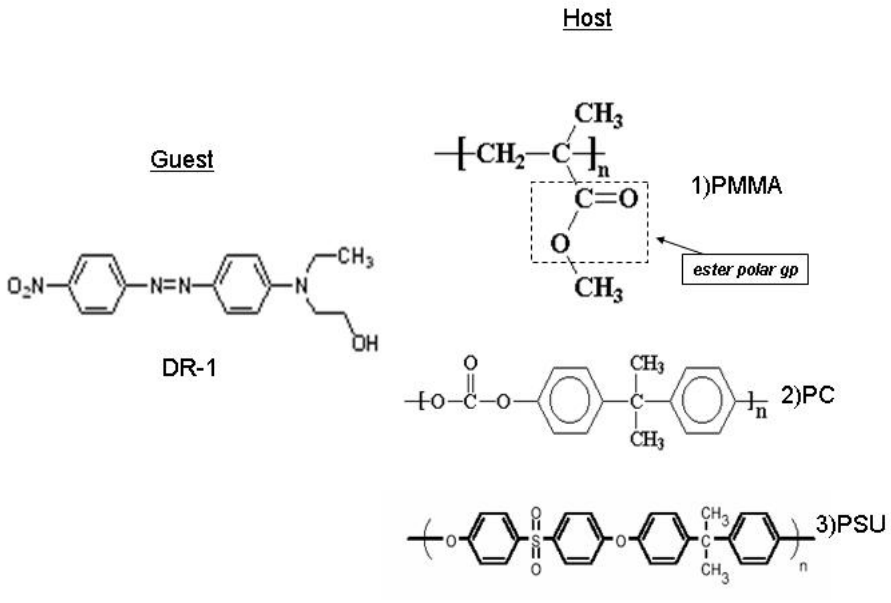

Fig. 5.4 Chemical structure of guest molecule (DR1), amorphous host polymers (poly(methyl methacrylate)-PMMA, poly(carbonate)-PC and poly(sulfone)-PSU)

For each SHG measurement, the samples were first poled at temperatures and voltage shown in **Table 5.2**, then cooled at 1°C/min and stabilized to room temperature before the SHG measurement to monitor the temporal profile of the decay. The relaxation behaviour of these films was measured using 1064 nm as fundamental wavelength.

Polymer	T_g ***(°C)***	T_{poling} ***(°C)***	t_{poling} ***(min)***	V_{poling} ***(kV)***
DR1-doped PMMA	114	80	10	5
DR1-doped PC	149	120	10	5
DR1-doped PSU	190	150	30	5

Table 5.2 Poling parameters used for DR1-doped PMMA, PC and PSU

In the case of conventional decay time evaluation method, a poled sample, together with its unpoled twin, are kept at room temperature for long time and SH intensities are monitored time by time as a measure of the residual value of NLO coefficient. However, for materials with very long decay times (of the order of years), it results hard to estimate decay time with sufficient accuracy

within a feasible time using this isothermal decay method at room temperature. In order to access at longer relaxation times, accelerated aging procedures were performed. In case of NLO systems based on chromophores in polymers, where the decrease of functionality can be correlated to dipole de-orientation (**Chapter 3**), temperature is the most important driving force. The general procedure we pursued consisted in studying isothermal decay in the temperature range 40-100°C.

Fig. 5.5 shows decays of d_{33} of DR1-doped PMMA systems at two different temperatures. As the temperature increases, the decay of d_{33} accelerates. This decay is well represented by the sum of two exponential terms

$$d_{33norm} = (1 - A) \cdot e^{\left(-\frac{t}{\tau_1}\right)} + A \cdot e^{\left(-\frac{t}{\tau_2}\right)} \qquad \textbf{(5.1)}$$

where τ_1 and τ_2 represent the time constants of faster and slower relaxation process, respectively, and A is a constant. The initial faster decay of the nonlinearities is thought to be related to the rotation of dopant molecules in polymer matrices. The slower decay process is due to thermal relaxation of the whole host-guest system. (**Suzuki, 1994**) Values of τ_1 and τ_2 from our experiments of decay time estimations at elevated temperatures are shown in **Table 5.3**.

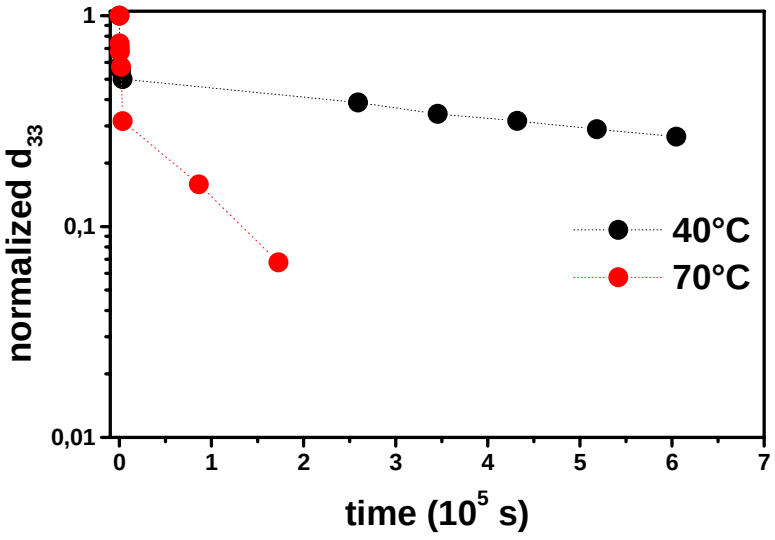

Fig. 5.5. Decays of d_{33} at elevated temperatures (DR1-doped PMMA films)

T_{baking} (°C)	τ_1 (s)	τ_2 (s)
	DR1-doped-PMMA	
40	$6\ 10^4$	$7.5\ 10^6$
70	$1.2\ 10^3$	$1\ 10^5$
100	$6.6\ 10^2$	$2.9\ 10^4$
	DR1-doped-PC	
40	$1.2\ 10^5$	$1\ 10^7$
70	$6\ 10^4$	$5.4\ 10^6$
100	$8.4\ 10^2$	$6.6\ 10^4$
	DR1-doped-PSU	
60	$3.5\ 10^5$	$2.8\ 10^7$
80	$2.2\ 10^5$	$6.4\ 10^6$
100	$3\ 10^5$	$3\ 10^6$

Table 5.3 Temperature dependencies of nonlinearities and decay time constants

As previously discussed in **Chapter 3**, the rotational diffusion model predicts a double exponential behaviour (**Eq. 3.23**) for the chromophore randomization process, with time constants ratio $\tau_2/\tau_1 = 6$. We didn't found such behaviour: the ratio τ_2/τ_1 is far from 6 as can be deduced from **Table 5.3**. Such results can be explained considering the fact that the model assumes for the two relaxation mechanism the same rotational constant D_R. This assumption is far from the reality if we consider the different nature of the two relaxation processes.

The slower relaxation times τ_2, the most important for device applications, are plotted as a function of the reciprocal temperature 1/T as shown in **Fig. 5.6**. Straight-line behaviour over this temperature range is consistent with the Arrhenius equation.

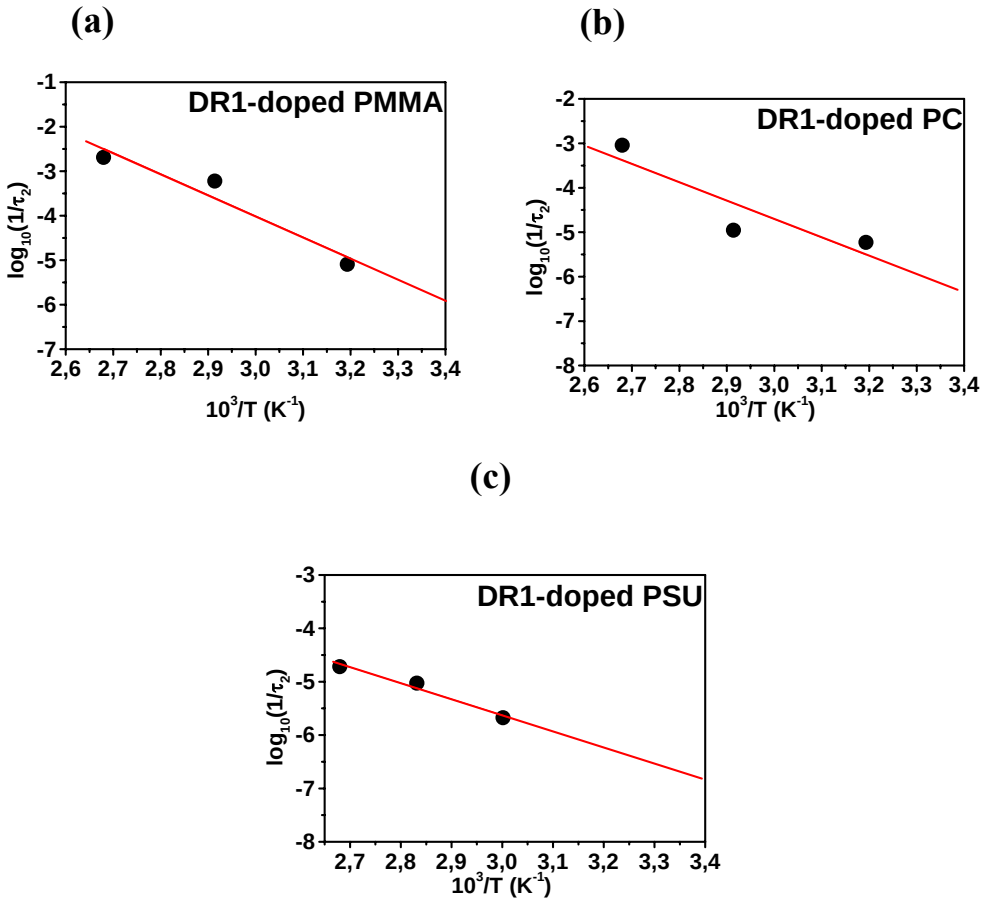

Fig. 5.6 Temperature dependencies of $1/\tau_2$ for **(a)** DR1-doped PMMA, **(b)** DR1-doped PC, **(c)** DR1-doped PSU

The decay times τ_2 of these systems can, therefore, be estimated using this method at an arbitrary temperature below T_g. The decay times τ_2 at room temperature evaluated from this Arrhenius relationship are shown in **Table 5.4**.

Polymer	***τ_2(25°C) (days)***
DR1-doped PMMA	307
DR1-doped PC	835
DR1-doped PSU	2190 (~6 years)

Table 5.4 τ_2 at 25°C estimated from decay data of nonlinearities at elevated temperatures

The time constant around room temperature of PMMA, PC and PSU systems range approximately from one to six years. In general, the host-guest systems with high T_g were understood to have long decay time leading to the consideration that thermal stability is the main factor of nonlinearity decay. However, these values are still not sufficient for electrooptic applications.

Doolittle proposed in **1951** the free-volume theory which assumes a linear dependence of the fractional free volume on temperature.

The relaxation below the T_g is primarily due to the non-equilibrium free volume associated with the finite cooling rate from the poling temperature to ambient temperature. In the conventional poling procedure, the time taken to cool the poled polymer from its poling temperature to ambient temperature is typically half an hour. To check the influence of the cooling process on the temporal stability, we included an annealing step in the poling process.

DR1-doped PSU was used to illustrate the effect of this new poling procedure on the stability. The sample was poled at around its T_g and then cooled down following the scheme shown in **Fig. 5.7**.

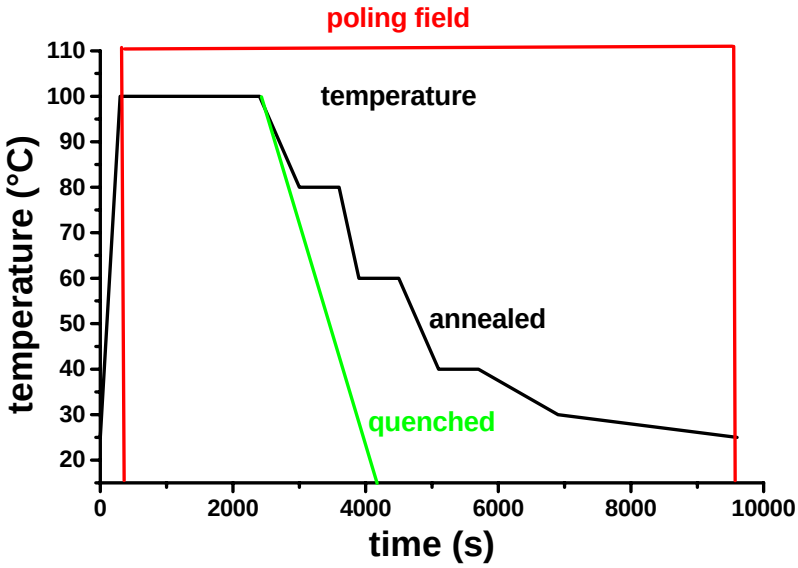

Fig. 5.7 Schematic representation of the poling procedure

The relaxations of this polymer was monitored at 80°C and compared with that of the sample which was poled without the annealing step (see previous section). A number of conclusions can be drawn from the results shown in **Table 5.5**.

Polymer	τ_1 *(s)*	τ_2 *(s)*
quenched	$2.2\ 10^5$	$6.4\ 10^6$
annealed	$9\ 10^4$	$6.5\ 10^6$

Table 5.5 Relaxation time constants of DR1-doped PSU

Beyond the initial fast relaxation, the slower relaxation part appears to be unchanged by the annealing process. So, following **Doolittle**'s theory, the initial fast decay is a result of the largest free volumes, because only this part of the relaxation seems to be affected, followed by the slower decay of the remaining "bulk" free-volumes.

5.2.2 DR19-doped Polyimide Films

The polyimide (**Fig. 5.8(a)**) was prepared by condensation of 4,4'-(1,3-phenylenedioxy)diphtalic anhydride with 4,4'-(4,4'-Isopropylidenediphenyl-1,1'-diyldioxy)dianiline by the chemistry group of Dr. Zaopo (Pirelli Labs.).

4,4'-(1,3-phenylenedioxy)diphtalic anhydride (Russian Chemical Products, 97%) was recrystallized from acetic anhydride and dried under reduced pressure at 200°C. 4,4'-(4,4'-Isopropylidenediphenyl-1,1'-diyldioxy)dianiline (Aldrich, 98%) was used as received. Acetic anhydride (Aldrich, 99+ %), dimethylformamide (Aldrich, 99.9+ %), methanol (Aldrich, 99.8+ %), 1,1,2,2-tetrachloroethane (Aldrich, 98%) and cyclohexanone (Aldrich, 99.8%) were used without further purification. The resulting polymer was triple reprecipitated from dimethylformamide solution to methanol and dried under reduced pressure at 120°C. Inherent viscosity is 0.84 dL/g in dimethylformamide at 25°C, glass transition temperature T_g is 196°C.

Guest chromophore DR19 (Aldrich, 95%) (**Fig. 5.8 (b)**) was recrystallized from ethanol and then dried under reduced pressure (mp>300°C). Thin films of active material were prepared deposing by spin-coating on Corning glass substrates solutions of polyimide and chromophore (3% w/w) in a mixture of tetrachloroethane and cycloexanone 7:3. All films were immediately baked at 80°C under reduced pressure for several hours to remove residual solvent; final thickness was about 3-4 μm

(a) Polyimide

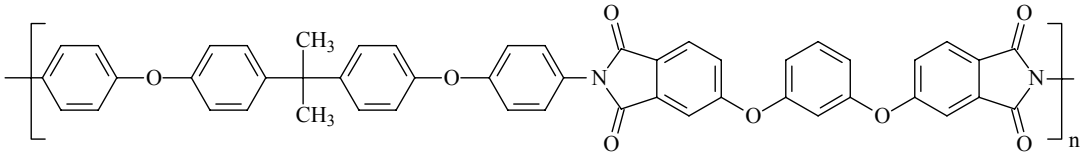

(b) DR19

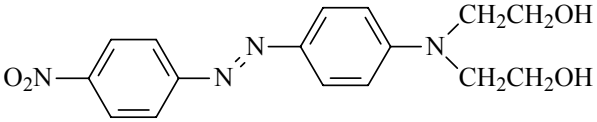

Fig.5.8 Polymer **(a)** and chromophore **(b)** used in this study

NLO characterization was carried out by performing in-situ SHG measurements using 1368 nm as fundamental wavelength. The typical poling procedure used for these samples consisted heating for 30 min at a temperature of 140°C, with the electric field on. The films were then cooled down to room temperature before the electric field was removed as shown schematically in **Fig. 5.9**. In addition, absorption spectra measurements of the films were performed before and immediately after poling procedure to estimate independently the polar order of the dipoles through the decrease of the absorption coefficients.

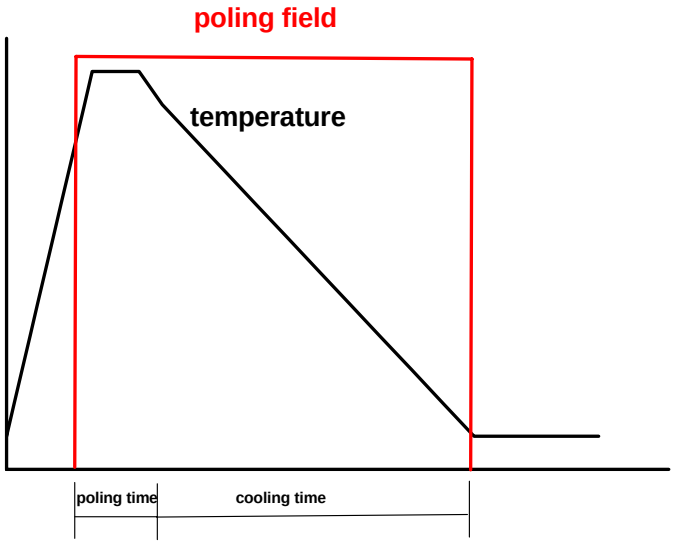

Fig. 5.9 Schematic representation of the poling procedure

The poling time at a poling temperature was determined by the minimum time required for poling equilibrium to be reached. It was minimized in order to avoid possible chemical degradation of the NLO polymer at elevated temperatures and to minimize the probability of dielectric breakdown. The SHG intensity of the poled samples was monitored for samples isothermally heated at fixed temperatures in the range of 35-100°C.

As already mentioned, the absorption spectrum of a system changes with electric field poling. The orientation degree can be expressed by the order parameter defined as:

$$\Phi = 1 - \left(\frac{A_{\perp}}{A_0} \right) \qquad \textbf{(5.2)}$$

where $A_{\perp}$ is the absorbance of a poled sample with light polarized perpendicular to the poling direction and A_0 is the absorbance of an unpoled one (measured at the peak wavelength). As already mentioned, a variety of functional decay forms have been used to describe time-dependent process in disordered systems, like the stretched exponential function or the two exponential one. In many cases it is difficult to distinguish between these two functional forms from the experimental decays alone.

In this thesis, comparing the relaxation of samples kept at different baking temperatures (**Fig. 5.10**), we have chosen to describe the relaxation behaviour by means of the two exponential model.

Values of decay time τ'_1 and τ'_2 obtained by the fitting of the decay of parameter Φ are shown in **Table 5.6**.

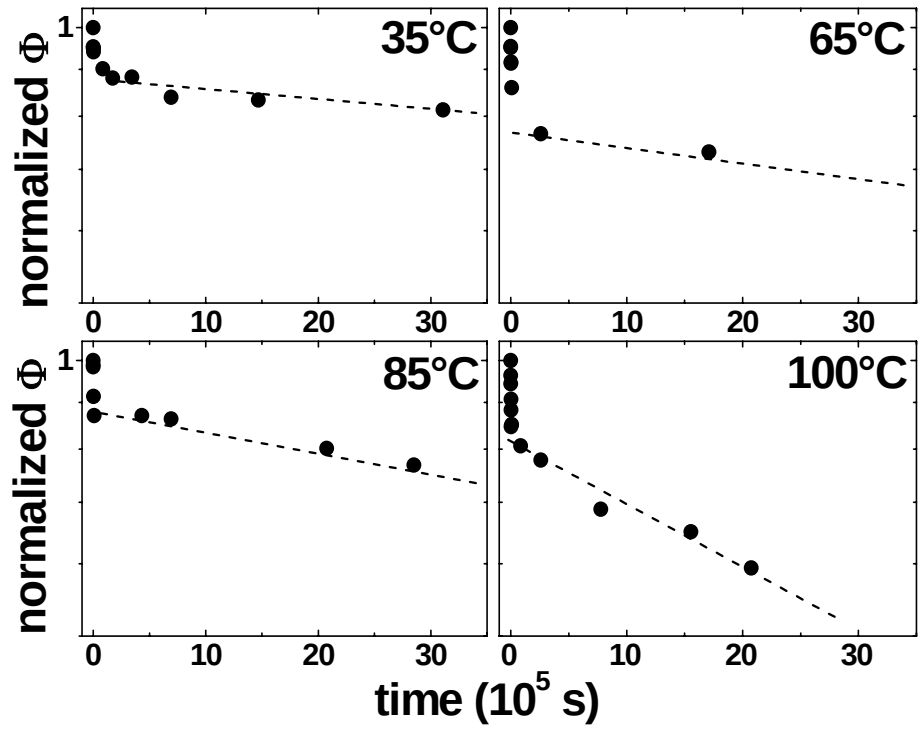

Fig. 5.10 Effect of temperature on the polar order Φ. The line is a guide for the eyes

T_{BAKING} (°C)	τ'_1 (s)	τ'_2 (s)
35	-----	----
65	$8.6\ 10^3$	$3\ 10^7$
85	$1.7\ 10^3$	$2.2\ 10^7$
100	$1.7\ 10^3$	$6\ 10^6$

Table 5.6 Relaxation time of order parameter as a function of temperature

Fig.5.11 shows decays of d_{33} at elevate temperatures for several films. The experimental decays of the second order nonlinear coefficient d_{33}, proportional to the square root of the SH intensity, can be fitted, as usual, with a double exponential function.

Isothermal decays of the SHG signal from samples stored at different temperatures in the range 35-100°C were recorded during 30 days and compared with the SHG reference signal of a Y-cut quartz in order to correct for long term fluctuation of the incident laser power. Values of τ_1 and

τ_2 of decay time estimations are shown in **Table 5.7**. As the temperature increases, the decay of nonlinear d_{33} accelerates.

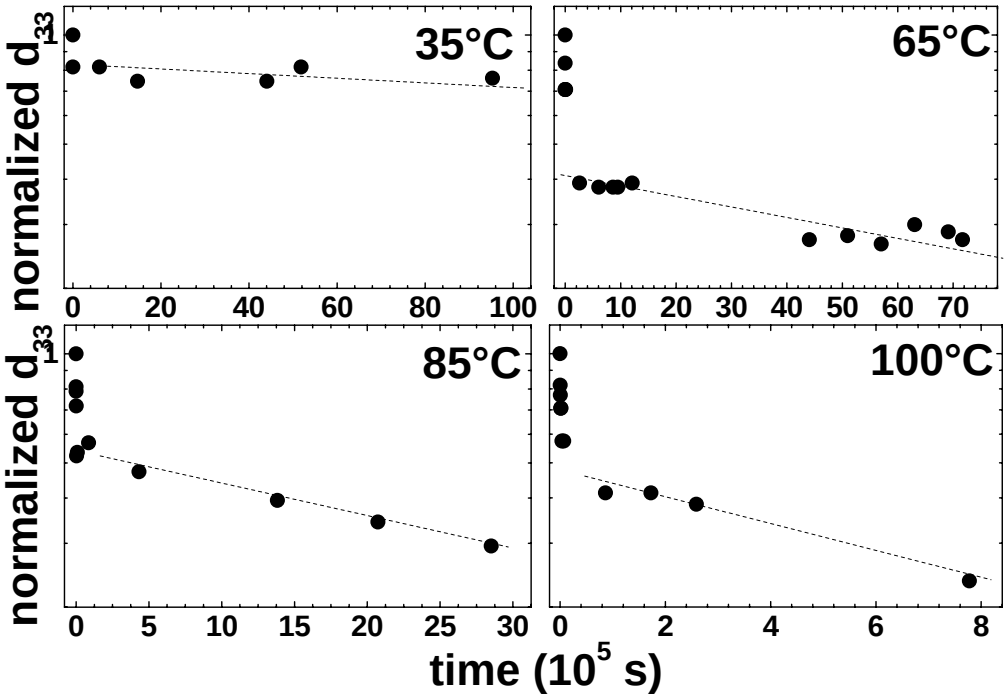

Fig. 5.11 Decay of normalized nonlinear coefficient d_{33} at four different temperatures. The line is a guide for the eyes

T_{BAKING} (°C)	τ_1 (s)	τ_2 (s)
35	--	--
65	$4.3\ 10^3$	$1.5\ 10^7$
85	$8.4\ 10^2$	$4.4\ 10^6$
100	$8.4\ 10^2$	$7.8\ 10^5$

Table 5.7 Relaxation time of d_{33} as a function of temperature

These results indicate that polar order decay is slower than decay of second order nonlinear effects such as SHG in disagreement with theorical studies. (**Wu, 1991**); this difference in decay times is much evident with increasing baking temperature, as can be noted comparing **Table 5.6** with **5.7**. Such studies predict that the linear properties decay in time with a single decay constant and assume

for linear and nonlinear relaxation phenomena the same diffusion constant D_R. We believe that the discrepancy with the experimental data belong from this assumptions as already discussed in **Section 5.2.1** for the τ_2/τ_1 ratio.

Assuming that the Arrhenius relationship holds between the decay probability $1/\tau_2$ and the inverse temperature 1/T, a τ_2 value at room temperature of 31 years can be predicted (**Fig 5.12**). Such a value is very long compared with the PMMA systems. The high T_g of the matrix, 196°C, about 100° higher than polymethylmetacrylate and its dimension, play a crucial role in this excellent time stability. Moreover, retaining of the orientation induced by poling is preserved by formation of hydrogen bonds between the two hydroxyethyl functionalities of DR19 and 1,3-phenylenedioxy moieties of the polymer chain. Indeed, the origin of the polar stability lies in the fact that considerable segmental motion in the polymer backbone is necessary if it is to move. This motion of the polymer chain is therefore severely restricted if the chromophores are attached to it via hydrogen bonding.

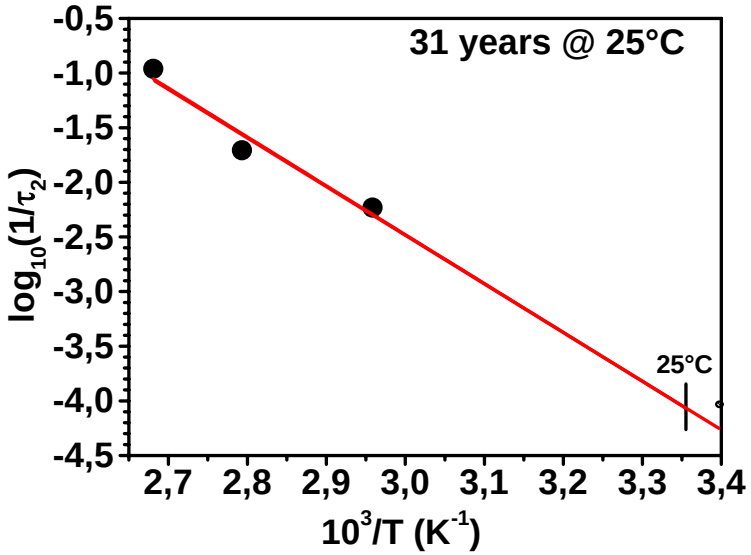

Fig. 5.12 Temperature dependence of the relaxation time τ_2

5.3 Relaxation Processes in Chemical Bounded Polymeric Systems

5.3.1 Side-Chain IMI/BZI-based Films

In this section we report the NLO behaviour of some homopolymers based on the two chromophores shown in Fig. **5.13**.

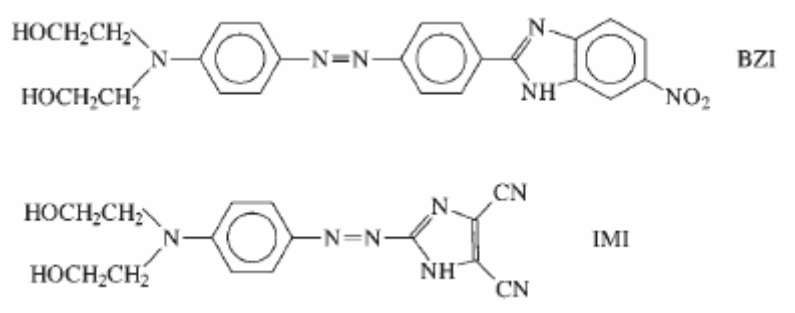

Fig. 5.13 BZI and IMI chromophores

Both chromophores contain good hydrogen bonding donor and acceptor groups within the NLO active unit. We note that few reports found in the literature about polymers based on benzimidazole-containing chromophores all deal with 1-alkyl-5-nitrobenzimidazole isomers, which are less NLO active as it was proved both theoretically and experimentally (**Carella, 2004**) and which lack the hydrogen bonding donor group. Both chromophores show good chemical stability and moderately good second order molecular nonlinearity, as measured by the EFISH technique (**Carella, 2004**) (see **Table 5.8**).

Chromophore	$\beta\mu^{(a)}$ ***(10^{-48} esu)***	$\lambda max^{(b)}$***(nm)***
BZI	940	472
IMI	1050	462

(a) measured by the EFISH technique in DMF at 1907 nm

(b) measured in DMF

Table 5.8 NLO properties of chromophores

Starting from these new chromophores, the polymers shown in **Fig. 5.14** were synthesized by the chemistry group of Prof. Roviello and Prof. Centore.

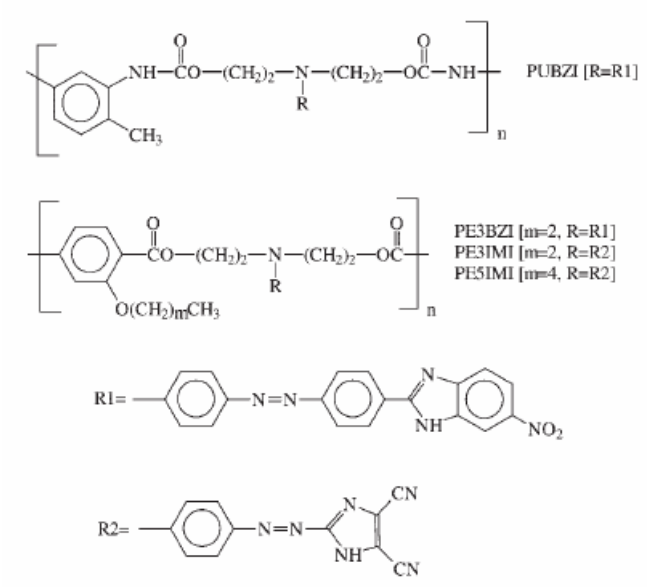

Fig. 5.14 Polymers synthesized from chromophores

NLO characterization was carried out by performing SHG measurements on 0,1 μm thick films deposited on BK7 Corning glass slides by spin coating. For this purpose, appropriate amounts of the polymers were dissolved in *N*-methyl-2-pyrrolidone (NMP) and the solution was filtered on 0,20 μm Teflon filters. The spinner operated at 1000 rpm for 30 s at room temperature. Residual solvent was removed by keeping the films at 100°C under a vacuum.

Some thermal and analytical data of the polymers under investigation are reported in **Table 5.9**. The time stability of the NLO activity of poled polymers has been studied by means of the accelerated ageing test. Poled films of all polymers were kept in a oven at three different temperatures (35, 65 and 85°C) and their d_{33} values were periodically measured at 1368 nm (utilizing the same procedure described previously) over a period of 60 days. For each oriented sample, the same thermal treatment was also performed on a non-oriented film and its UV-Vis spectrum periodically recorded. These showed no change which allowed us to exclude chemical degradation of the material due to the thermal treatment. In **Fig. 5.15** we report, as an example, the time behaviour of the normalized d_{33} coefficient of PE5IMI at two different baking temperatures.

Sample	T_g *(°C)*	T_d *(°C)*	T_{poling} *(°C)*	d_{33} *(pm/V)*
PUBZI	188	291	180	4.0
PE3BZI	152	285	140	3.5
PE3IMI	152	305	140	2.0
PE5IMI	131	291	120	1.8

Table 5.9 Thermal, analytical and NLO data of polymers

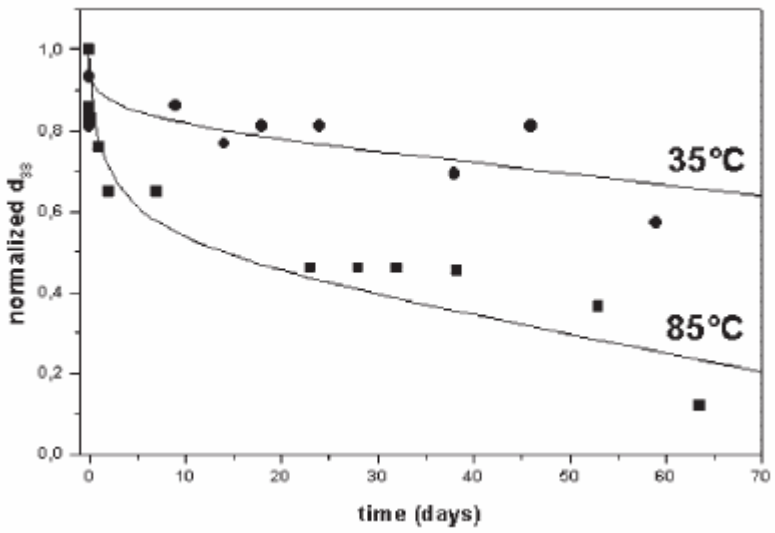

Fig. 5.15 Plot of normalized d_{33} vs time for PE5IMI at 35°C (circles) and 85°C (squares)

For all samples, the time decay of normalized d_{33} is compatible with a bi-exponential fit. Relaxation times at room temperature were calculated through the Arrhenius-type fit and the τ_2 values extrapolated to 25°C for all the polymers are reported in **Table 5.10**.

Polymer	τ_2 *(25°C) (days)*
PUBZI	1040
PE3BZI	370
PE3IMI	440
PE5IMI	280

Table 5.10 Extrapolated τ_2's at 25°C

Actually, although the correlation between the extrapolated τ_2's and the T_g of the polymers is clear (see **Tables 5.9**, **5.10** and **Fig. 5.16**), the presence of hydrogen bonding donor/acceptor groups in the chromophore unit seems to play an additional, and in some cases predominant, role if we consider that the glass transition temperatures of the polymers are not particularly high and if their behaviour is compared with similar polymers but based on chromophores lacking donor H bonding groups, for which relaxation times far lower have been reported. (**Chang, 1997, Choi, 2001**)

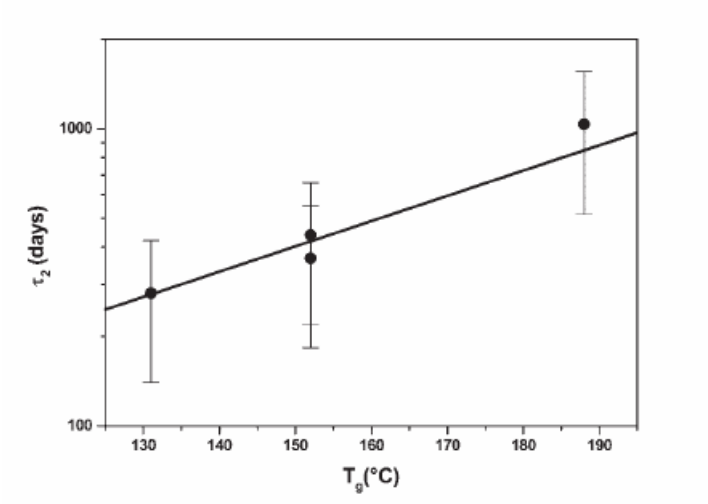

Fig. 5.16 Semilogarithmic plot of τ_2 extrapolated at 25°C versus the T_g of polymers

5.4 Relaxation Processes in Sol-Gel-based Systems

Silica films doped with different nonlinear chromophores were prepared in collaboration with the Material Sector of the Mechanical Engineering Department (Dr. Brusatin and Dr. Della Giustina, University of Padova). **Table 5.11** shows the structures and properties of the compounds used for the starting solution.

Name	*Chemical structure*	*Molecular weight*
GPTMS	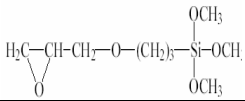	236.34
GPDMMS	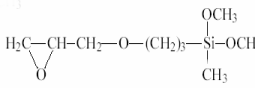	220.34
AEAPTMS	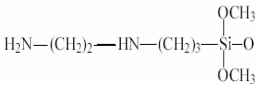	226.36
TEOS	$(CH_3\text{-}CH_2\text{-}O)_4Si$	208.33
ACN	$CH_3\text{-}C\equiv N$	41.05
MeOH	$CH_3\text{-}OH$	32.04
MeOEtOH	$CH_3\text{-}O\text{-}CH_2CH_2OH$	76.09

Table 5.11 Sol-gel precursors structures and solvents used to prepare sol-gel starting solution of hybrid films doped with organic nonlinear chromophores.

For these samples, infrared absorption spectra in the range 4000-500 cm^{-1} were recorded by Fourier Transform IR spectroscopy (FTIR) (Perkin-Elmer 2000), with a resolution of ±1 cm^{-1}, on film deposited on silicon substrates.

From the FTIR spectra we can have informations on the intensity of following main peaks:

- Si-O-Si bond @ 1070 cm^{-1}
- epoxy ring @ 3060 cm^{-1}
- Si-OH bond @ 910-950 cm^{-1}
- OH group @ 3400 cm^{-1}
- $R^*\text{-}CH_2\text{-}NR_2$ bond @ 1472 cm^{-1}
- Si-O-Me** or Si-O-Et @ 2900-3000 cm^{-1}

* R = Radicals

** Me = Methanol

5.4.1 Hybrid Matrices

GTA48

Hybrid sol-gel materials were prepared as shown in **Fig. 5.17**: TEOS, GPTMS (Aldrich) were co-hydrolized in MeOH 4 hours under reflux at 80°C, with molar ratios MeOH:Si = 1,7, GPTMS: TEOS = 7:3, H_2O:(TEOS+GPTMS) = 1,65. The use of TMESPE modifies the inorganic SiO_2 network via amine moieties and at the same time determines a basic catalyst of the sol. The basic environment used to prepared these hybrid sols, avoids the chemical degradation of this chromophore normally observed in an acidic media. After 20 min stirring at room temperature, the sol was ready for film deposition or doping with the organic chromophores.

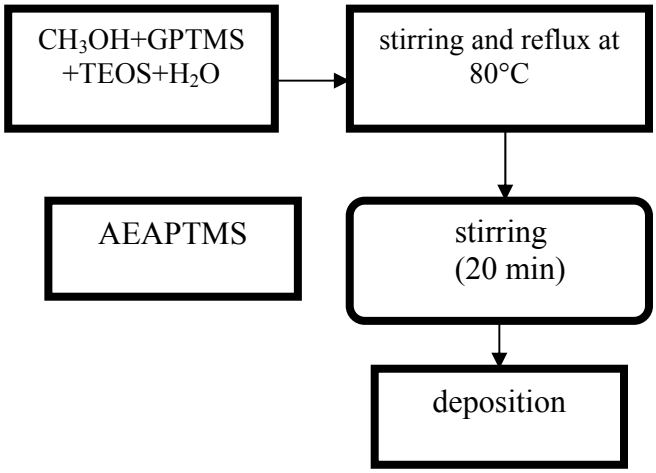

Fig. 5.17 Flowchart for preparation of GTA48 matrix

GdA40NaOH

For preparing the solution to fabricate the thin films, AEAPTMS was added to GPDMMS in the molar ratio AEAPTMS: GPDMMS = 0,4. The solution was stirred for 5 min and then H_2O was added (H_2O/ GPDMMS = 1 and H_2O/AEAPTMS = 1,5). For hydrolysis, NaOH and MeOH were added during stirring, as shown schematically in **Fig. 5.18**.

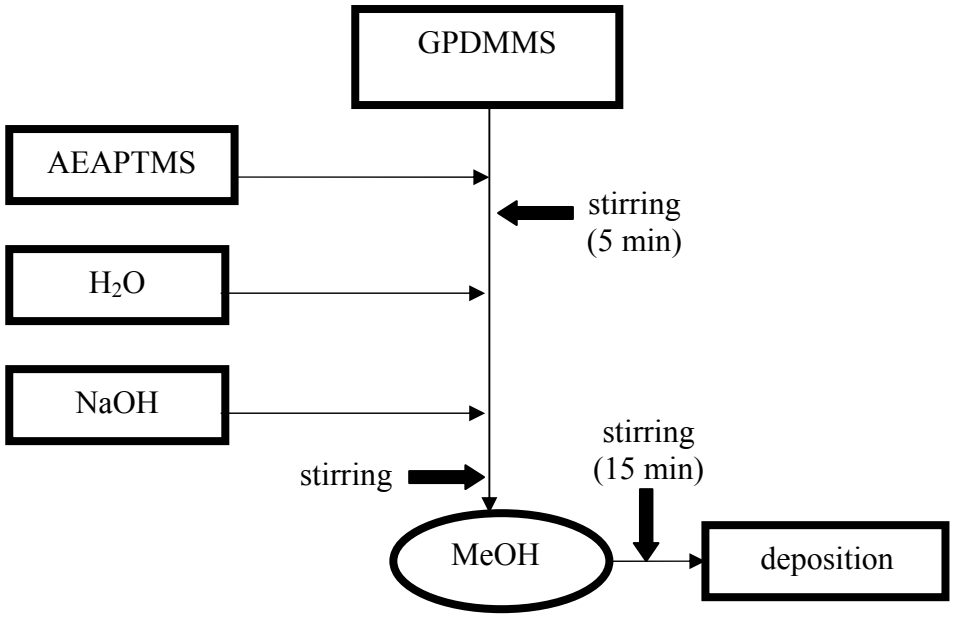

Fig. 5.18 Flowchart for preparation of GdA40NaOH matrix

5.4.2 BisOHPETCN in GTA48

After 20 min stirring at room temperature the GTA48 sol was ready for film deposition and doping with BisOHPETCN (synthesized by the group of Prof. Pagani at the University of Milano "Bicocca") and hydroxyethylcarbazole (CbOH) dissolved in 2MeOEtOH (**Fig. 5.19**) (**Brusatin, 2004**)

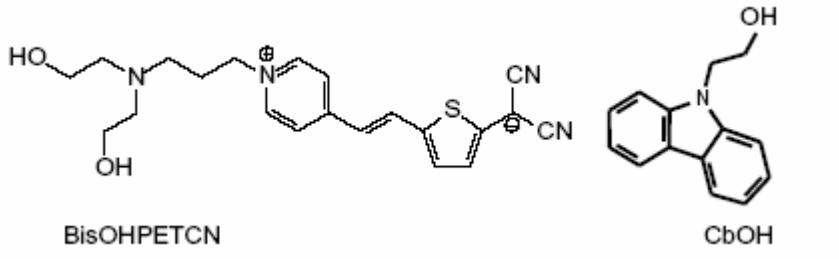

Fig. 5.19 Dihydroxy functionalized chromophore BisOHPETCN and CbOH

Both molecules were functionalized with OH groups to permit chemical bound with the sol-gel matrix and larger solubilities in the sol. The amount of BisOHPETCN was indicated by the molar ratio BisOHPETCN:Si = 0.20 and in this case film co-doped with CbOH were prepared, with BisOHPETCN/CbOH = 0.4. Films (3 μm thick) were deposited by spinning on Corning microscope

slides and then dried at 70°C under vacuum. **Fig. 5.20** reports absorption spectra of a dried doped film. In the spectra the broad intense absorption band due to BisOHPETCN Intramolecular Charge Transfer (ICT) is clearly visible, peaked around 620 nm. The spectrum shows also an intense absorption at 330-340 nm, characteristic of the carbazole molecules, which disappears after treatment at 140°C. The band at 380 nm is probably due to the presence of degraded species, while the presence of chromophore clusters is ruled out, because their absorption would be found around 430 nm. It was noted that introducing CbOH units strongly reduce the chromophore aggregation that would occur at this concentration, allowing the achieve higher chromophore loadings with a good dispersion within the matrix.

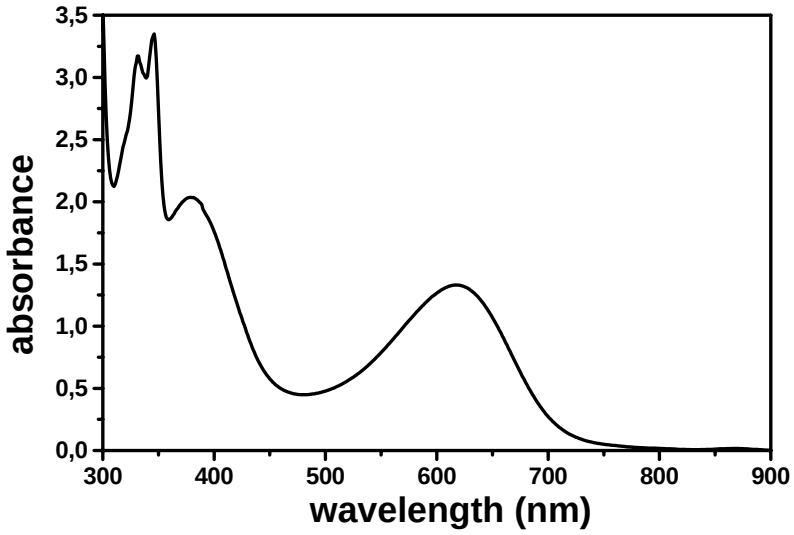

Fig. 5.20 Absorption spectra of hybrid films doped with BisOHPETCN (20%)/CbOH

In general, the thermal treatment of the solid hybrid material should determine the progress of the inorganic condensation reaction inside the sol-gel film. This was evident from the decrease of the band at 3380 cm^{-1} at 140°C of the bonded OH (molecular water bounded to the silica surface of hydrogen bonded hydroxyl groups) in the IR spectra; indicating a progressive condensation of residues silanols. Moreover, in the case of these specific matrices containing amine moieties and epoxy groups, during the thermal treatment and poling procedure the progress of the coupling reaction between amine and epoxy groups occurs (**Fig. 5.21**), enhancing the network crosslinking of the structure.

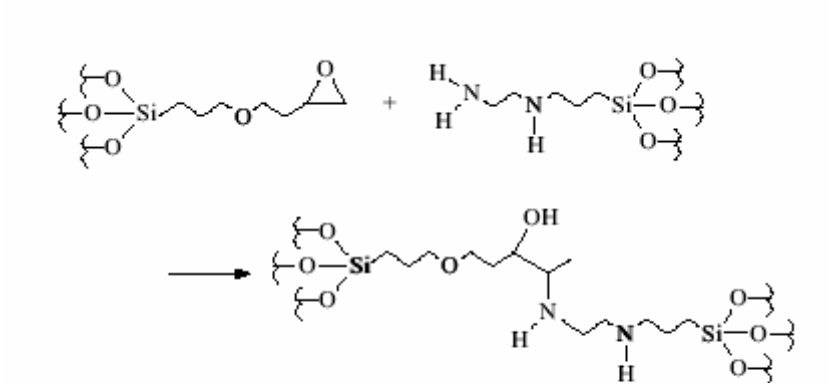

Fig. 5.21 The coupling reaction between the residual amines and epoxy rings

Following these informations, we optimized the poling parameters. Poling process was performed at increasing temperature until 120°C at 6 kV in nitrogen atmosphere, because a BisOHPETCN degradation was expected at 140°C (**Fig. 5.22**).

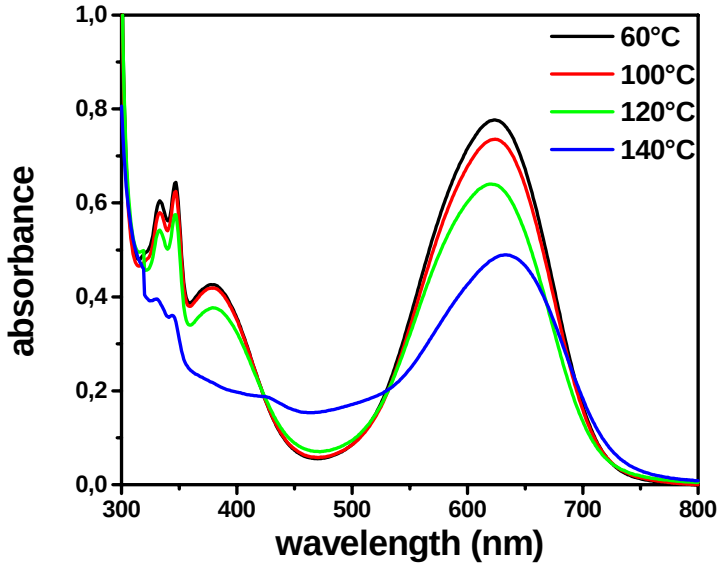

Fig. 5.22 UV-Vis absorption spectra of BisOHPETCN/CbOH-GTA48 films at different temperatures

Poling for lower times and temperatures was ineffective. The orientation efficiency suddenly increased after 2 hours poling and its effect was probably due to the elimination of free charges that were produced from the completion of sol-gel condensation reactions in the hybrid film due to the

thermal treatment. The presence of these charges decreased the electrostatic field intensity and prevented them to orientate the chromophore dipoles. The temperature effect is particularly important in the presence of the CbOH molecules. In fact, lower poling temperatures are necessary to observe SHG signals if the films were not co-doped with carbazole molecules. In this case it is probably that chromophore orientation is effective only after the spacers degradation i.e. when CbOH units are not influencing the chromophores dipoles. This degradation is almost completed at 120°C, as it can be seen from the UV-Vis spectra of **Figs. 5.22** and **5.23**.

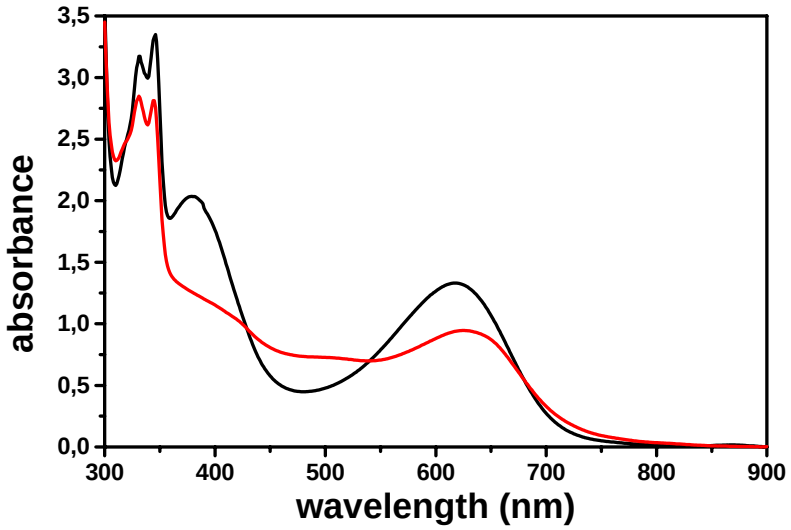

Fig. 5.23 Absorption spectra of hybrid doped films before (**black line**) and after (**red line**) poling

An intense SHG signal was revealed only after 2 hours. **Fig. 5.24** shows that after poling off, the SHG immediately broke down at a lower but stable and still high values. BisOHPETCN was not damaged during the poling treatment, because the main ICT absorption band of the chromophore was maintained as shown in **Fig. 5.23** and an order parameter Φ of 0.29 was calculated.

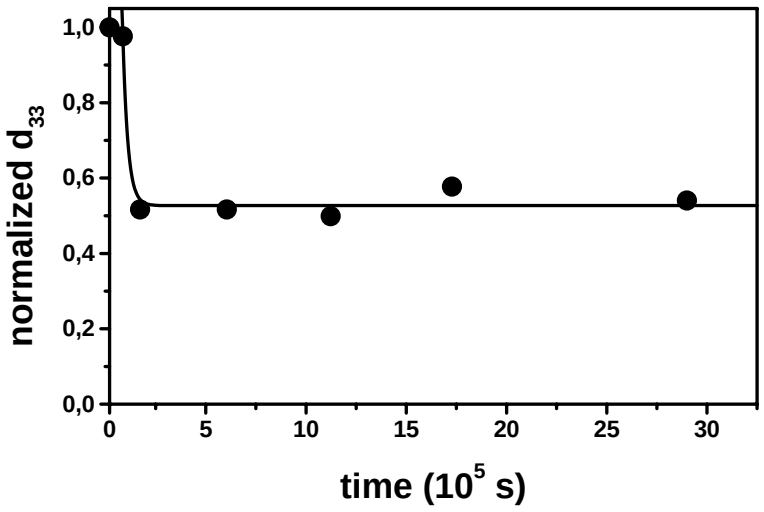

Fig. 5.24 Evolution of the nonlinear coefficient d_{33} at room temperature after poling off

In sol-gel systems, accelerated tests using temperature as degrading agent are ineffective because baking temperature helps the condensation reaction to take place, thus blocking the alignment of the chromophore dipoles. The main consequence of the network condensation normally observed in sol-gel materials is on the chromophore orientation time stability, that was found to be excellent in this poled system. The inorganic condensation is decisive for time stability of chromophore orientation being an indication of the increase of the network densification and rigidity during the thermal treatment. For these reasons we followed the orientational decay at room temperature.

As can be noted from the previous graph, there are also in this case two relaxation mechanisms with no long-term relaxation. This result is very encouraging. Experiments have shown that these systems can effectively freeze the aligned chromophores due to the material properties. In fact, the hybrid sol-gel has inorganic networks, which have a more rigid structure than organic polymers and, hence, can reduce the relaxation of the aligned chromophore molecules.

The NLO coefficient value, 9 pm/V, was found for incident light at 1368 nm where the refractive indices at 1368 and 684 nm are 1.554 and 1.593, respectively.

5.4.3 DR19 in GTA48

Hybrid materials containing nonlinear DR19 and carbazole pendant groups (Aldrich) were also synthesized. Samples were obtained using 2MeOEtOH as solvent, with the following molar ratio:

DR19/CbOH:Si = 0.35. Films (3 μm thick) were deposited on glass slides and then dried at 70°C under vacuum.

For this experiment, we poled the sample at 6 kV reaching a maximum temperature of 140°C because no damage was observed until 150°C in the chromophore absorption band of an unpoled sample cured at different temperatures (**Fig. 5.25**). Also in this case, a SHG signal was observed after almost two hours of poling, as shown in **Fig. 5.26 (a)**.

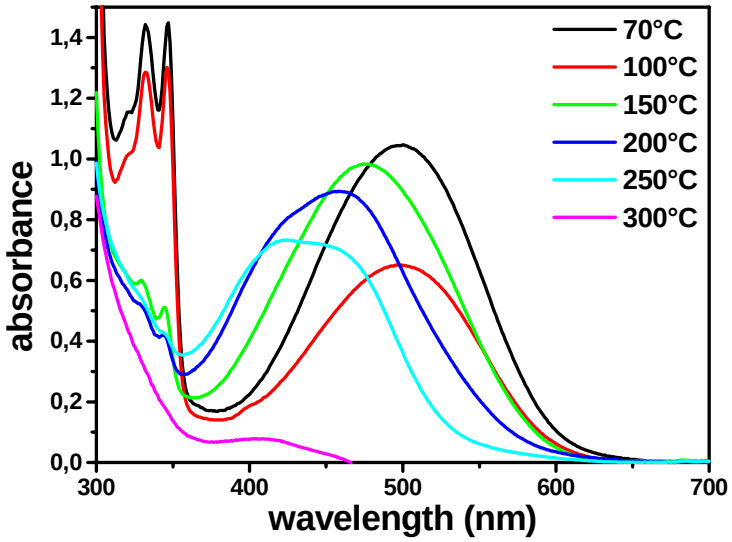

Fig. 5.25 UV-Vis absorption spectra of DR19/CbOH-GTA48 cured at different temperatures

(a)

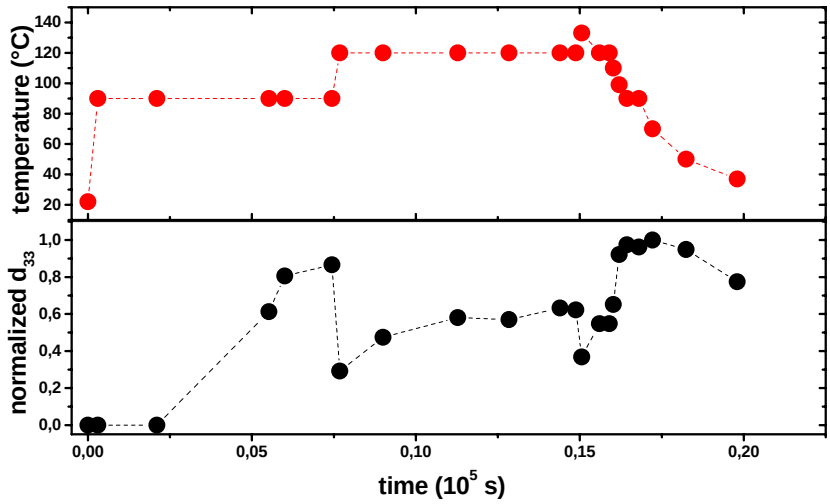

(b)

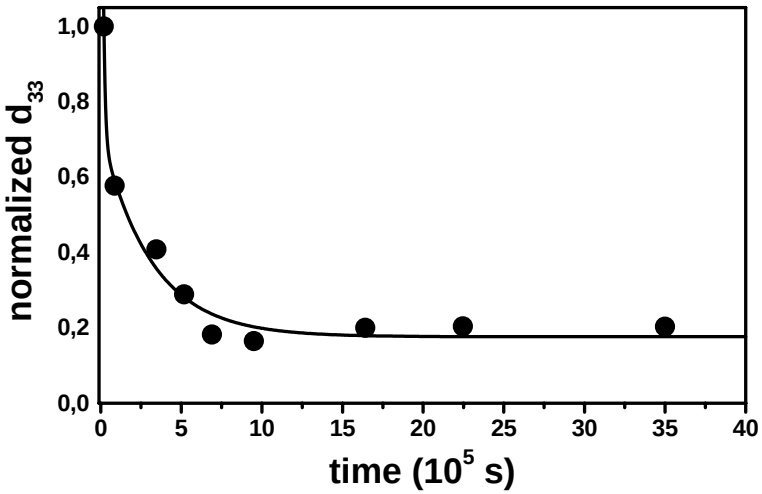

Fig. 5.26 Temporal behaviour of the nonlinear coefficient d_{33} of DR19/CbOH-GTA48 film. **(a)** growth and **(b)** decay

During the poling a reduction of intensity of the SHG signal with increasing temperature of the film took place. This is a typical behaviour of these materials which denotes that the local free volume surrounding each chromophore is still "liquid-like". This feature was confirmed by switching off the voltage during poling procedure. The signal was observed to drop instantaneously and to recover when the voltage was switched on again.

The NLO coefficient value, 6 pm/V was evaluated at 1368 nm, by considering n(@1368 nm) = 1.562 and n(@684 nm) = 1.590, estimated from ellipsometric measurements and an order parameter $\Phi = 0.20$ estimated from absorbance spectra shown in **Fig. 5.27**.

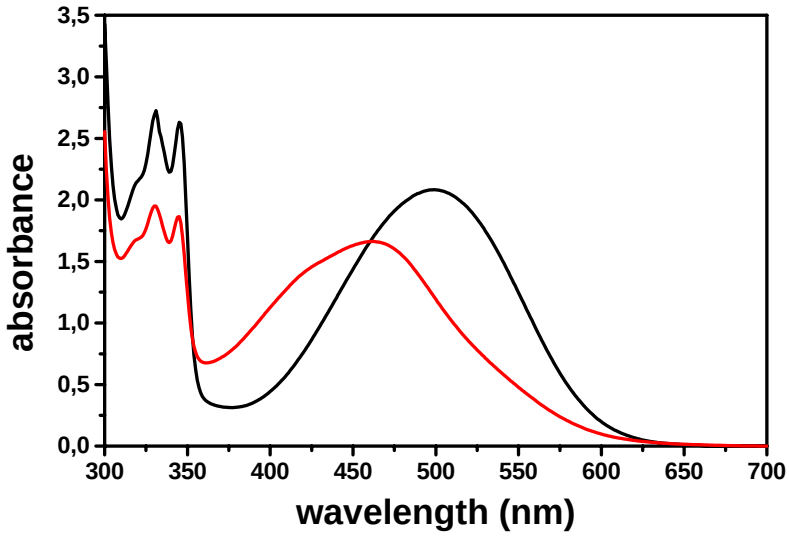

Fig. 5.27 UV-Vis absorption spectra of DR19-GTA48, **before** and **after** poling

5.4.4 BZI in GdANaOH

Hybrid materials containing nonlinear BZI-E-SGM were also synthesized by the group of Dr. Brusatin and Dr. Della Giustina. Chromophore structure is shown in **Fig. 5.28**.

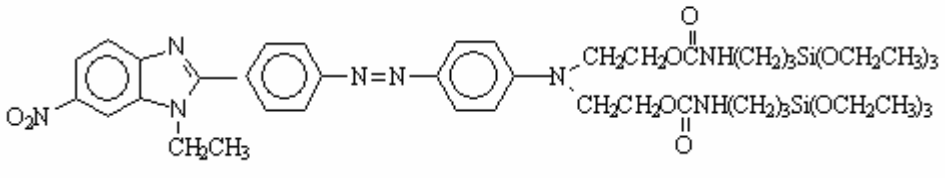

Fig. 5.28 BZI 1-E-SGM chemical structure

Hybrid materials containing BZI-E-SGM chromophore were prepared by using 2MeOtOH as solvent. The curing behaviour was determined by absorbance and FTIR characterization. By baking the hybrid doped samples at temperatures in the range 25-300°C, a substantial degradation was observed over 120°C as shown in **Fig. 5.29**.

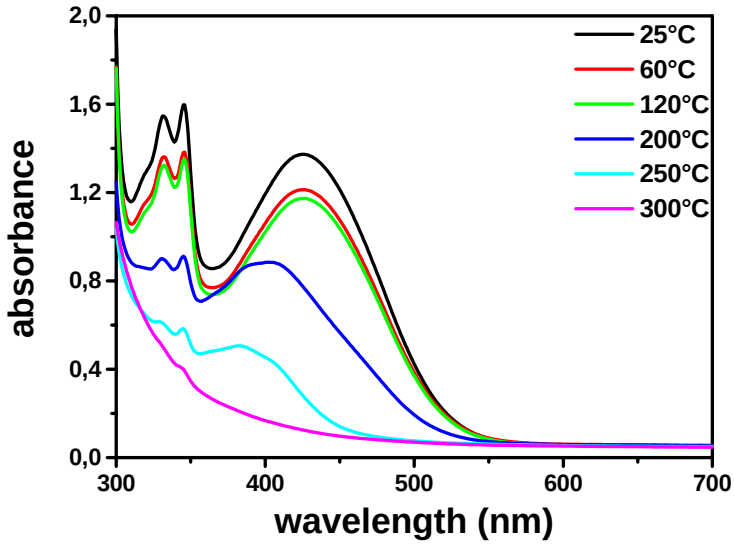

Fig. 5.29 Absorption spectra of BZI-E-SGM (20%)-GdA40NaOH cured at different temperatures

Curing the organically modified inorganic NLO sol-gel material at temperatures in the range 25-150°C (**Fig. 5.30**), an appreciable decrease of the OH groups at 60°C and an increase of the Si-O-CH_3 peak (2850 cm-1) around 90°C was observed.

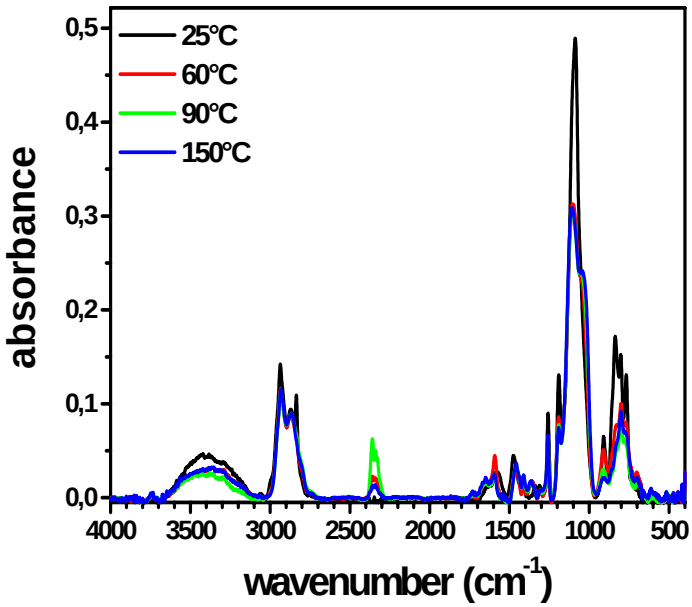

Fig. 5.30 Change of IR spectrum under curing at different temperatures

Taking into consideration the previous informations, we applied 7 kV of the corona field to the sample, reaching a maximum temperature of 120°C as shown in **Fig. 5.31**.

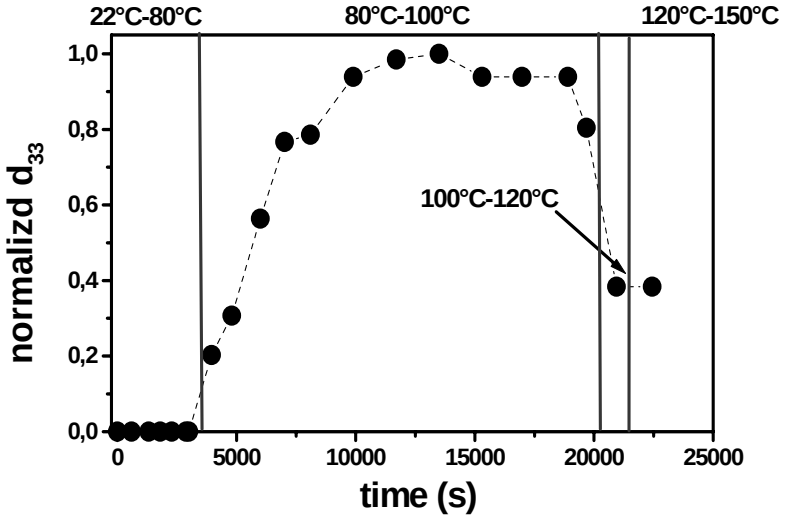

Fig. 5.31 *In situ* measurement of d_{33} during poling treatment

The temporal characteristic of the sample exhibits a relatively poor temporal stability (almost 10 days at room temperature). We believe that the condensation between silicon hydroxide did not proceed enough to form a highly organized silicon oxide network. This was tested during poling procedure. After the sample reached 100°C, we turned off the voltage to check the stability of the SH signal. The signal felt down to 10% of initial one. After the voltage was turned on again, the signal recovered to the same value as that measured before turning off the applied field. These results indicated that the chromophore was still in a "liquid-like" environment.

The poling effect on the absorption behaviour of these NLO systems was measured by UV-Vis spectroscopy (**Fig. 5.32**) and the order parameter, 0.43, denotes that a chromophore –breaking occurred during poling.

d_{33} values of BZI-E-SGM(20%)-GdANaOH and BZI-E-SGM(40%)-GdANaOH were 4 and 2 pm/V (at 1368 nm), respectively.

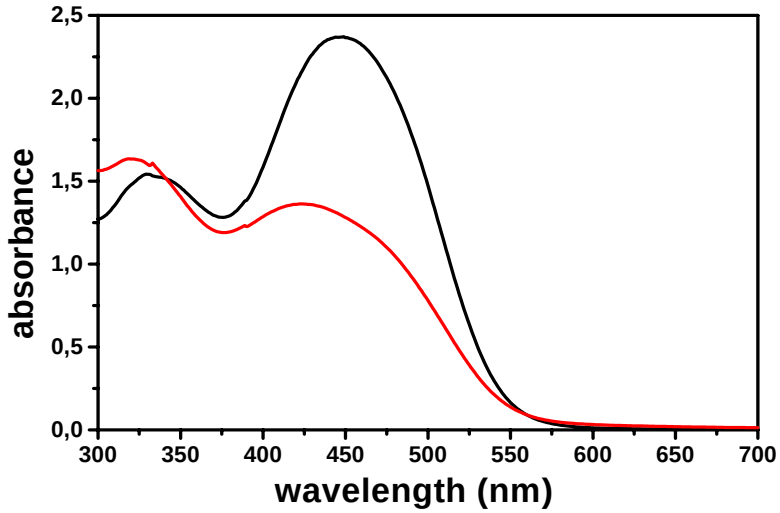

Fig. 5.32 UV-Vis absorption spectra of BZI-E-SGM-GdANaOH, **before** and **after** poling

Chapter 6

Characterization of NLO Materials Oriented by All-Optical Poling

A comparison of AOP among guest-host and side-chain polymers has been performed. The characteristic kinetic of decay of induced second order susceptibility was measured by SHG. All the observed decay evolutions reflect the following two relaxation processes: the thermal cis-to-trans back-reaction, which in different polymer systems may vary from second to minutes, corresponding to the faster decay component and the loss of the polar order of the trans molecules by thermal diffusion, corresponding to the slower decay component. It is shown that the polar order relaxation follows the duration of the poling process (seeding): the longer the poling, the slower the polar relaxation time. Causes of the orientation relaxation retardation are also discussed.

In addition, photoinduced dipolar orientation dynamic was studied in films obtained via sol-gel process using Zirconium(IV)propoxide (Zr), tetramethylorthosilicate (TMOS) and 3-Glycidoxypropiltrimethoxysilane as precursors (Gly). All these measurements have been performed at the ***Laboratoire des Propriétés Optiques des Matériaux et Applications (POMA)*** *at the University of Angers.*

6.1 Dynamics of Photoinduced Second Order Nonlinearity in Guest-Host Polymeric Systems

6.1.1 DR1-doped Polymer Films

Azo-dye (DR1) was dispersed into three different polymers (PMMA, PC and PSU) with different T_g, as already mentioned in **Chapter 5**. All the starting products were purchased by Aldrich Chemical Company Inc.. The chromophore was dissolved in a solution of the host polymer in $ChCl_3$ at a concentration such to obtain samples absorbing approximately 1 O.D. at 532 nm. Each solution was filtered on 0.20 μm Teflon filters and cast by spin coating at 1000 rpm for 30 seconds on standard cleaned microscope slides. The film thickness was typically 1 μm.

The experimental setup is described in detail in **Chapter 4**. Pulse energies of the ω and 2ω beams, 16 mJ and 6 μJ respectively, were carefully optimized for DR1-doped PMMA systems according to previous studies in order to prevent surface damage. (**Fiorini, 1997**)

Fig. 6.1 shows the square root of SH signal as a function of poling (seeding) time in DR1-doped PMMA films.

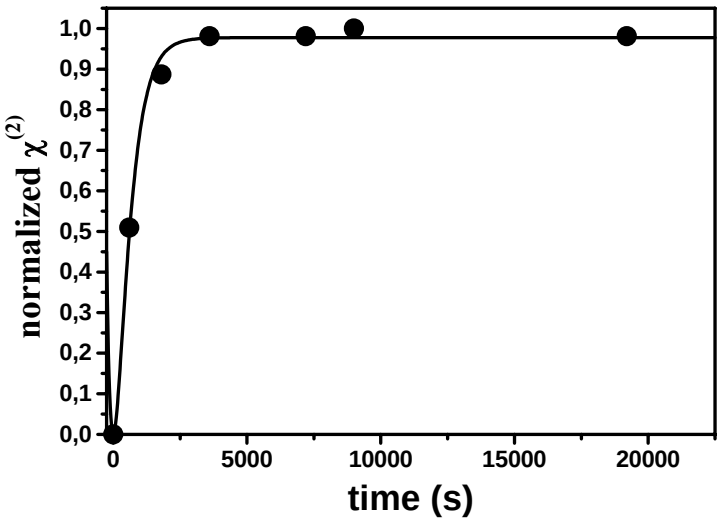

Fig. 6.1 Growth of the square root of SH signal in DR1-doped PMMA film

The SH growth in this system is a growing function saturated after about 60 minutes of seeding. The SH signal increases rapidly during first minutes of seeding and then reaches some constant value. After 5 hours of seeding, the SH signal remains comparable with the maximum SH achieved in the first minute of poling. The fit of the experimental points to the following equation (**Apostoluk, 2003**)

$$y = a\left[1 - e^{\left(-\frac{t}{\tau}\right)^b}\right]^2 \qquad \textbf{(6.1)}$$

where $y = \chi^{(2)}(t)/\chi^{(2)}_{MAX}$, a, b and τ are constants, gives the following results:

a	1.0
b	7.9
τ (s)	$3.8\ 10^3$

Table 6.1 Fitting parameters obtained from **Eq. (6.1)**

In order to test the temporal stability of the oriented films, the decay evolution of the induced $\chi^{(2)}$ was measured by probing the SHG of the samples after seeding process. The decay of nonlinear susceptibility of the polymeric films at room temperature is shown in **Fig. 6.2** for different seeding times.

According to the mechanism of AOP, when the seeding process is just finished, there are two kinds of noncentrosymmetries contributing to the SHG. One of them comes from the *cis* isomer produced by the photoinduced *trans*-to-*cis* isomerization during seeding, the other comes from the polarly oriented *tran*s molecules. All the observed decay evolutions in **Fig. 6.2** reflects, respectively, the following two relaxation processes: the thermal *cis* -to- *trans* back-reaction, which in different polymer systems may vary from seconds to minutes, corresponding to the faster decay component and the loss of the polar order of the *trans* molecules by thermal diffusion, corresponding to the slower decay component.

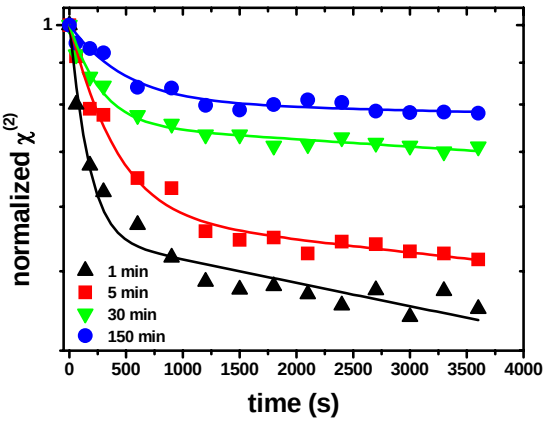

(a)

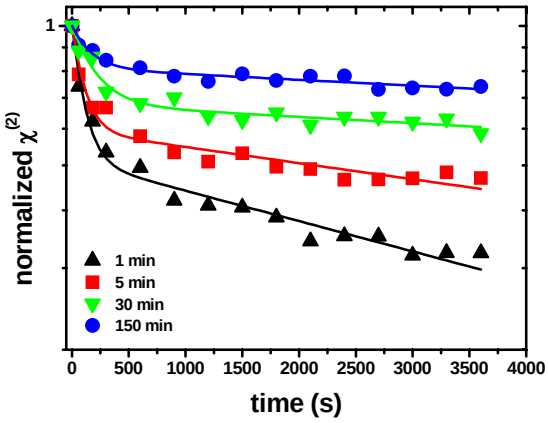

(b)

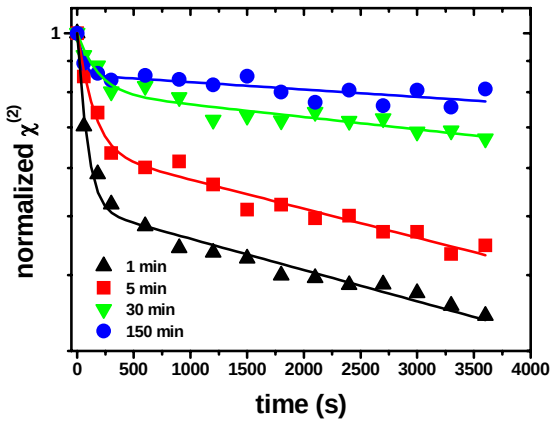

(c)

Fig.6.2 Decay of normalized photoinduced $\chi^{(2)}$ of DR1-doped PMMA **(a)**, PC **(b)** and PSU **(c)** systems for varying seeding times

We found again that all the decay curves can be approximately fit to a bi-exponential function given by:

$$y = (1 - A) \cdot e^{\left(-\frac{t}{\tau_1}\right)} + A \cdot e^{\left(-\frac{t}{\tau_2}\right)} \qquad \textbf{(6.2)}$$

where y is the normalized $\chi^{(2)}$ at time t after stopped seeding, i.e., $y=|\chi^{(2)}|/|\chi_{MAX}^{(2)}|$.
The first and the second terms describe, respectively, the decay process of the faster component with time constant τ_1 and the slower one with τ_2 and A is a constant between 0 and 1 which describes the loss of the polar order. **Table 6.2** summarize the fitting parameters of τ_1, τ_2 and *A*.

SEEDING TIME	***DR1-doped PMMA***			***DR1-doped PC***			***DR1-doped PSU***		
(min)	***A***	***τ_1(s)***	***τ_2(s)***	***A***	***τ_1(s)***	***τ_2(s)***	***A***	***τ_1(s)***	***τ_2(s)***
1	0.55	138	$1.5\ 10^4$	0.51	102	$6.6\ 10^3$	0.51	74	$8.4\ 10^3$
5	0.58	342	$3.1\ 10^4$	0.59	108	$1.3\ 10^4$	0.64	126	$9\ 10^3$
30	0.75	246	$5\ 10^4$	0.67	210	$3.2\ 10^4$	0.8	168	$2.1\ 10^4$
150	0.8	456	$1.4\ 10^5$	0.81	168	$3.5\ 10^4$	0.85	48	$3.6\ 10^4$

Table 6.2 Parameters derived from the fitting of the decay of the photoinduced $\chi^{(2)}$ curves shown in **Fig. 6.2**

The slow decay constant τ_2 increases with increased poling time for the three NLO polymers studied. In addition, the relative weight *A* of the slow decay component $Ae^{-t/\tau 2}$ increases upon prolonged AOP. This suggest that during AOP, the local polymeric environment surrounding azo-dyes is hardened or densified in such a way that dye dopant orientation relaxation is retarded. The fast decay component τ_1 is not relevant for interpreting the orientation relaxation because few

minutes after starting the $\chi^{(2)}$ decay measurements, *cis-trans* thermal back isomerization is still an important contribution to the decay rate.

Referring to **Table 6.2**, the rate of increase of the slow decay constant τ_2 upon AOP of DR1-doped PMMA is far higher than that of DR1-doped PC and PSU, although DR1-doped PMMA has the lowest T_g among them. (**Chan, to be submitted**) It indicates that retardation of the orientation relaxation upon AOP is not related to the first-order α-relaxation (T_g) of polymer matrix as previously seen in corona poling measurements, leading to the conclusion that the time constants τ_1 and τ_2 have a different nature in the two poling process. This is clear if we consider that AOP is performed at room temperature where the effect of the matrix are not relevant.

6.2 Dynamics of Photoinduced Second Order Nonlinearity in Chemical Bounded Polymeric Systems

6.2.1 Side-Chain BZI-based Films

Copolymers PA**BZI**-E (polymer E) and PA**BZI**-B5F (polymer B), shown in **Fig. 6.3 (a)** and **(b)**, synthesized by the group of Prof. Roviello and Centore, were dissolved in freshly distilled NMP. After deposition, residual solvent was removed by heat-treating the films at 100°C. The T_g of polymer E and B is 210°C and 214°C, respectively.

(a) Polymer E

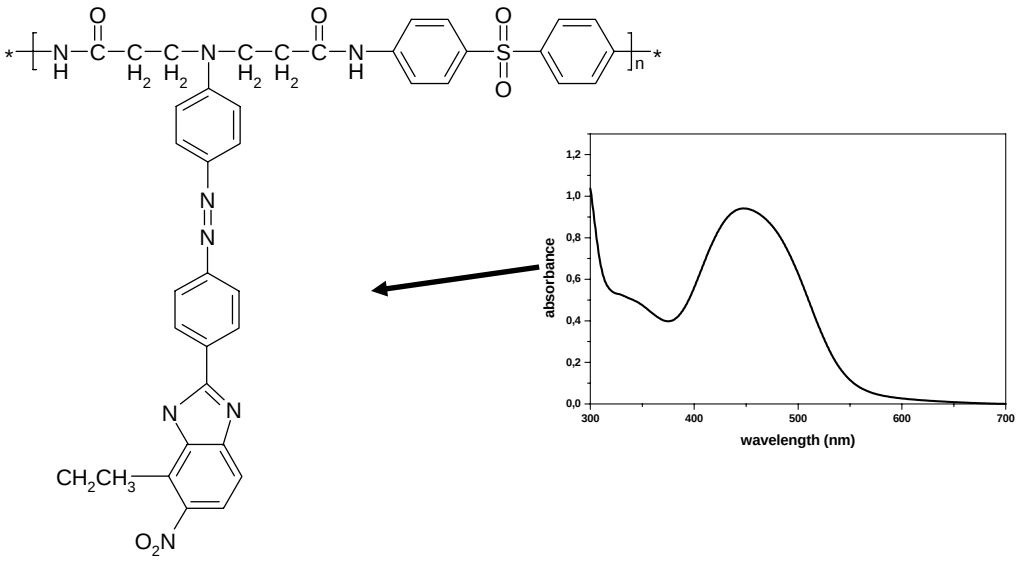

(b) Polymer B

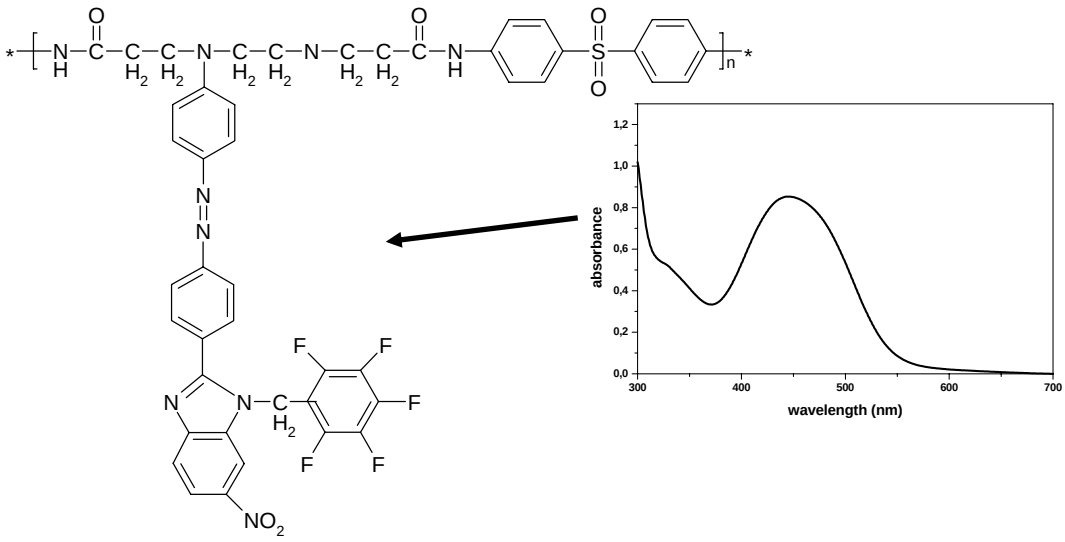

Fig.6.3 Chemical structures of Polymer E **(a)** and Polymer B **(b)**

The NLO characterization was carried out by performing SHG measurements on 1 μm thin films deposited at a rate of 1200 rpm for 30 sec at room temperature in a clean room. The decays of nonlinear susceptibility of polymeric films at room temperature for two different seeding times are shown in **Figs. 6.4** and **6.5** and the parameters derived from the fitting of the decay curves are represented in **Table 6.3** and **6.4**.

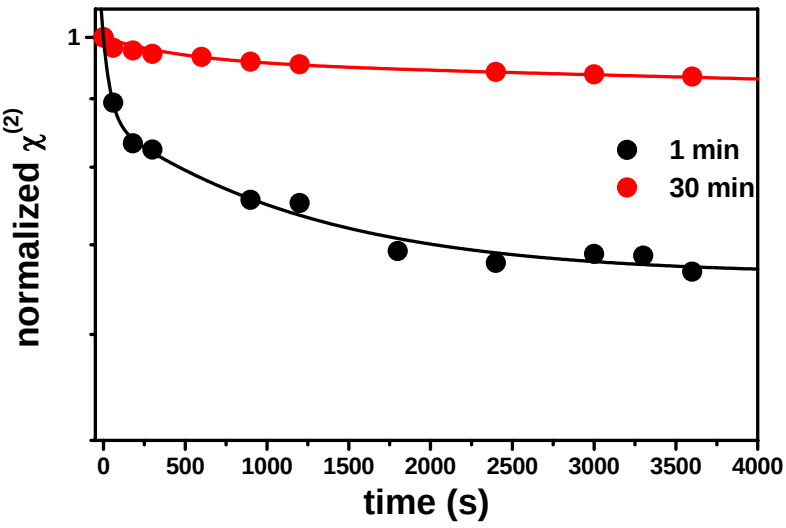

Fig. 6.4 Decay of normalized photoinduced $\chi^{(2)}$ of Polymer E

SEEDING TIME(min)	τ_1*(s)*	τ_2*(s)*
1	90	$2\ 10^4$
30	82	$8\ 10^4$
90	/	/

Table 6.3 Parameters derived from the fitting of the decay of the photoinduced $\chi^{(2)}$ curves shown in **Fig. 6.4**

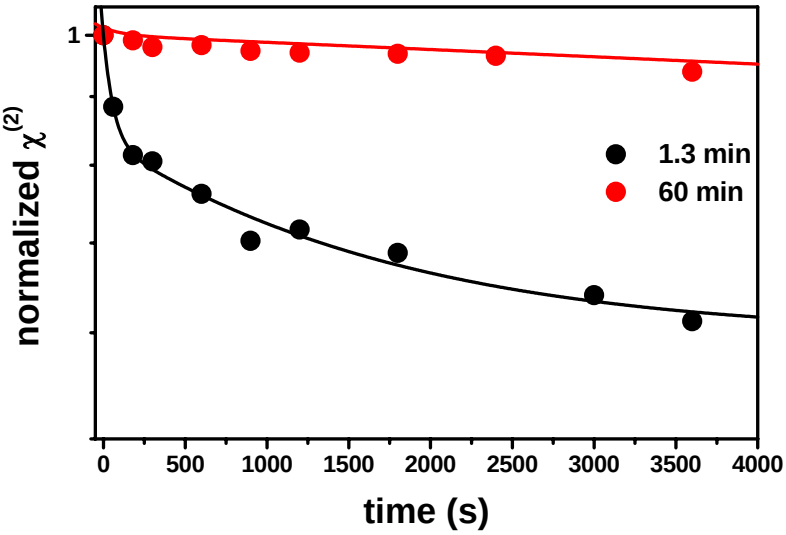

Fig. 6.5 Decay of normalized photoinduced $\chi^{(2)}$ of Polymer B

SEEDING TIME	τ_1*(s)*	τ_2*(s)*
1.3 min	102	$1.4\ 10^4$
5 min	600	$3.4\ 10^4$
30 min	23	$6\ 10^4$
60 min	188	$1\ 10^5$
310 min	/	/

Table 6.4 Parameters derived from the fitting of the decay of the photoinduced $\chi^{(2)}$ curves shown in **Fig. 6.5**

Considerations about chemical structures and orientation stability can be done comparing the decay evolutions of these systems with those one of simply doped polymers (**Table 6.2**). In fact, in guest-host systems, where the azo chromophores are not attached to the polymer backbone, there is no additional restriction to their rotation, leading to a faster relaxation if compared with the time evolution of side-chain Polymer E and B.

6.3 Dynamics of Photoinduced Second Order Nonlinearity in Sol-Gel-based Systems

6.3.1 DR1-doped Sol-Gel Films

Inorganic-organic materials have also been investigated. The azo-dye used was DR1, which was purchased from Aldrich and used as received. Hybrid films were prepared with Zirconium(IV)propoxide (**Zr**), tetramethylorthosilicate (**TMOS**) and 3-Glycidoxypropyltrimethoxysilane (**Gly**) as precursors. Doping of the composite matrix was carried out by directly adding the dye powder to the sol-gel solution which was filtered and casted on glass substrates.

Fig. 6.6 shows the photoinduced $\chi^{(2)}$ as a function of poling time in sol-gel samples. The SH growth is a growing function saturated after about 4 hours of seeding. The SH signal increases rapidly during first hour of seeding, and then drops to some constant value.

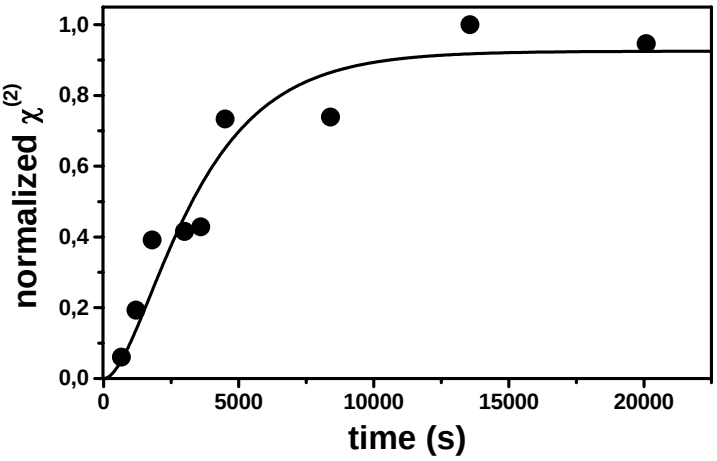

Fig. 6.6 Photoinduced $\chi^{(2)}$ growth of DR1-Zr/TMOS/Gly optically poled

The fit of the experimental points to **Eq. (6.1)** gives the following results:

a	0.9
b	8.6
τ (s)	$2\ 10^4$

Table 6.5 Fitting parameters obtained from **Eq. (6.1)**

The gradual growth of the photoinduced $\chi^{(2)}$ and its saturation seems to be slower respect to the case of DR1-doped PMMA (**Fig. 6.1**). After the preparation process is stopped, we observed a relaxation regime close to what we showed for polymer systems.

The decay process is also double exponential like AOP in azo-polymers as shown in **Fig. 6.7**. We tested also the difference in decay evolutions between a fresh and an old (after 6 hours from deposition) sample and **Table 6.6** summarizes the fitting parameters.

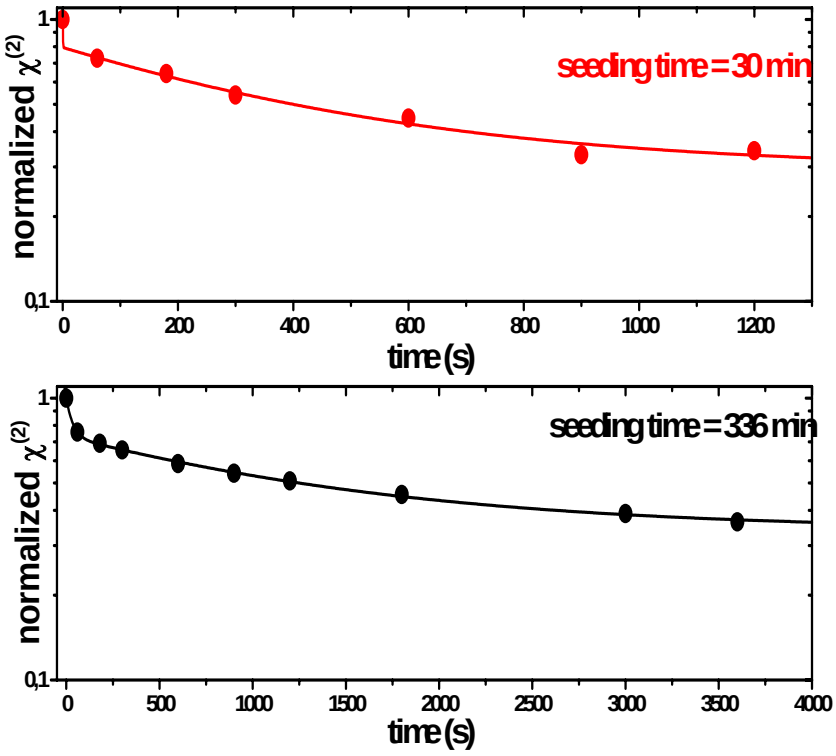

Fig.6.7 Decay of normalized photoinduced $\chi^{(2)}$ of DR1-Zr/TMOS/Gly

SEEDING TIME	τ_1*(s)*	τ_2*(s)*
30 min fresh	42	$1.4\ 10^3$
30 min old	84	$4\ 10^3$
336 min	54	$5\ 10^3$

Table 6.6 Parameters obtained by fitting the relaxation curves of photoinduced $\chi^{(2)}$ to **Eq. (6.2)**

As already shown for guest-host systems, the decay times of the slower components increase with the seeding time and it becomes stable for higher writing times. In despite of corona poling measurements, the decay of the SH signal in hybrid samples is faster comparing with azobenzene-contained polymers. Such behaviour confirms that upon AOP, the slower decay time is not solely related to the T_g.

Conclusions

Organic and hybrid second order NLO materials have gained in recent years strong consideration. This thesis has reported some achievements in the field, paying particular attention to the time stability of NLO properties of such systems. In particular, it was reported the relaxation behaviour at different temperatures of linear (PAS) and nonlinear properties (d_{33}) of films containing different NLO chromophores. Key role of orientation techniques, able to induce the mandatory polar symmetry, has been focused; in particular, *corona* and *all-optical poling* techniques were discussed. All the decay curves were fitted by a double exponential function. An extrapolation of the slower relaxation time at room temperature using the Arrhenius model, permitted to obtain the stability of nonlinear properties at room temperature. Attention was paid to the relationship between chemical, physical and optical properties of polymers and hybrid sol-gel materials, such as chromophore concentration and nonlinear activity (d_{33}), glass transition temperature (T_g) and stability and, in the case of *all-optical poling*, seeding procedure and stability. A short review of the results in polymeric and sol-gel based systems has been given as well. As a matter of facts, it seems that a good control of temporal stability of NLO properties, rather than a further increasing of their absolute value, can be reached. That is an essential requisite to be obtained for practical uses.

During the PhD time:

- Solutions were directly prepared by the candidate herself and deposited on glass slides in the clean room.

- Corona poling procedures were calibrated as a function of the poling parameters (poling time, poling temperature and poling voltage) for organic and hybrid organic-inorganic systems.

- Accelerated life tests technique using temperature as degrading agent was adapted to thin polymeric films, leading to a fast estimation of the second order coefficient d_{33} relaxation time at room temperature and an evaluation of the relationship between stability and T_g.

- All-optical poling was performed on new polymers and new hybrid organic-inorganic films. The reading procedure was optimized and relaxation process were studied at room temperature as a function of time and seeding duration.

- Solid State Raman Shifter was calibrated and aligned to the Nd:YAG laser in order to shift the main wavelength and obtain off-resonance d_{33} coefficients.

- A *Matlab* programming was adapted to the new setup and wavelengths in order to obtain the d_{33} coefficients of the samples, using a Quartz (010) crystal slab as reference.

- A new corona poling setup was realized using Macor®, which can tolerate high temperatures (up to 300°C). Moreover, the horizontal position of the sample holder permits to orient dopants in sol-gel samples immediately after the deposition, when the condensation is still in progress.

At least two promising materials were found, a polyimide-based and a hybrid sol-gel-based system, and the fabrication of a prototype of electrooptic modulator is envisaged in collaboration with the research centers of some Italian private companies. The properties of these materials enable the chromophore molecules to have rigid free volume and can be well controlled in the aligned status, which leads to the high temporal stability and helps the devices to withstand short-term thermal shock present during processing and packaging.

Appendix 1

*In **Chapter 1**, we have shown how nonlinearities in the response of a material system to an intense laser field can cause the polarization of the medium to develop new frequency components not present in the incident radiation field. In the present Appendix, we examine how Maxwell's equations describe the generation of these new components of the field with particular attention to SHG.*

The Electromagnetic Formulation of the Nonlinear Interaction: SHG

Let us consider the form of the wave equation for the propagation of light through a nonlinear optical medium. We begin with *Maxwell*'s equations, which we write in gaussian units in the form

$$\nabla \cdot \tilde{\boldsymbol{D}} = 4\pi\tilde{\rho} \tag{A.1}$$

$$\nabla \cdot \tilde{\boldsymbol{B}} = 0 \tag{A.2}$$

$$\nabla \times \tilde{\boldsymbol{E}} = -\frac{1}{c}\frac{\partial \tilde{\boldsymbol{B}}}{\partial t} \tag{A.3}$$

$$\nabla \times \tilde{\boldsymbol{H}} = \frac{1}{c}\frac{\partial \tilde{\boldsymbol{D}}}{\partial t} + \frac{4\pi}{c}\tilde{\boldsymbol{J}} \tag{A.4}$$

We are primarily interested in the solution of these equations in regions of space that contain no free charges, so that

$$\tilde{\rho} = 0 \tag{A.5}$$

and that contain no free currents, so that

$$\tilde{\boldsymbol{J}} = 0 \tag{A.6}$$

We assume that the material is nonmagnetic, so that

$$\tilde{\boldsymbol{B}} = \tilde{\boldsymbol{H}} \tag{A.7}$$

However, we allow the material to be nonlinear in the sense that the fields $\boldsymbol{D}$ and $\boldsymbol{E}$ are related by

$$\tilde{\boldsymbol{D}} = \tilde{\boldsymbol{E}} + 4\pi\tilde{\boldsymbol{P}} \tag{A.8}$$

where in general the polarization vector $\boldsymbol{P}$ depends nonlinearly upon the local value of the electric field strength $\boldsymbol{E}$.

We now proceed to derive the optical wave equation in the usual manner. We take the curl of the curl-$\boldsymbol{E}$ *Maxwell* **Eq. (A.3)**, interchange the order of space and time derivatives on the right-hand side of the resulting equation, and use **Eqs. (A.4)**, **(A.6)** and **(A.7)** to replace $\nabla\times\boldsymbol{B}$ by $(1/c)(\partial\boldsymbol{D}/\partial t)$, to obtain the equation

$$\nabla\times\nabla\times\widetilde{\boldsymbol{E}}+\frac{1}{c^2}\frac{\partial^2\widetilde{\boldsymbol{D}}}{\partial t^2}=0 \qquad \textbf{(A.9a)}$$

We now use **Eq. (A.8)** to eliminate $\boldsymbol{D}$ from this equation, and we thereby obtain the expression

$$\nabla\times\nabla\times\widetilde{\boldsymbol{E}}+\frac{1}{c^2}\frac{\partial^2\widetilde{\boldsymbol{E}}}{\partial t^2}=-\frac{4\pi}{c^2}\frac{\partial^2\boldsymbol{P}}{\partial t^2} \qquad \textbf{(A.9b)}$$

This is the most general form of the wave equation in nonlinear optics. Under certain condition it can be simplified. For example, by using an identity from vector calculus, we can write the first term on the left-hand side of **Eq. (A.9b)** as

$$\nabla\times\nabla\times\widetilde{\boldsymbol{E}}=\nabla\left(\nabla\cdot\widetilde{\boldsymbol{E}}\right)-\nabla^2\widetilde{\boldsymbol{E}} \qquad \textbf{(A.10)}$$

In the linear optics of isotropic source-free media, the first term on the right-hand side of this equation vanishes because the *Maxwell* equation $\nabla\cdot\boldsymbol{D}=0$ implies that $\nabla\cdot\boldsymbol{E}=0$. However, in nonlinear optics this term is generally nonvanishing even for isotropic materials, owing to the more general relation **(A.8)** between $\boldsymbol{D}$ and $\boldsymbol{E}$. Fortunately, in nonlinear optics the first term on the right-hand side of **Eq. (A.10)** can usually be dropped for cases of interest. For example, if $\boldsymbol{E}$ is of the form of a transverse, infinite plane wave, $\nabla\cdot\boldsymbol{E}$ vanishes identically.

More generally, the first term can often be shown to be small, even when it does not vanish identically, especially when the slowly-varying amplitude approximation is valid.

It is often convenient to split $\boldsymbol{P}$ into its linear and nonlinear part as

$$\widetilde{\boldsymbol{P}}=\widetilde{\boldsymbol{P}}^{(1)}+\widetilde{\boldsymbol{P}}^{NL} \qquad \textbf{(A.11)}$$

Here $\boldsymbol{P}^{(1)}$ is the part of $\boldsymbol{P}$ that depends linearly on the electric field strength $\boldsymbol{E}$. We can similarly decompose the displacement field $\boldsymbol{D}$ into its linear and nonlinear parts as

$$\tilde{\boldsymbol{D}} = \tilde{\boldsymbol{D}}^{(1)} + 4\pi\tilde{\boldsymbol{P}}^{NL} \qquad \textbf{(A.12a)}$$

where the linear part is given by

$$\tilde{\boldsymbol{D}}^{(1)} = \tilde{\boldsymbol{E}} + 4\pi\tilde{\boldsymbol{P}}^{(1)} \qquad \textbf{(A.12b)}$$

In terms of this quantity, the wave equation **(A.9)** becomes

$$\nabla\times\nabla\times\tilde{\boldsymbol{E}} + \frac{1}{c^2}\frac{\partial^2\boldsymbol{D}^{(1)}}{\partial t^2} = -\frac{4\pi}{c^2}\frac{\partial^2\boldsymbol{P}^{NL}}{\partial t^2} \qquad \textbf{(A.13)}$$

To see why this form of the wave equation is useful, let us first consider the case of a lossless, dispersionless medium. We can then express the relation between $\boldsymbol{D}^{(1)}$ and $\boldsymbol{E}$ in terms of a real, frequency-independent dielectric tensor $\boldsymbol{\varepsilon}^{(1)}$ as

$$\tilde{\boldsymbol{D}}^{(1)} = \varepsilon^{(1)}\cdot\tilde{\boldsymbol{E}} \qquad \textbf{(A.14a)}$$

For the case of an isotropic material, this relation reduces simply to

$$\tilde{\boldsymbol{D}}^{(1)} = \varepsilon^{(1)}\tilde{\boldsymbol{E}} \qquad \textbf{(A.14b)}$$

where $\varepsilon^{(1)}$ is a scalar quantity. For this (simpler) case of an isotropic material, the wave equation **(A.13)** becomes

$$\nabla\times\nabla\times\tilde{\boldsymbol{E}} + \frac{\varepsilon^{(1)}}{c^2}\frac{\partial^2\tilde{\boldsymbol{E}}}{\partial t^2} = -\frac{4\pi}{c^2}\frac{\partial^2\tilde{\boldsymbol{P}}^{NL}}{\partial t^2} \qquad \textbf{(A.15)}$$

This equation has the form of a driven (i.e., inhomogeneous) wave equation; the nonlinear response of the medium acts as a source term which appears on the right-hand side of this equation. In the

absence of this source term, **Eq. (A.15)** admits solutions of the form of free waves propagating with velocity c/n, where $n = [\varepsilon^{(1)}]^{1/2}$ is the linear index of refraction.

For the case of a dispersive medium, we must consider each frequency component of the field separately. We represent the electric, linear displacement and polarization fields as the sums of their various frequency components

$$\widetilde{\boldsymbol{E}}(\boldsymbol{r},t) = \sum_n{}' \widetilde{\boldsymbol{E}}_n(\boldsymbol{r},t) \tag{A.16a}$$

$$\widetilde{\boldsymbol{D}}^{(1)}(\boldsymbol{r},t) = \sum_n{}' \widetilde{\boldsymbol{D}}_n(\boldsymbol{r},t) \tag{A.16b}$$

$$\widetilde{\boldsymbol{P}}_n^{NL}(\boldsymbol{r},t) = \sum_n{}' \widetilde{\boldsymbol{P}}_n^{NL}(\boldsymbol{r},t) \tag{A.16c}$$

where the summation is to be performed over positive field frequencies only, and we represent each frequency component in terms of its complex amplitude as

$$\widetilde{\boldsymbol{E}}_n(\boldsymbol{r},t) = \boldsymbol{E}_n(\boldsymbol{r}) \cdot \boldsymbol{e}^{-i\omega_n t} + \boldsymbol{c.c.}, \tag{A.17a}$$

$$\widetilde{\boldsymbol{D}}_n^{(1)}(\boldsymbol{r},t) = \widetilde{\boldsymbol{D}}_n^{(1)}(\boldsymbol{r}) \cdot \boldsymbol{e}^{-i\omega_n t} + \boldsymbol{c.c.}, \tag{A.17b}$$

$$\widetilde{\boldsymbol{P}}_n^{NL}(\boldsymbol{r},t) = \boldsymbol{P}_n^{NL}(\boldsymbol{r}) \cdot \boldsymbol{e}^{-i\omega_n t} + \boldsymbol{c.c.} \tag{A.17c}$$

If dissipation can be neglected, the relationship between $\boldsymbol{D}^{(1)}_n$ and $\boldsymbol{E}_n$ can be expressed in terms of a real, frequency-dependent dielectric tensor according to

$$\widetilde{\boldsymbol{D}}_n^{(1)}(\boldsymbol{r},t) = \varepsilon^{(1)}(\omega_n) \cdot \widetilde{\boldsymbol{E}}_n(\boldsymbol{r},t) \tag{A.18}$$

When **Eqs. (A.16)** through **(A.18)** are introduced into **Eq. (A.13)**, we obtain a wave equation analogous to **(A.15)** that is valid for each frequency component of the field

$$\nabla \times \nabla \times \widetilde{\boldsymbol{E}}_n + \frac{\varepsilon^{(1)}(\omega_n)}{c^2} \cdot \frac{\partial^2 \widetilde{\boldsymbol{E}}_n}{\partial t^2} = -\frac{4\pi}{c^2} \frac{\partial^2 \widetilde{\boldsymbol{P}}_n^{NL}}{\partial t^2} \tag{A.19}$$

As mentioned above in connection with **Eq. (A.10)**, the first term on the left-hand side of this equation can often be replaced by $-\nabla^2 \boldsymbol{E}_n$.

The general case of a dissipative medium is treated by allowing the dielectric tensor to be a complex quantity that relates the complex field amplitudes according to

$$\tilde{\boldsymbol{D}}_{\boldsymbol{n}}^{(1)}(\boldsymbol{r}) = \varepsilon^{(1)}(\omega_{\boldsymbol{n}}) \cdot \boldsymbol{E}_{\boldsymbol{n}}(\boldsymbol{r}) \qquad \textbf{(A.20)}$$

This expression, along with **Eqs. (A.16)** and **(A.17)**, can be introduced into the wave equation **(A.13)**, to obtain

$$\nabla \times \nabla \times \boldsymbol{E}_{\boldsymbol{n}}(\boldsymbol{r}) - \frac{\omega_{\boldsymbol{n}}^2}{c^2} \varepsilon^{(1)}(\omega_{\boldsymbol{n}}) \cdot \boldsymbol{E}_{\boldsymbol{n}}(\boldsymbol{r}) = \frac{4\pi\pi_{\boldsymbol{n}}^{\,2}}{c^2} \boldsymbol{P}_{\boldsymbol{n}}^{\boldsymbol{NL}}(\boldsymbol{r}) \qquad \textbf{(A.21)}$$

When the first term on the left-hand side of this expression can be reduced simply to the negative of the Laplacian of $\boldsymbol{E_n}$, this equation has the form of an inhomogeneous *Helmholtz equation*.

SHG

We assume that the medium is lossless both at the fundamental frequency ω_1 and at the second harmonic frequency $\omega_2 = 2\omega_1$, so that the nonlinear susceptibility obeys the condition of full permutation symmetry. Our discussion closely follows that of one of the first theoretical treatments of SHG.

We take the total electric field within the nonlinear medium to be given by

$$\tilde{E}(z,t) = \tilde{E}_1(z,t) + \tilde{E}_2(z,t) \qquad \textbf{(A.22)}$$

where each component is expressed in terms of a complex amplitude $E_j(z)$ and slowly varying amplitude $A_j(z)$ according to

$$\tilde{E}_j(z,t) = \tilde{E}_j(z) \cdot e^{-i\omega_j t} + c.c. \qquad \textbf{(A.27)}$$

where

$$E_j(z) = A_j(z) \cdot e^{ik_j z} \qquad \textbf{(A.28)}$$

and where the wave number and the refractive index are given by

$$k_j = \frac{n_j \omega_j}{c}, n_j = \left[\varepsilon^{(1)}\left(\omega_j\right)\right]^{\frac{1}{2}} \quad \textbf{(A.29)}$$

We assume that each frequency component of the electric field obeys the driven wave equation **A.19**

$$\frac{\partial^2 \tilde{E}_j}{\partial z^2} - \frac{\varepsilon^{(1)}\left(\omega_j\right)}{c^2}\frac{\partial^2 \tilde{E}_j}{\partial t^2} = \frac{4\pi}{c^2}\frac{\partial^2 \tilde{P}_j}{\partial t^2} \quad \textbf{(A.30)}$$

The nonlinear polarization is represented as

$$\tilde{P}^{NL}\left(z,t\right) = \tilde{P}_1\left(z,t\right) + \tilde{P}_2\left(z,t\right) \quad \textbf{(A.31)}$$

with

$$\tilde{P}_j\left(z,t\right) = P_j\left(z\right)\cdot e^{-i\omega_j t} + c.c.\,; j = 1,2 \quad \textbf{(A.32)}$$

The expressions for P_j are given according to **Eq. (1.8)** by

$$P_1\left(z\right) = 4dE_2E_1^* = 4dA_2A_1^* e^{i(k_2-k_1)z} \quad \textbf{(A.33)}$$

and

$$P_2\left(z\right) = 2dE_1^2 = 2dA_1^2 e^{2ik_1 z} \quad \textbf{(A.34)}$$

we obtain coupled-amplitude equations by using **Eq. (A.19)**. We find that

$$\frac{dA_1}{dz} = \frac{8\pi i\omega_1^2 d}{k_1 c^2} A_2 A_1^* e^{-i\Delta k z} \quad \textbf{(A.35)}$$

and

$$\frac{dA_2}{dz} = \frac{4\pi i \omega_2^2 d}{k_2 c^2} A_1^2 e^{ik\Delta z} \qquad \textbf{(A.36)}$$

where

$$\Delta k = 2k_1 - k_2 \qquad \textbf{(A.37)}$$

It is convenient to express these amplitudes A_1 and A_2 in dimensionless form. We hence write the complex, slowly varying field amplitude as

$$A_1 = \left(\frac{2\pi I}{n_1 c}\right)^{\frac{1}{2}} u_1 e^{i\phi_1}, \qquad \textbf{(A.38a)}$$

$$A_2 = \left(\frac{2\pi I}{n_2 c}\right)^{\frac{1}{2}} u_2 e^{i\phi_{21}}. \qquad \textbf{(A.38b)}$$

Here we have introduced the total intensity of the two waves

$$I = I_1 + I_2 \qquad \textbf{(A.39)}$$

where the intensity of each wave is given by

$$I_j = \frac{n_j c}{2\pi} \left| A_j \right|^2 \qquad \textbf{(A.40)}$$

We next introduce a normalized distance parameter $\xi = z/l$, where

$$l = \left(\frac{n_1^2 n_2 c^3}{2\pi I}\right)^{\frac{1}{2}} \frac{1}{4\pi\omega_1 \chi^{(2)}} \qquad \textbf{(A.41)}$$

is the characteristic distance over which the fields exchange energy.

We now assume that the initial conditions are

$$u_1(0) = 1; u_2(0) = 0. \qquad \textbf{(A.42)}$$

These conditions imply that no second-harmonic light is incident on the nonlinear crystal, as is the case in most experiments. In this case the solutions for **Eqs. (A.35)** and **(A.36)** are

$$u_2(\xi) = tanh\xi \qquad \textbf{(A.43a)}$$

$$u_1(\xi) = sech\xi \qquad \textbf{(A.43b)}$$

All these considerations are valid for the case of perfect phase matching (***Δk* = 0**). When this condition is fulfilled the individual atomic dipoles that constitute the material system are properly phased so that the field emitted by each dipole adds coherently in the forward direction. The total power radiated by the ensemble of atomic dipoles thus scales as the square of the number of atoms that participate.

When the phase matching condition is not satisfied, the intensity of the emitted radiation is smaller than for the case of ***Δk* = 0**. The amplitude of second harmonic intensity at the exit plane of the nonlinear medium is given by the following expression

$$I_2 = \frac{128\pi^5 \left(\chi^{(2)}\right)^2 I_1^2}{n_1^2 n_2 \lambda_2^2 c} L^2 \sin c^2 \left(\Delta k \cdot \frac{L}{2}\right) \qquad \textbf{(A.44)}$$

This expression predict a dramatic decrease in the efficiency of SHG when the condition of perfect phase matching is not satisfied.

Behaviour of the sort predicted by **Eq. (A.44)** was first observed experimentally by **Maker at al. (1962)**. Their experiment involved focusing the output of a pulsed ruby laser into a single crystal of quartz and measuring how the intensity of the second harmonic signal varied as the crystal was rotated, thus varying the effective path length L through the crystal. The wave vector mismatch Δk was nonzero and approximately the same for all orientations used in their experiment.

The phase matching condition $\Delta k = 0$ is often difficult to achieve because the refractive index of materials that are lossless in the range ω_1 to ω_2 shows an effect known as normal

dispersion: the refractive index is an increasing function of frequency. As a result, the condition for perfect phase matching with collinear beams,

$$n(\omega_1) = n(\omega_2) \qquad \textbf{(A.45)}$$

which is clearly not possible when $n(\omega)$ increases monotonically with ω.

Appendix 2

In this Appendix, we present the results in the nonlinear optics field, published on scientific journals and obtained during the Ph.D. studies.

Methacrylate Polymers based on 2-[4-(N-methyl,N-hydroxyethylamino)phenylazo]-phenyl-6-nitrobenzoxazole Chromophores

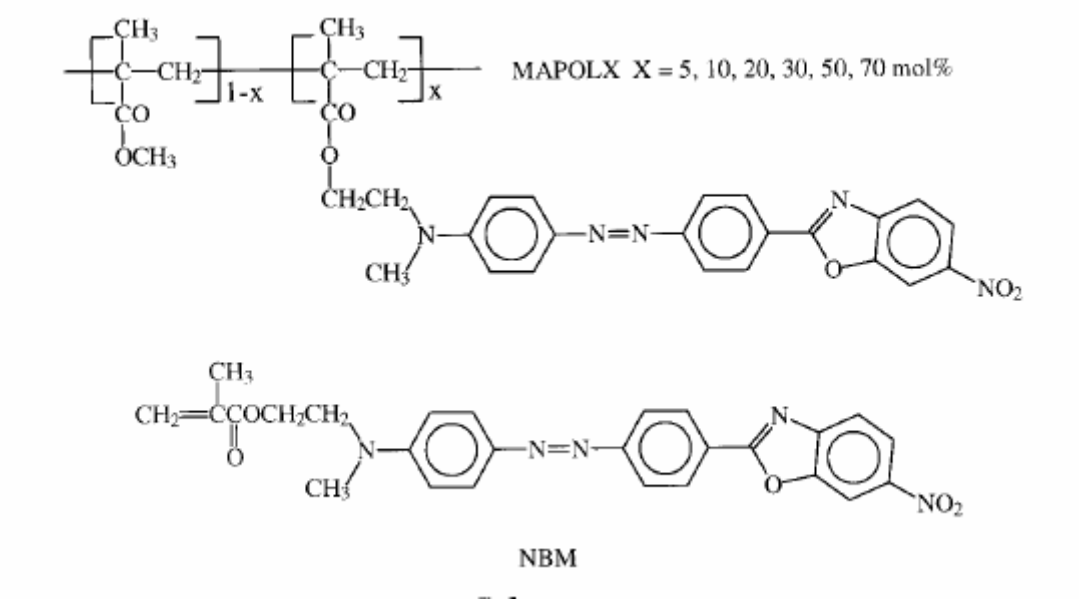

Polymer	T_g (°C)	d_{33}@1064 nm (pm/V)	τ_2(25°C) (days)
MAPOL5 6%*	128	40	/
MAPOL10 9%*	130	50	/
MAPOL20 17%*	130	60	/
MAPOL30 33%*	133	50	/

** content of chromophores in the polymer (mol-%)*

P. Persico, R. Centore, A. Sirigu, M. Casalboni, **A. Quatela**, F. Sarcinelli

Synthesis and Nonlinear Optical Properties of Methacrylate Polymers Based on 2-[4-(N-methyl,N-hydroxyethylamino)phenylazo]-phenyl-6-nitrobenzoxazole Chromophores

J Polym. Sci A, **41**, 1841 (2003)

Pd(II)-based Organometallic Side-Chain Polymers with C, N or N, O Chelating Chromophore Ligands

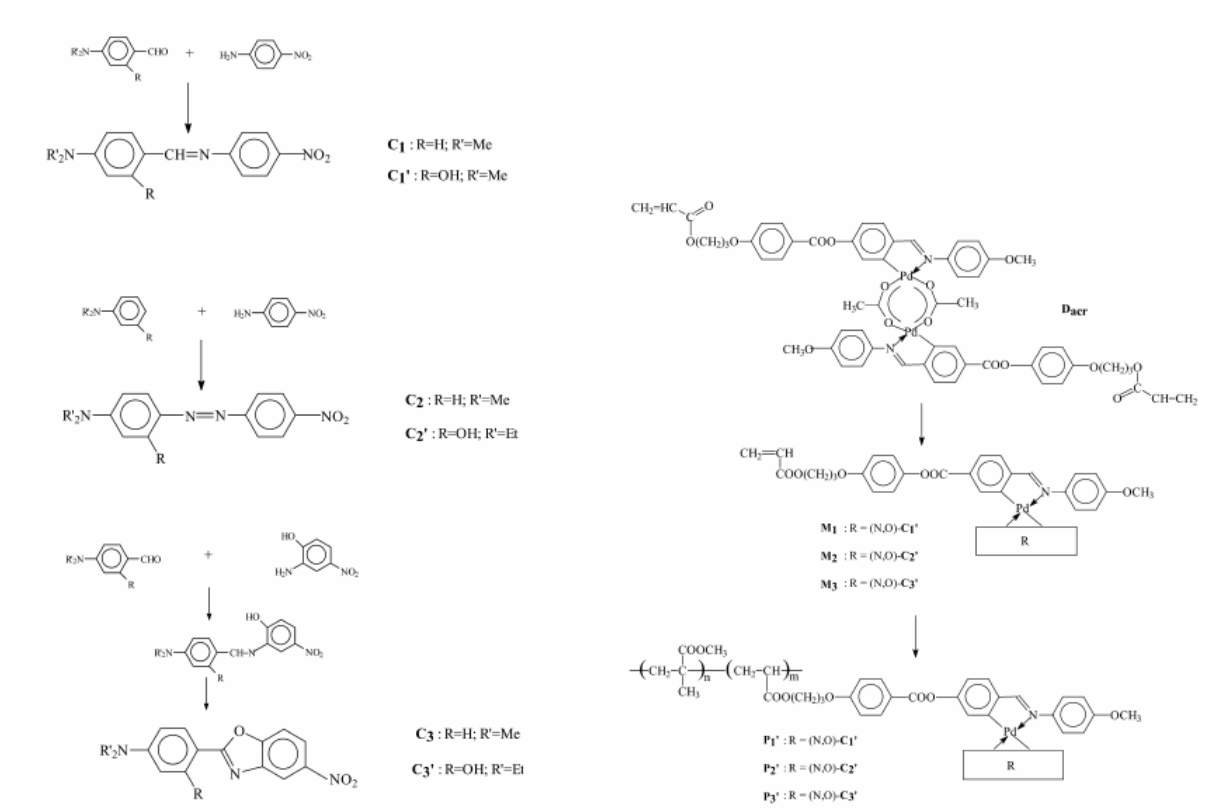

Polymer	T_g *(°C)*	d_{33} *@ 1064 nm (pm/V)*	τ_2*(25°C) (days)*
P'1	129	20	/
P'2	175	25	/
P'3	152	10	/

I. Aiello, U. Caruso, M. Ghedini, B. Panunzi, **A. Quatela**, A. Roviello, F. Sarcinelli

NLO active Pd(II)-based organometallic side-chain polymers with C,N or N,O-chelating chromophoric ligands

Polymer, **44**, 7635 (2003)

Polymers Containing Imidazole and Benzimidazole Chromophores

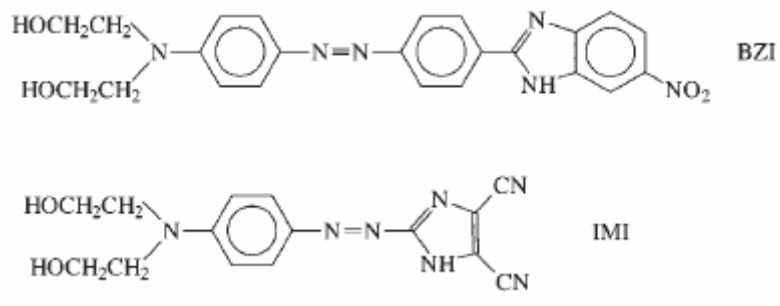

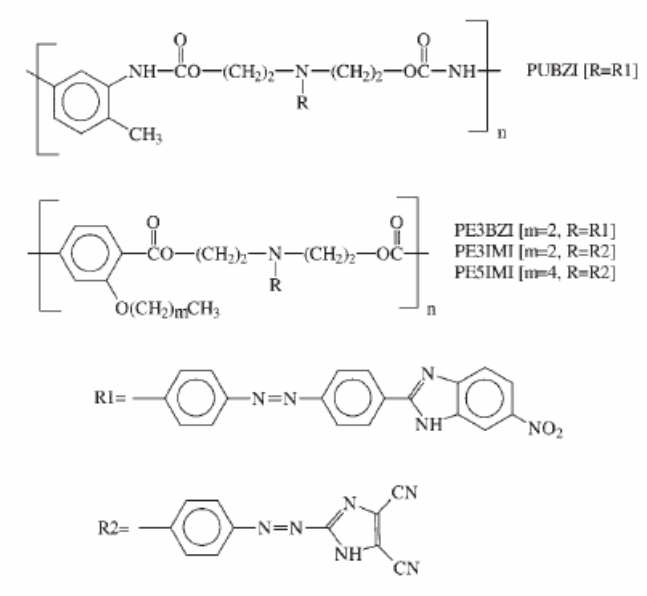

Polymer	***T_g (°C)***	***d_{33}@ 1368 nm (pm/V)***	***τ_2 (25°C) (days)***
PUBZI	188	4.0	1040
PE3BZI	152	3.5	370
PE3IMI	152	2.0	440
PE5IMI	131	1.8	280

A. Carella, R. Centore, A. Sirigu, A. Tuzi, **A. Quatela**, S. Schutzmann, M. Casalboni

Second order nonlinear optical performances of polymers containing imidazole and benzimidazole chromophores

Macromol. Chem. Phys., **205**, 1948 (2004)

New Polyurethanes and Polyesters

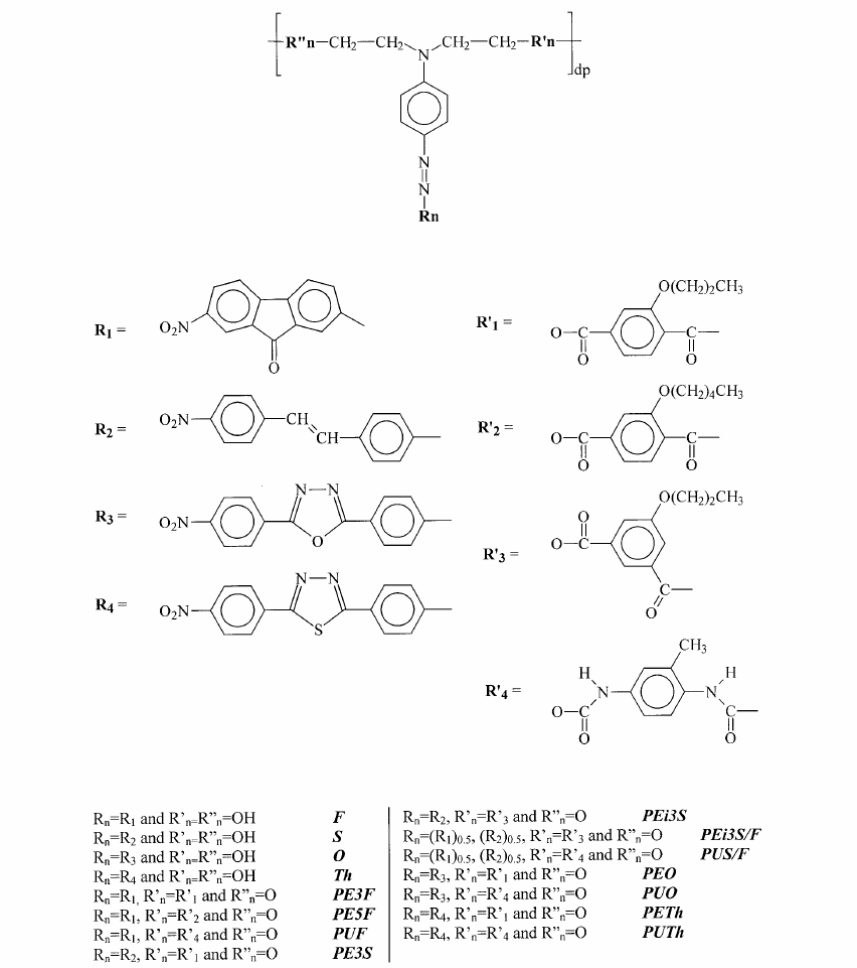

Polymer	T_g *(°C)*	d_{33} *@ 1064 nm (pm/V)*	τ_2*(25°C) (days)*
PE5F	128	25	/
PUF	183	18	/
PEi3S/F	130	18	/

M. Casalboni, U. Caruso, A. De Maria, M. Fusco, B. Panunzi, **A. Quatela**, A. Roviello, F. Sarcinelli, A. Sirigu

New polyurethanes and polyesters for second-order nonlinear optical applications

J Polym. Sci Part A-Pol. Chem. **42**,3013, (2004)

Polymethacrylate Copolymers Containing 4,5-Dicyanoimidazole-based Chromophores

(a)

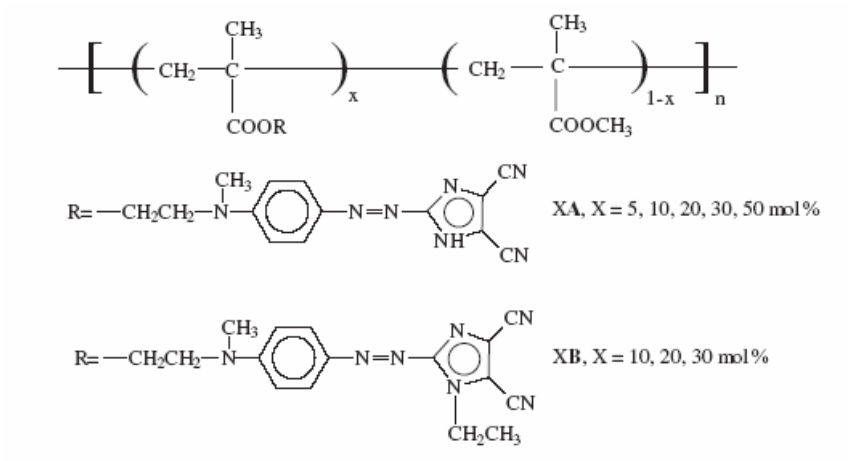

(b)

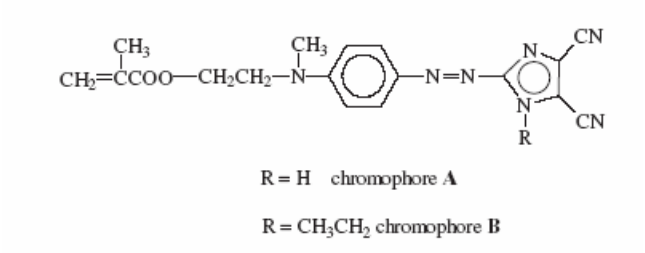

Polymer	*T_g (°C)*	*d_{33} @ 1368 nm (pm/V)*	*τ_2(25°C) (days)*
5A 4%*	138	0.2	/
10A 8.9%*	146	1.1	/
20A 15%*	159	3.3	/
30A 27%*	170	1.0	/
50A 50%*	182	0.7	/
10B 8%*	131	1.4	/
30B 29.5%*	138	3.0	/
50B 42%*	149	1.7	/

**content of chromophores in the polymer (mol-%)*

A. Carella, R. Centore, P. Riccio, A. Sirigu, **A. Quatela**, C. Palazzesi, M. Casalboni

Polymethacrylate copolymers containing 4,5-dicyanoimidazole based chromophores and their nonlinear optical behaviour

Macromol. Chem. Phys. **206**, 1399-1404, 2005

Thiophene Copolymers

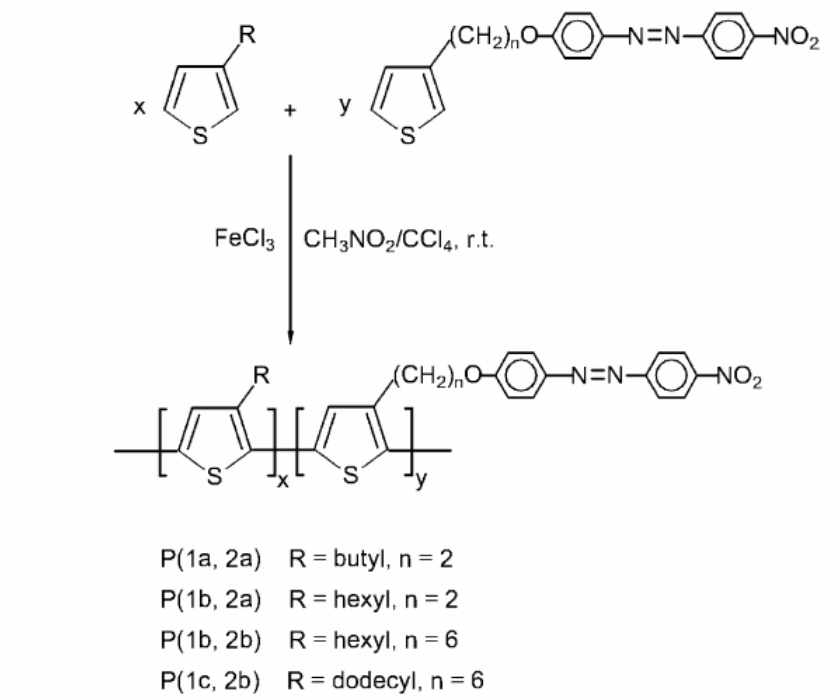

P(1a, 2a) R = butyl, n = 2
P(1b, 2a) R = hexyl, n = 2
P(1b, 2b) R = hexyl, n = 6
P(1c, 2b) R = dodecyl, n = 6

Polymer	***T_g (°C)***	***d_{33} @ 1064 nm (pm/V)***	***τ_2(25°C) (days)***
P(1a,2a)	67	4.7	/
P(1b,2a)	56	6.0	/
P(1b,2b)	40	2.1	/
P(1c,2b)	/	2.0	/

C. Della-Casa, A. Fraleoni-Morgera, M. Lanzi, P. Costa-Bizzarri, L. Paganin, F. Bertinelli, L. Schenetti, A. Mucci, M. Casalboni, F. Sarcinelli, **A. Quatela**,

Preparation and characterization of thiophene copolymers with second order non-linear optical properties

Eur. Pol. J.,**41**, 2360-2369, (2005)

DR1-doped Polymeric Systems

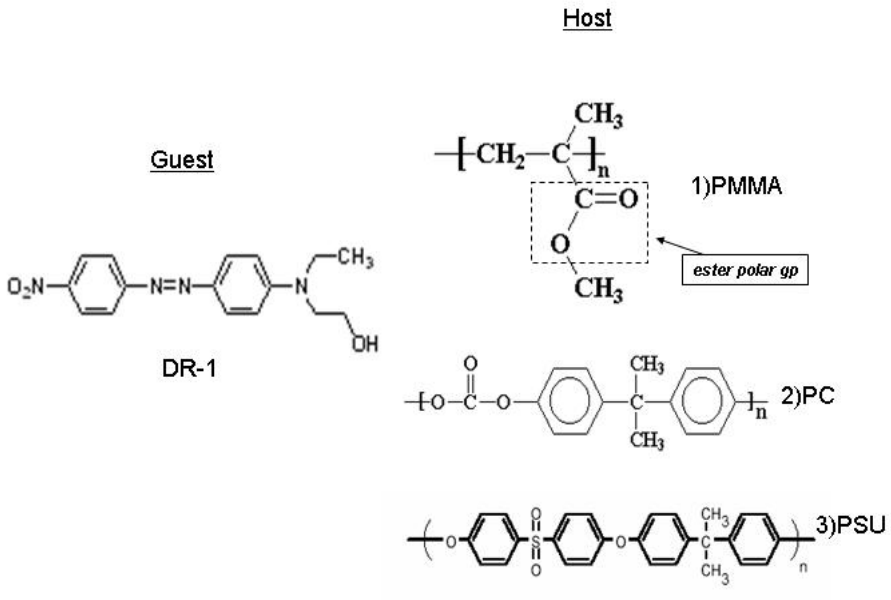

Polymer	T_g *(°C)*	d_{33} *(pm/V)*	τ_2*(25°C) (days)*
DR1-doped PMMA	114	/	307
DR1-doped PC	149	/	835
DR1-doped PSU	190	/	2190 (~6 years)

DR19-doped Polyimide Systems

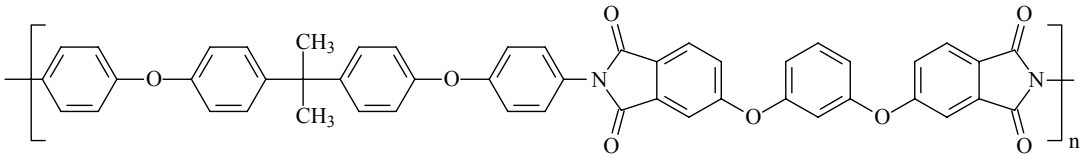

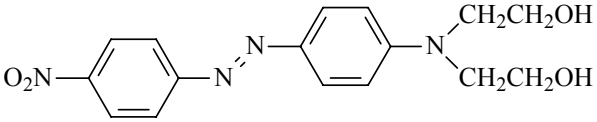

Polymer	T_g *(°C)*	d_{33}@	τ_2*(25°C) (days)*
DR19-doped Polyimide	196	/	11315

A. Quatela, F. De Matteis, M. Casalboni, M. Colombo, A. Zaopo

Relaxation processes of poled ordered azo-dye in polyimide films below the glass transition temperature

to be submitted

BISOHPETCN in Sol-Gel System GTA48

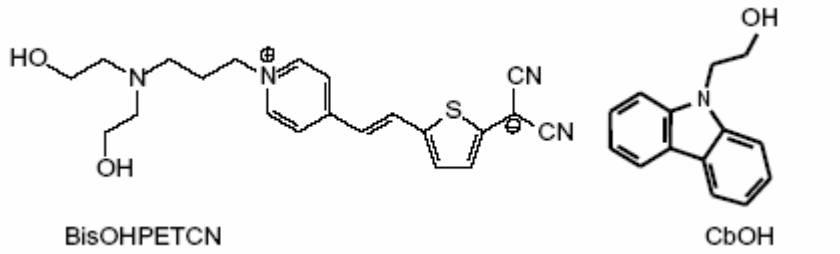

System	*d_{33} @ 1368 nm (pm/V)*	*τ_2(25°C) (days)*
BISOH in GTA48	9	/

DR19 in Sol-Gel System GTA48

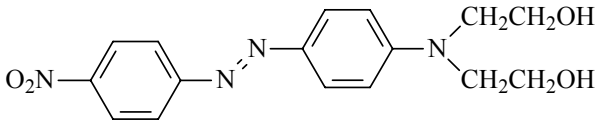

System	*d_{33} @ 1368 nm (pm/V)*	*τ_2(25°C) (days)*
DR19 in GTA48	6	/

Benzimidazole chromophore (BZI) in Sol-Gel System GdANaOH

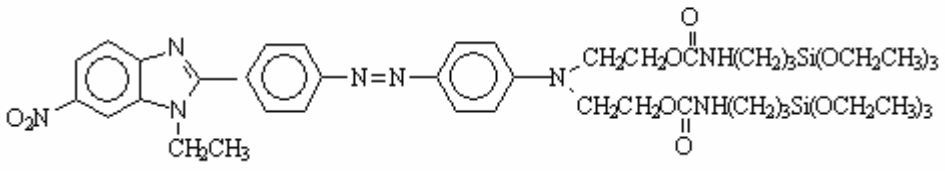

System	*d_{33} @ 1368 nm (pm/V)*	*τ_2(25°C) (days)*
BZI in GdANaOH 20%*	4	/
BZI in GdANaOH 40%*	2	/

** content of chromophores in the polymer (mol-%)*

Acknlowledgements

Con loro ho iniziato e terminato il percorso universitario, ho seguito le loro vicende lavorative e sentimentali. Sono sempre state pronte a sentire le mie lamentele e i miei sfoghi, a consolarmi e a farmi aprire gli occhi, quando necessario (mai, perché hanno paura che mi arrabbi!). Per questo e per il fatto che sono ancora mie amiche, ringrazio la Dr. Danila Ambrosino, Eleonora Nicolai e Lara Castellano (e consorti, ovviamente!).

Je remercie tous les PhD du Laboratoire POMA, Dr. Serge Maabou, Dr. Gabriela Aldea, Dr. Sohrab Ahamadi, Dr. David Chapron, Dr. Sudhir Cherukulappurath, Dr. Unni Narayanan, Dr. Lian Nedelchev, Dr. Anna Migalska…… pour avoir rendu le travail en Angers amusant et stimulant. En particulier, je voudrais remercier le Dr. Wallace Chan pour m' avoir supportée pendant 2 mois e pour le spécial dîner chinois.

À tout le monde, je m'excuse pour mon français!

Deseo agradecer a mis buenos amigos: Dr. Katherine Pacheco y Dr. Daniela Coelho para ser tan bueno con mí. Han sido muy importantes cuando estaba en encolerizo. Me animaron y apoyaron en todo: estudio, trabajo y compras. Espero que nuestra amistad dure por siempre. ¡A usted, el Capítulo 6 es dedicado!

Специальная благодарит к Andrey сделало меня множество чая.

Ik zou graag een speciaal persoon, Dr. Emile van Veldhoven, willen bedanken, die mij de schoonheid de wetenschap tonde en die nij aanmoedigde en stende in mijn gehele PhD tijd (en dat niet alleen). Ik herinner, met liefde, alle uren die wij in het donker hebben doorgebracht en al het snoep dat we hebben gegeten! Voor hem, een speciale gedachte en dank.

Ringrazio la Dr. Valentina Cascella, per tutta la calma che ha saputo infondermi e per l'enorme sforzo che fa ogni qualvolta cerca di spiegarmi qualche legge e/o regola della comunità europea.

Un ringraziamento particolare va ai miei "compagni di viaggio", che hanno condiviso con me le gioie e i dolori della ricerca: il direttore della CIA, Dr. Luca Marinucci, la migliore shopping-friend che esista, Dr. Giordana Roma, la mia nuova collega, Dr. Roberta Pagliacci, Mr. Universo (che sia lui o il fratello) Dr. Marcello Burattini, il "gentilino" padovano, Dr. Gioia della Giustina, il vampiro, Dr. Alexandru Udvar e i miei personal trainer, Dr. Federica Stella e Dr. Serena Pietrantoni.

Besonders, bedanke ich den *playboy* Doktor des Laboratoriums Christian Palazzesi, mit dem hoffe ich viele mailändisch Reisen zu teilhaben.

Ringrazio infinitamente il Dr. Stefano Schutzmann, il quale a "colpi di vena" e di sincera amicizia ha saputo accompagnarmi ed aiutarmi nel mio lavoro. Ringrazio ***Brewsted,*** che illuminando la mente del mio collega, lo ha trasformato nel "*Signore dell'indice di rifrazione"*!

Un grazie alla Dr. Giovanna Brusatin dell'Università di Padova, al Prof. Antonio Roviello e Roberto Centore dell'Università Federico II di Napoli per il loro contributo a questa tesi e per avermi fatto appassionare alla chimica.

Un remerciement particulier va au Prof. J.-M. Nunzi pour m'avoir donnée la possibilité de travailler dans son groupe. Je la remercie pour m'avoir faite sentir comme chez moi e pour les nombreuses discussions scentifiques qui m'ont illumineé dans le mystérieux monde del' *All Optical poling*.

Een speciale dank voor Dr. Paolo Prosposito, ten eerste hij is een vriendelijk persoon, ten tweede zijn doorzettingsvermogen in onderzoek. Hij straalt in de donkere periodes en hij maakt me altijd aan het lachen in de harde tijden. Hij zal altijd mijn speciale Hollandse koffie trainer.

Mi è difficile ringraziare il Dr. Fabio De Matteis perché non so da dove cominciare. La sua onestà e diplomazia mi hanno sempre affascinato, ma ancor di più la sua disponibilità e curiosità scientifica. Se dovessi scegliere un modello a cui aspirare, probabilmente sceglierei lui anche se ciò è impossibile….non posso digerire così tanti zuccheri!!!

Le parole non sono sufficienti per ringraziare il Prof. Mauro Casalboni. Lo ringrazio per avermi dato fiducia e per avermi supportato in ogni mia scelta scientifica. Mi ha saputo guidare nella ricerca senza mai intromettersi nelle mie, spesso discutibili, scelte. Ha sempre (vero?) sopportato la mia impulsività e per questo lo ringrazio.

Ringrazio infinitamente la mia famiglia per il loro affetto e supporto e per avermi dato la possibilità di intraprendere questa strada. Un grazie speciale a Dario perché senza di lui non sarei diventata la persona che sono oggi. La sua fiducia è per me una spinta a fare sempre meglio.

Ringrazio chi, da lassù mi segue; chi, per primo, mi ha guidato in questo lavoro; chi mi ha trasmesso la passione per la ricerca. La sua grande energia mi ha travolto e spero di non averlo deluso.

A te, Felice, questa tesi è dedicata. Grazie.

References

A

Apostoluk A., Chapron D., Gadret G., Sahraoui B. and Nunzi J. M., *Optics. Lett*., 27, 2028 (2002)

Arfken G., *Mathematical Methods for Physicists*, 3rd ed.; Academic Press: New York, 1985

B

Bartkowiak W., Zalesny R., Leszczynski J., *Chem. Phys*., 287, 103 (2003)

Bauer S*., J. Appl. Phys*. 80 (10), 5531 (1996)

Boyd R. W., *Nonlinear Optics*, Academic Press Inc., San Diego, CA, USA (1992)

Brinker C. J. and Scherer G. W., Sol-*Gel science: the physics and chemistry of sol-gel processing*, ACADEMIC PRESS, INC., San Diego, USA

Brown R. P., *Polymer Testing*, 14, 403 (1995)

Brusatin G., Abbotto A., Beverina L., Pagani G. A., Casalboni M., Sarcinelli F., Innocenzi P., *Adv. Func. Mat.*, 14, 1166 (2004)

Burland D. M., Miller R. D. and Walsh C. A., *Chem. Rev*., 94, 31 (1994)

Butcher P. N. and Cotter D., *The Elements of Nonlinear Optics*, Cambridge University Press, Cambridge, UK (1990)

Byer R. L. and Harris S. E., *Phys. Rev*. **168**, 1064 (1968)

C

Carella A., Centore R., Fort A., Peluso A., Sirigu A. and Tuzi A., *Eur. J. Org. Chem*. 2004, 2620

Carella A., Centore R., Sirigu A., Tuzi A., Quatela A., Schutzmann S. and Casalboni M., *Macromol. Chem. Phys*., 205, 1948 (2004)

Casalboni M., *Organic electrooptical modulators*, to be published by SIF (2004)

Casalboni M. Sarcinelli F., Pizzoferrato R., D'Amato R., Furlani A. and Russo M.V., *Chem. Phys. Lett.*, 319, 107 (2000)

Chan S. W., Nunzi J.-M., Quatela A., Casalboni M., *in preparation*

Chang J. Y, Kim T. J., Han M. J., Choi D. H. and Kim N., *Polymer*, 38, 4651 (1997)

Charra F., F. Kajzar, J. M. Nunzi, P. Raimond and E. Idiart, *Opt. Lett*., 18, 941 (1993)

Cheng L. T., Tam W., Stevenson S. H., Meredith G. R., Rikken G. and Marder S. R., *J. Phys. Chem.*, 95, 10631-10643 (1991)

Choi D. H., Kang J. S. and Hong H. T., Polymer, 42, 793 (2001)

D

M., Fetterman H., Shi Y., Mustacich R. V., Jen K. Y., Shea K. J., *Chem. Mater*. 7, 1060 (1995)

Dalton L., Harper A. W., Ren A., Wong F., Todorova G., Chen J., Zhang C., Lee M., *Ind. Eng. Chem. Res* 38, 8 (1999)

Dao P. T., Williams D. J., McKenna W. P., Goppert-Berarducci K., *J. Appl. Phys*., 73, 2043 (1993)

Dhinojwala A., Wong G. K. and Torkelson J. M., *Macromolecules*, 26, 5943 (1993)

Dulcic A. and Sauteret C., *J. Chem. Phys*., 69, 3453 (1978)

Doolittle A. K., *J. Appl. Phys*., 22, 1471 (1951)

Dumont M., Froc G. and Hosotte S., *Nonl. Optics*, 9, 327 (1995)

E

Ermer S., Valley J. F., Lipscomb G. F., Van Eck T. E. and Girton D. G*., J. Appl. Phys*., 61, 2272 (1992)

F

Fiorini C., Charra F., Nunzi J. M. and Raimond P., *J. Opt. Soc. Am. B*, 14, 1984 (1997)

Flytzanis C., *Quantum Electronics, a Treatise*, *Vol 1*, Academic Press, New York, USA (1975)

Franken P. A., Hill A. E., Peters C. W. and Weinreich G., *Phys. Rev. Lett*. **7**, 118 (1961)

G

Garret C. G. B. and Robinson F. N. H., *IEEE J. Quantum. Electron*. **2**, 328 (1966)

Goudket H., Canva M. and Lévy Y., *J. Appl. Phys*. 90 (12), 6044 (2001)

H

Harper A. W., Sun S., Dalton L. R., Garner S. M., Chen A., Kalluri S., Steier W. H., Robinson B. H., *J. Opt. Soc. Am. B*, 15, 329 (1998)

Harris S. E., Oshman M. K. and Byer R. L., *Phys. Rev. Lett*. **18**, 732 (1967)

Havinga E. L. and Van Pelt P., *Phys. Chem*., 83, 816 (1979)

Hayden L., Sauter G., Ore F., Pasillas P., Hoover J., Lindsay G., Henry R., *J. Appl. Phys*. 68, 456 (1990)

Houe M., Townsed P. D., *J. Phys. D*, 28, 1747 (1995)

Hutchinson J. M., *Prog. Polym. Sci*., 20, 703 (1995)

J

Jerphagnon J. and Kurtz S. K., *J. Appl. Phys*., 41, 1667 (1970)

K

Kajzar F. and Nunzi J. M., *Molecular Orientation Techniques* in *Beam Shaping and Control with Nonlinear Optics*, edited by Kajzar F. and Reinisch R., Plenum Press New York, USA (1998)

Kajzar F., Charra F., . Nunzi J. M, Raimond P., Idiart E. and Zagorska M., in *Proceedings of International Conference on Frontier of Polymers and Advanced Materials*, Jakarta, 1995

Kleinman D. A., *Phys. Rev*. **126**, 1977 (1962)

L

Lee M., Katza H. E., Erben C., D. Gill M., Gopalan P., Heber J. D. and McGee D. J., *Science*, 298, 1401 (2002)

Levine B. F., *J. Chem. Phys*., 63, 115 (1975)

Liang J., Levenson R., Rossier C., Toussaere E., Zyss J., Rousseau A., Boutevin B., Foll E. and Bose D., *J. Phys. (France) III*, 4, 2441 (1994)

Lindsay G. A., Henry R. A. and Hoover J. M., *Macromolecules*, 25, 4888 (1992)

M

Marder S. R., Bretan D. N., Cheng L. T., *Science* 252, 103 (1991)

Matsumoto S., Kubodera K., Kurihara T. and . Kaino T, *Appl. Phys. Lett*., 51, 1 (1987)

McConell J., *Rotational Brownian Motion and Dielectric Theory*; Academic Press: New York, 1980

Middleman S. and Hochberg A. K., *Process Engineering Analysis in Semiconductor Device Fabrication*, McGraw-Hill (1993)

Miller R. C., *Appl. Phys. Lett*. **5**, 17 (1964)

Möhlmann G. R., *Chemisch Magazine*, 49, 786-828 (1987)

Morley J. O. and Pugh D., *Spec. Publ. Soc. Chem*., 69, 28 (1989)

Morley J. O., Docherty V. J., and Pugh D., *J. Chem. Soc. Perkin Trans*., 2, 1351 (1987)

Mortazavi M. A., Knoesen A., Kowel S. T., Higgins B. G. and Dienes A., *J. Opt. Soc. Am. B*, 6, 733 (1989)

Maker P.D., Terhune R. W., Nisenoff M. and Savage C. M., *Phys. Lett*. 8, 21 (1962)

N

Newell A. C. and Moloney J. V., *Nonlinear Optics*, Addison-Wesley Publishing Company, Redwood City, USA (1992)

Nunzi J. M., Charra F., Fiorini C. and Zyss J., *Chem. Phys. Lett*., 219, 349 (1994)

O

Osterberg U. and Margulis W., *Optics Lett*. 11, 516 (1986)

Oudar J. L. and LePerson H., *Opt. Comm*., 15, 258 (1975)

Oudar J.L. and Chela D.S., *J. Chem. Phys*., 66, 2664-68 1977

Oudar J.L., *J. Chem. Phys.,* 67, 446-457 1977

P

Persico P., Centore R., Sirigu A., Casalboni M., Quatela A., and Sarcinelli F*., J. of Pol. Sci.: Part A: Pol. Chem.*, 41, 1841 (2003)

Q

Quatela A.,COST P8 Mission Report 2003-2004

R

Reliasoft Coorporation, © 1998-2002, http://www.weibull.com

Reyes-Esqueda J., Darracq B., Garcia-Macedo J., Canva M., Blanchard-Desce M., Chaput F., Lahil K., Boilot J. P., Brun A. and Lèvy J., *J. Opt. Commun*., 198, 207, (2001)

Rong-Ho-Lee, Ging-Ho-Hsiue, Che-Kai Hsu, Jenn-Chiu Hwang and Ru-Jong Jeng, *Polymer*, 39, 26 (1998)

S

Saleh B. E. A. and Teich M. C., *Fundamentals of Photonics*, John Wiley & Sons Inc., New York, USA (1991)

Saleh B. E. and Teich M. C., *Fundamentals of Photonics*, John Wiley & Sons, INC., New York, USA (1991)

Sarcinelli F. and Casalboni M., *Recent. Res. Devel. Applied Phys*., 6, 663-694 2003

Sekkat Z. and Dumont M., *Nonl. Optics*, 2, 359 (1992)

Singer K. D., Sohn J. E. and Lalama S. J., *Appl. Phys. Lett*., 49, 248 (1986)

Singer K., Sohn J. E., Lalama S. J., Appl. Phys. Lett. 49, 248 (1986)

Suzuki A. and Matsuoka Y., , *J. Appl. Phys*. 77 (3), 965 (1995)

W

Williams D. J., *Angew. Chem. Int. Ed. Engl.*, 23, 690 (1984)

Wong K. K., *Properties of Lithium Niobate*, Institution of Electrical Engineers London, UK (2002)

Wu J. W., *J. Opt. Soc. Am. B*, 8, 142 (1991)

Y

Yariv A., *Quantum Electronics*, John Wiley & Sons Inc., New York, USA (1975)

Yilmaz S., Bauer S., Gerhard-Multhampt R., *Appl. Phys. Lett*., 64, 2770 (1994)

Candidate's Bibliography

P.Prosposito, M. Casalboni , F. De Matteis, M. Glasbeek , **A. Quatela**, E. van Veldhoven, H. Zhang
Femtosecond dynamics of ir-molecules in hybrid materials
J. Lumin., **94-95**, 641 (2001)

P.Prosposito, M. Casalboni , F. De Matteis, **A. Quatela**, M. Glasbeek , E. van Veldhoven, H. Zhang
IR-luminescent-molecules in hybrid materials
J. Sol-Gel Science Tech., **26**, 909 (2003)

M. Casalboni, F. De Matteis, P. Prosposito, **A. Quatela**, F. Sarcinelli
Fluorescence efficiency of four infrared polymethine dyes
Chem. Phys. Lett., **373**, 372 (2003)

P. Persico, R. Centore, A. Sirigu, M. Casalboni, **A. Quatela**, F. Sarcinelli
Synthesis and Nonlinear Optical Properties of Methacrylate Polymers Based on 2-[4-(N-methyl,N-hydroxyethylamino)phenylazo]-phenyl-6-nitrobenzoxazole Chromophores
J Polym. Sci A, **41**, 1841 (2003)

P. Costa-Bizzarri, M. Lanzi, L. Paganin, C. Della-Casa, F. Bertinelli, M. Casalboni, F. Sarcinelli, **A. Quatela**
Versatile synthesis of soluble multifunctional thiophene copolymers with NLO activity
Macromol. Chem. Phys., **204**, 1982 (2003)

I. Aiello, U. Caruso, M. Ghedini, B. Panunzi, **A. Quatela**, A. Roviello, F. Sarcinelli
NLO active Pd(II)-based organometallic side-chain polymers with C,N or N,O-chelating chromophoric ligands
Polymer, **44**, 7635 (2003)

A. Carella, R. Centore, A. Sirigu, A. Tuzi, **A. Quatela**, S. Schutzmann, M. Casalboni
Second order nonlinear optical performances of polymers containing imidazole and benzimidazole chromophores
Macromol. Chem. Phys., **205**, 1948 (2004)

M. Casalboni, U. Caruso, A. De Maria, M. Fusco, B. Panunzi, **A. Quatela**, A. Roviello, F. Sarcinelli, A. Sirigu
New polyurethanes and polyesters for second-order nonlinear optical applications
J Polym. Sci. Part A-Pol. Chem. **42**,3013, (2004)

A. Carella, R. Centore, P. Riccio, A. Sirigu, **A. Quatela**, C. Palazzesi, M. Casalboni
Polymethacrylate copolymers containing 4,5-dicyanoimidazole based chromophores and their nonlinear optical behaviour
Macromol. Chem. Phys. **206**, 1399-1404, 2005

C. Della-Casa, A. Fraleoni-Morgera, M. Lanzi, P. Costa-Bizzarri, L. Paganin, F. Bertinelli, L. Schenetti, A. Mucci, M. Casalboni, F. Sarcinelli, **A. Quatela**,
Preparation and characterization of thiophene copolymers with second order non-linear optical properties
Eur. Pol. J.,**41**, 2360-2369, (2005)